RELATIONSHIPS BETWEEN MECHANICAL PROPERTIES AND BOREHOLE HEAT EXCHANGERS THERMAL FORCING IN CLAYEY SUBSOIL ICEA 2014

Niccolò Giuliani

UNIVERSITÀ
DEGLI STUDI
DI PADOVA

Second Cycle Degree in Environmental Engineering
ICEA Department

Master thesis

Niccolò Giuliani

RELATIONSHIPS BETWEEN MECHANICAL PROPERTIES AND BOREHOLE HEAT EXCHANGERS THERMAL FORCING IN CLAYEY SUBSOIL

The case study of Venice

Supervisor:
Prof. Raffaele Sassi

Co-Supervisors:
Prof. Antonio Galgaro
Ing. Giorgia Dalla Santa

A.Y. 2013-2014

Relationships between mechanical properties and borehole heat exchangers thermal forcing in clayey subsoils

Niccolò Giuliani

Academic year 2013\2014

A mia Madre

Contents

Introduction

Borehole heat exchanger (BHE) is a device installed into vertical drilled wells which is part of closed loop geothermic exchange system, used for buildings conditioning. BHE can reach more than 100 meters depth and, coupled with a heat pump, transfers heat between ground and buildings by the carrier fluid flowing inside the pipes filled into the borehole (Figure 0.0.1).

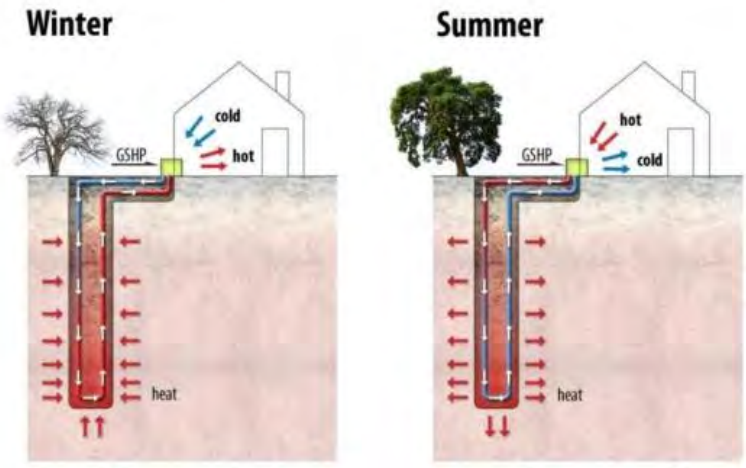

Figure 0.0.1: Closed loop geothermal heat pump during winter heating and summer conditioning functioning

This research wants to investigate the effects of the thermal stress induced by the BHE on the mechanical behaviors of the subsoil. In fact, to satisfy peak buildings heat demands, an extensive heat extraction occurs, or in case of under-sizing of the BHE field design, the carrier fluid temperatures drop below 0°C (even less than -5°C). Therefore it is necessary to mix anti-freeze additives in the working fluid. Consequently, freezing of the BHE surrounding grout and of the surrounding ground is possible. This process is commonly referred to as freeze-thaw-cycle (FTC).

FTC processes cause changes to the underground mechanical properties, in particular on cohesive sediments. This may result in considerable damages to the buildings stability, as BHEs are often installed close to, or even below, the buildings. FTC in the subsoil could also lead to underground hydraulic hazard. In fact, BHEs penetrate different deposition horizons and need to be sealed. FTC induces changes in soil permeability leading unwonted vertical water flow or possible aquifers connections.

In order to implement and design BHE, it is necessary to become aware of the possible hazards.

Venezia and the *COGET* project

The research focuses on the FTC effect on clayey subsoils and, in particular, on the effects on the FTC processes of salt concentration in the interstitial water. The study case is the Venetian subsoil, which is rich in cohesive sediments and susceptible to saltwater intrusion. In fact, this research derives and is part of the project named *COGET*[1], which is a research partnership between the Padua University and the *Provincia di Venezia*. This partnership is the prosecution of *AGAVE*[2] project, aim of which is to investigate the environmental impacts of the geothermal solutions in Venetian area, in order to avoid the possible hazards. The problem arises from the particular environmental sensitivity of the lagoon area, which is also characterized by other subsidence problems, but also from the need to protect the urban area of Venice, rich in cultural and historical architectures.

The urban area of Venice is located in a high urbanized coastal area, and could be used to develop guidelines and standard parameters for geothermal heat pump utilization, applicable also to other areas with the same characteristics. In fact, in densely urbanized areas, the lack of open spaces combined with the increased attention to energy efficiency, leads to BHE installation even directly under the buildings, affecting portions of subsoil which interact with the foundations. Moreover the proximity to the sea makes coastal and lagoon areas different from the others. In fact, saltwater intrusion as also the marine-continental transitional deposition environment, strongly interacts with FTC processes.

The energy question

Geothermal heat pumps are very high efficient and of relatively new diffusion systems for building conditioning. It is therefore necessary to improve our knowledges about the possible hazards, in order to promote a safety implementation of these technologies.

Nowadays the entire world's energy system is based on the combustion of fossil fuels and the demand for energy is rising sharply, mainly due to the growth of developing countries. Firstly, fossil resources are non-renewable and will finish, but, more importantly, their exploitation is causing serious medium and long-term environmental impacts. Global warming has become unmistakably important with widespread melting of ice, noticeable climate changes, and rising sea levels. This is now recognized by almost everyone as caused by greenhouse gases, mainly carbon dioxide, produced by burning fossil fuels. For these reasons it is necessary to gradually change the entire system of energy production, turning as soon as possible to energy conservation and efficiency as well as renewable resources.

[1] Analysis of the geomechanical behavior of the Venetian sediments in relation to thermal stresses induced by vertical geothermal borehole

[2] Geotechnical analysis of the effects induced by thermal variations in the clay sediments of the lagoon of Venice

In recent years many efforts have been made both locally and internationally for the development and application of renewable and energy-saving technologies, in order to improve the energy efficiency of the global system and start giving answers to the energy issue. A first step is to modernize the electricity and conditioning infrastructures even of small residential units, which are often outdated and inefficient. Governments and local institutions implement various policies in order to increase the diffusion of these technologies, such as subsides, tax-free and legal obligation. The current standard regulation in Italy, refers to the D.M. 28/12/2012 [21] and the D.Le n.28 [19], in which are defined all the incentives for energy saving and renewable resources measures.

The innovation of the research

A lot of efforts (numbers of papers and reviews) have been done in order to understand freezing and thawing mechanism in soils. But all of these papers and studies refer to the freezing and thawing of the active layer of *permafrost*. Permafrost is permanently frozen subsoil, occurring at high latitudes but also at high altitudes. The upper layer of permafrost, named *active layer*, is subjected to seasonal freezing and thawing with consequences on the structures stability, consequentially it is an important engineering topic in cold regions such as Canada and northern Europe. Figure 0.0.2 shows the seasonal temperature variability in permafrost and its spatial distribution. One of the most important processes involved is the *frost heave.* Frost heave is basically an upward swelling of soil during freezing conditions caused by an increasing presence of ice as it grows towards the surface.

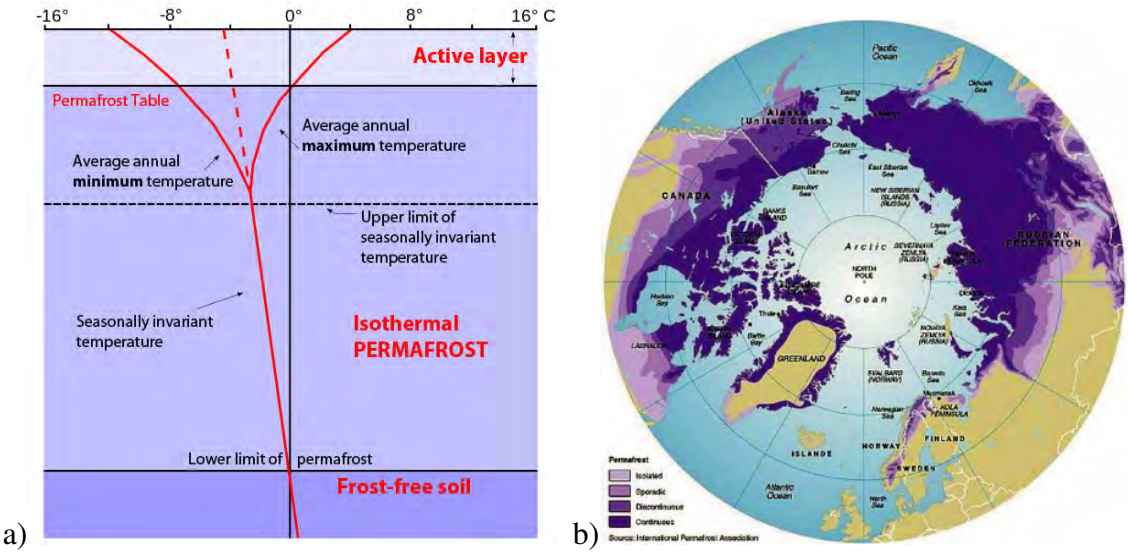

Figure 0.0.2: (a) vertical temperature profile in Permafrost. (b) Permafrost distribution map

The innovation of this research is to apply the investigation of freezing and thawing soil mechanism to the BHE. To be done, a change in the process geometry is required. Figure 0.0.3 shows the different geometry of the heat transfer processes between the FTC in permafrost and

BHEs induced. Permafrost freezing and thawing and frost heave are caused by the outdoor temperature variability. The heat transfer direction is vertical, form the external environment to the ground, during summer thawing, and in the other way around during freezing. In this case the freezing front is parallel to the ground surface.

In FTC induced by BHEs, the heat transfer principal direction is horizontal, radial respect to the pipes axis. From the ground to the borehole, in case of winter heating function; from the borehole to the surrounding ground during summer conditioning functioning. Consequentially the freezing front forms vertical, around the the borehole pipes.

These processes, even if they look similar, have different environmental consequences, as it will be discussed in the following chapters.

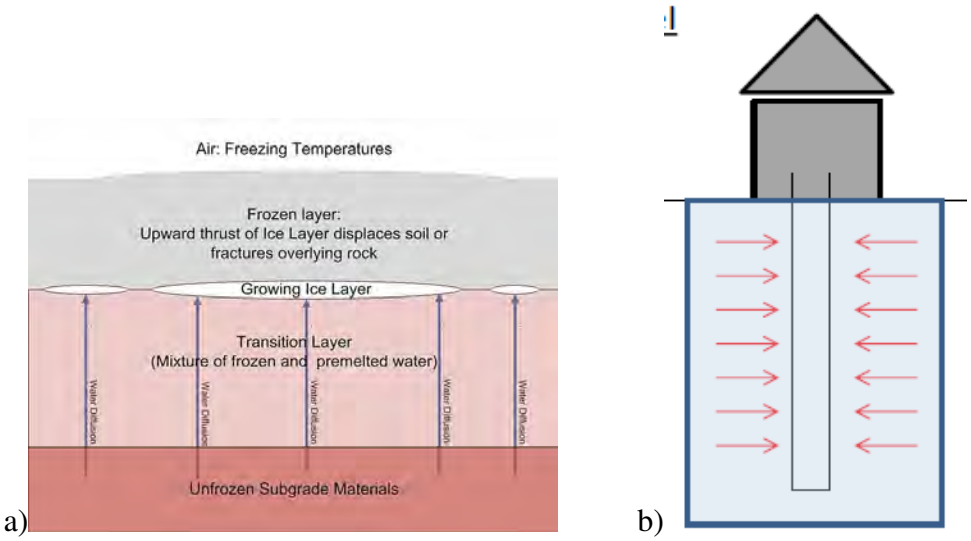

Figure 0.0.3: Change in process geometry. a) frost heave. b) borehole freeze-thaw cycles

Chapter 1

Geothermal systems

1.1 Heat pumps

A heat pump is a machine able to transfer thermal energy from a source of lower temperature, to another of higher temperature, generally with electrical energy consumption. The physical principle is known from a couple of centuries and nowadays one of the most common applications is the thermal conditioning of the interiors. During the winter season the heat pump transfers heat from a free outside cold source (air, sea, lake, underground), and 'pumps' it to the hot source, witch is the internal environment to be heated, by spending electrical power. During the summer, it absorbs heat from the cold internal environment, to be air-conditioned, and "pumps" outside. The heat pumps having this dual function winter - summer are said reversible, and, in most cases, the source from which we extract the thermal energy needed is the air (Figure1.1.1).

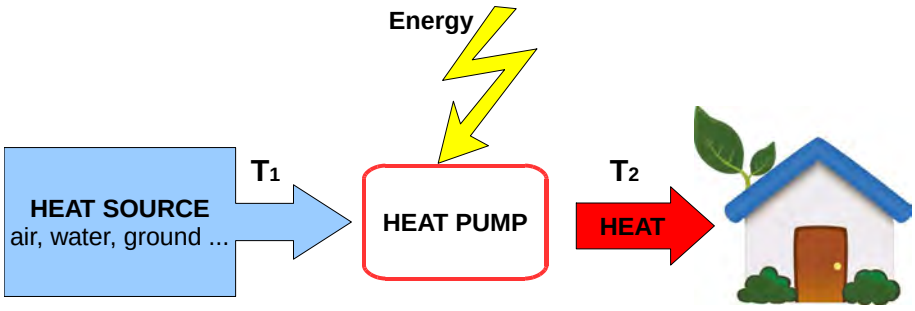

Figure 1.1.1: Conditioning heat pump diagram

The functioning of the heat pump is based on the Joule-Thomson effect: a gas which abruptly expands, undergoes a lowering of the temperature; on the contrary, if it is compressed, it increases its temperature. From the second principle of thermodynamics derives that, while the heat could spontaneously pass from a warmer body to a colder one, the passage of heat "unnatural" from a colder to a warmer body requires energy, necessary for the compression.

1.1.1 Thermodynamic cycle

The functioning of the heat pump is commonly described by the cycle represented in the diagram T-s (Figure1.1.2), in which is possible to see thermodynamic transformations of which the fluid undergoes in the passage through the two heat exchangers of high, the condenser, and low temperature, evaporator, the expansion valve and the compressor (Figure1.1.3) .

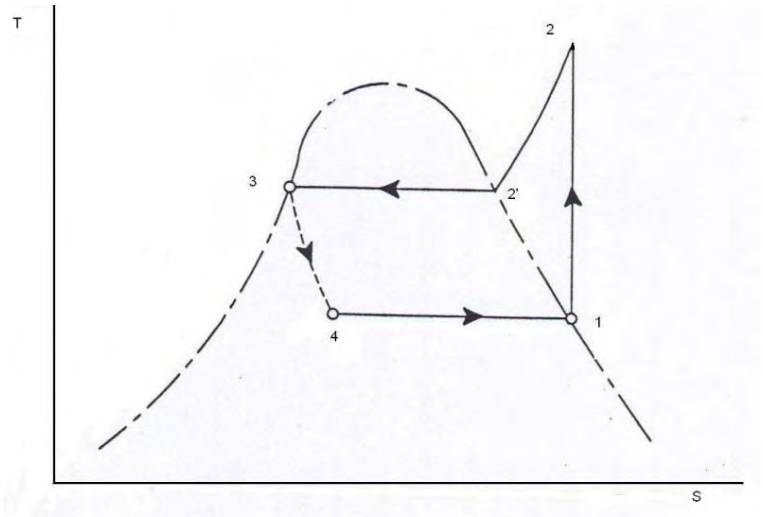

Figure 1.1.2: heat pump cycle in temperature - entropy diagram.

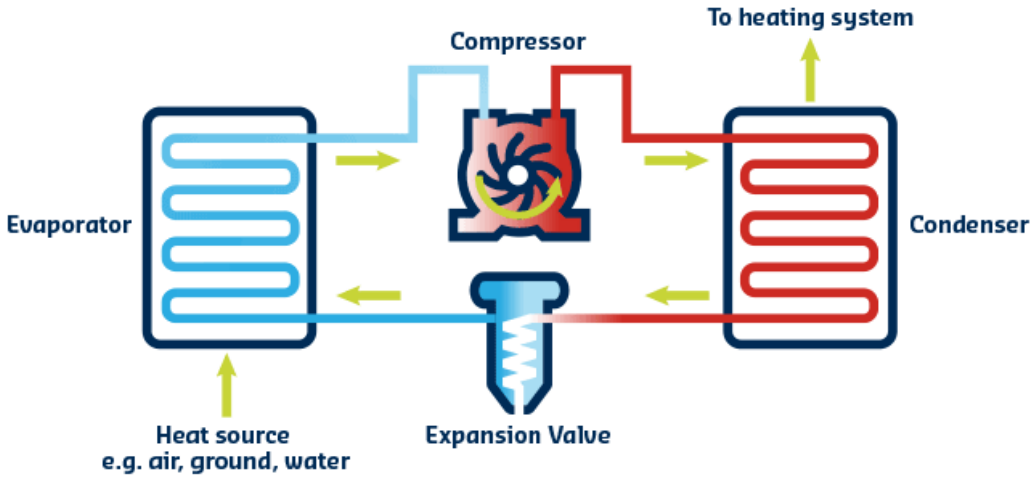

Figure 1.1.3: Heat pump component

The compression is normally assumed adiabatic, with a request of work from the outside. The evaporation, heat removed from the machine, and the condensation heat transferred from the machine, are assumed isobars and then isotherms, while lamination is a isoenthalpic transformation. If these four transformations are also reversible, then the cycle will named as the

reverse Carnot cycle (Figure1.1.4), a particular thermodynamic cycle to which referring when treating heat pumps.

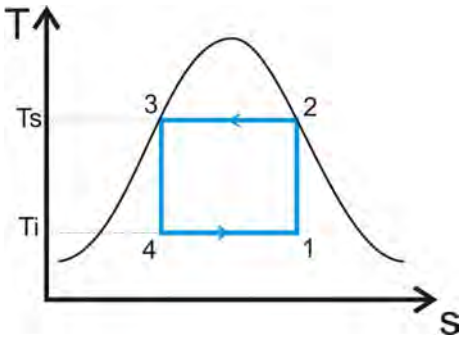

Figure 1.1.4: Carnot cycle

In the reality, instead, unavoidable irreversibility occurs and it is the reason for which the coefficient of performance of real value deviates from the theoretical one in the ideal conditions. The irreversibility are caused by frictional losses of the fluid flowing through the exchangers and along the connecting pipes between the various organs of the cycle (irreversibility however negligible), and the irreversibility in compression, characterized by its isoentropic efficiency. Beyond this, temperature differences between the condensing fluid and the hot tank, and the fluid between the evaporator and the cold source, have to take into account. They are not present in the ideal Carnot cycle, in which the transformations to the condenser and the evaporator are reversible.

Schematically (Figure1.1.5), the pump extracts heat (Qe) from a source and transfers (Qc) to a receiver thanks to the compressor which provides a quantity of labor (L) equal to the difference between heat lost and heat extracted. Therefore, to evaluate the performance of the heat pump,

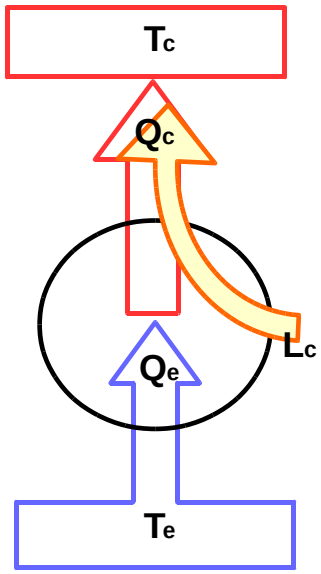

Figure 1.1.5: Heat pump scheme

is used the *coefficient of performance*, COP.

$$COP = \frac{Q_c}{L_c}$$

Rewriting the equation in function of the source and receive temperatures:

$$COP = \frac{T_c}{T_c - T_e}$$

This expression analytically shows how the heat pump improves its performance, much closer the sources temperatures are. It is the basic reason for which the usage of different type of heat source instead of the air, like the soil, could be an interesting alternative and provides a substantial energy saving.

When the pump is used to the internal cooling, the performances are evaluated with the *Energy Efficiency Ratio*, EER:

$$EER = \frac{Q_e}{L_c} = \frac{T_e}{T_c - T_e}$$

with the same consequences and considerations of the heating usage.

1.1.2 Air and geothermal heat pumps

Heat pumps could be classified according with the fluid used both in the user and in the source side:

Air-air pumps are pumps which use the external air as heat source and directly transfer heat with the internal air.

In **air-water** pumps the heat, taken from the external air, is transferred to the water in order to better carry and spread it.

Water-water pumps, instead, use a heat source different from the external air. It could be the streamflow, lake or sea water, as also the groundwater or the subsoil. In this case exploiting the geothermal resources.

The great advantage of using as source the subsoil instead of the external air derives from the fact that the ground maintains a constant temperatures in every conditions (around 15°C), which is considerably higher than that of air, especially when more power is required. As it has been explained, smaller is the ΔT between the source and the receiver, higher is the pump performance (COP) and smaller are the energy costs. In fact, using a normal air heat pumps for winter warming, when the external temperature decrease, the ΔT increase, decreasing the COP precisely when more heat transfer is needed. For this reason, the pump should be design in order to provide the necessary heat supply in extreme conditions, working at partial load in most of times, differently from the geothermal systems which utilize a constant temperature source.

The same considerations could be applied in summer with reverse heat pump. The usage of geothermal heat pumps cut down the energy loss because of the smaller ΔT compared to air heat pumps. An important advantage with geothermal pumps is the possibility of the so called *free cooling* or *natural cooling*, which provide the simple fluid circulation without energy consumption for the compression. It is possible exploiting the fact that the subsoil is cooler than the internal ambient with a natural heat transfer.

The advantages of the geothermal heat pumps are the constancy of the source (subsoil) temperature and the fact that it is a good starting temperature both for winter and summer usage, in order to maximize the COP and minimize the costs. The principal disadvantage of geothermal systems, instead, is represented by the high initial costs. In fact, it is important to evaluate the real economical benefit of a geothermal system, in particular regarding the climate. There is a real energy saving, compared to a traditional air heat pumps only if the the external temperature are low enough to cover the installation costs in a reasonable time (10-20 years).

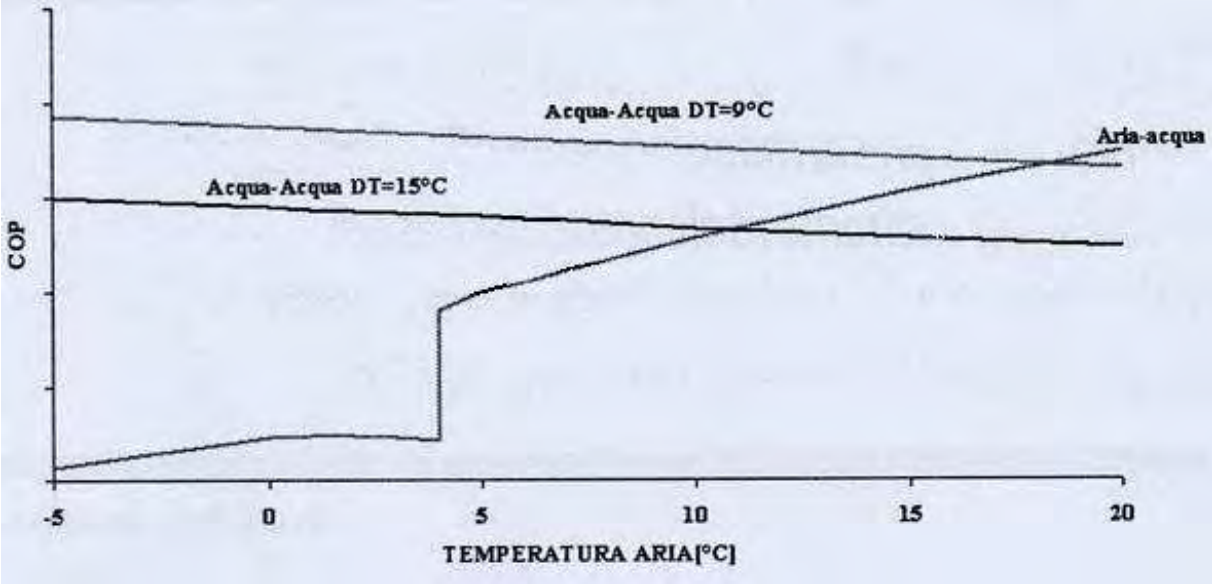

Figure 1.1.6: Performance comparison of air-air and water-water heat pumps

The Figure1.1.6 shows the result of a recent research focused on the comparison of the two sources [1]. It is possible to notice that water-water systems are highly convenient for operational temperatures below 10-15°C but becomes unnecessary when the temperature rises. This operational range of temperatures make the geothermal systems a good choice for example for the northern Italy climate such as in the Po Valley, but could be an unnecessary economic strain in more temperate areas.

The comparison is made only regarding the residential sector and only for the winter heating needs. It is possible to assume that benefits for the water-water systems will increase including also the tertiary sector and the air conditioning summer needs, because in the hottest periods, the subsoil temperature is almost always favorable compared to which of the air.

1.2 Geothermics

The term geothermics refers to the exploitation of the geothermal energy, i.e. that part of the ground heat potentially useful from the subsoil and used for human activity.

Geothermal energy is considered a renewable and sustainable resource, because its exploitation does not affect the planet thermal reserves, and its impacts, from the environmental point of view, are very low, if performed with the adequate precautions.

The most common classification of the geothermal energy is based on the enthalpy which is directly proportional to the temperature. Geothermal resources are so divided into: **low**, **medium** and **high enthalpy resources** (Table 1.1).

Enthalpy	Low	Medium	High
Temperature (°C)	< 90°	90° - 150°	> 150°

Table 1.1: Geo-resources classification [36]

The high enthalpy georesources refer to inhomogeneity of the temperature field due to tectonic and volcanic activity and are exploited by geothermal plants in order to produce electricity. Low enthalpy resources are the object of the geothermal heat pumps, also for domestic implants, exploitable in most of the planet regions and referred to the normal temperature field of the subsoil.

1.2.1 Temperature trend in the subsoil

The basic principle geothermal heat pumps is that they can exploit a tank with high accumulation capacity which could mitigate daily temperature fluctuations which instead are typical of the air, as well as to ensure a constancy of temperature already at a depth of a few meters, for the entire period of the year and that can be considered, with good approximation, equal to the site annual average air temperature.

The *thermal gradient* (T) indicates the temperature increasing with soil depth, and analytically is represented by the ratio between the geothermal heat flux (q) and the soil thermal conductivity (λ):

$$T = \frac{q}{\lambda} [^\circ\mathrm{K}]$$

In Italy, the thermal gradient is about 2,5° - 3° C / 100m (Figure 1.2.1).

By considering the subsoil as infinitely extended and homogeneous, is possible to study the temperature value at different depth. Fourier heat diffusion equation could analytically describe the phenomenon. From the surface, the temperature trend is sinusoidal and damped until certain depth (about 10 - 15). Soil has a damping effect on the surface temperature which, after few meters, stands at a constant value (Figure 1.2.1a).

Obviously, in order to better define the subsoil temperature trend, it is necessary a detailed geological investigation to identify the real subsoil properties.

Anyway, it is possible to define general behaviors. As it is shown in Figures 1.2.1 a and b, only the first meters of the subsoil are affected from the daily and annual temperature fluctuations and already at 10 meters depth is possible to have a temperature almost constant of about 12°-15° C.

It means that the installation of vertical probes at 100m depth can operate with undisturbed soil temperature, not influenced by seasonal changes that occur during the year. This is not true for the horizontal probes, which are more affected by solar radiation and air temperature, factors which plays a significant role in few meters of soil depth.

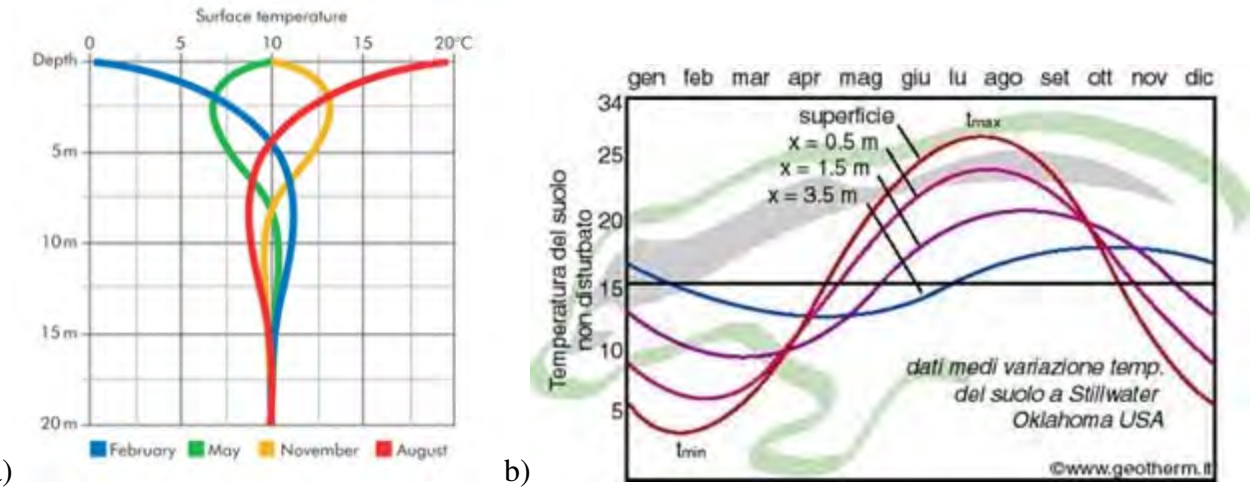

Figure 1.2.1: a) soil temperature trend with depth. b) Annual T trend in subsoil at different depth

1.2.2 Geothermal heat pumps

As already explained, geothermal heat pumps use the subsoil as the heat source. There are different type of technologies and it is possible a first classification based on how the heat extraction is performed, with the refrigerant fluid circulating inside a closed loop or directly using the groundwater.

GWHP Groundwater heat pumps. The groundwater is taken from an aquifer and, after its cooling, it is stored into another aquifer. During the winter season, this process will create a cold source (storage aquifer) ready to be used with the reverse process during the summer season.These pumps are subjected to strict bonds in order to minimize the environmental and hydro-geological impact on the groundwater compared with the undisturbed situation.

SWHP Superficial water heat pumps. They exchange heat with a superficial water body as example lakes or ponds. Normally they are a open loop and operate in the same way of the GWHP, but some times could be closed loop systems. As the high variability of the water body temperature, SWHP are just little more efficient than

a modern air-air heat pump. Moreover, like GWHP, they are subjected to limitation due to the water usage.

GCHP Ground coupled heat pumps. The system consists of a closed loop circuit (BHE) buried into the ground. The borehole could have different configurations according to the position inside the ground. Horizontal boreholes are less expensive from the point of view of the initial investment, because it is not needed deep drilling and perforation, but on the contrary its performances are much dependent from the temperature variability of the superficial ground. Vertical configuration instead, could reach more than 100meters depth and can fully benefit from the constancy of the subsoil temperature. On the other hand, drillings and perforations are expensive and, as the borehole penetrates aquifers and aquitards, they need to be sealed with grouting materials in order to prevent aquifers connections.

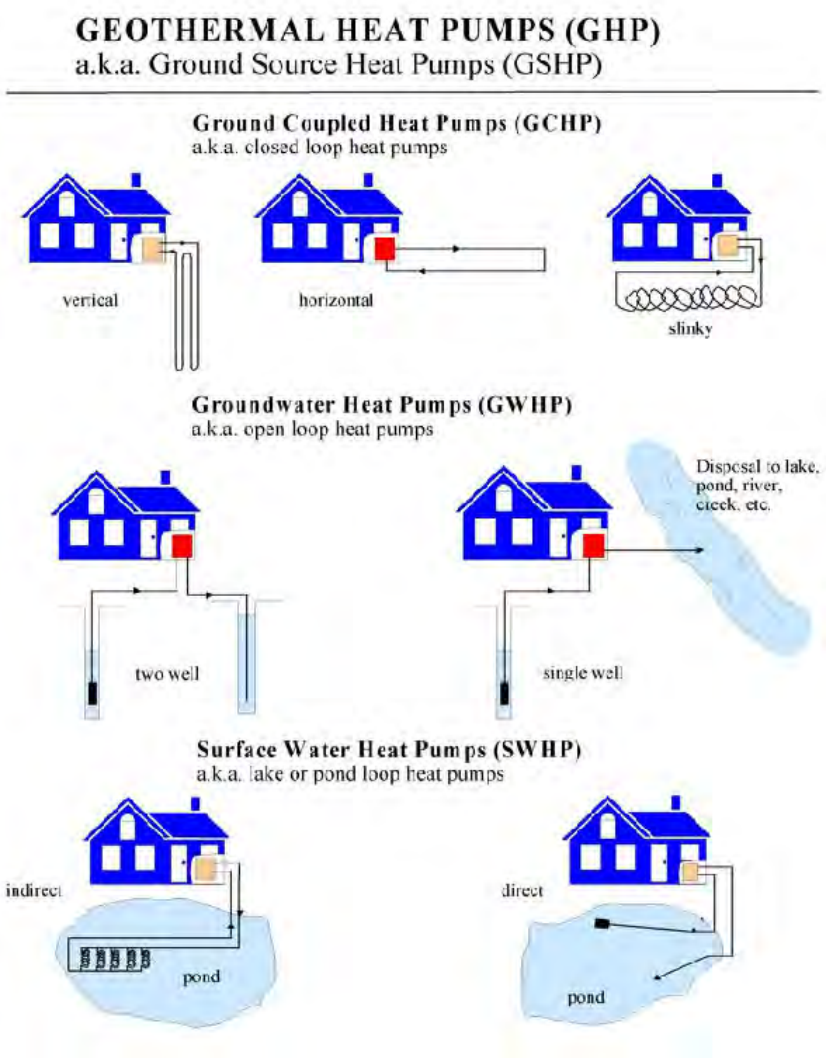

Figure 1.2.2: Ground Heat Pumps different configurations

Vertical closed loop BHE

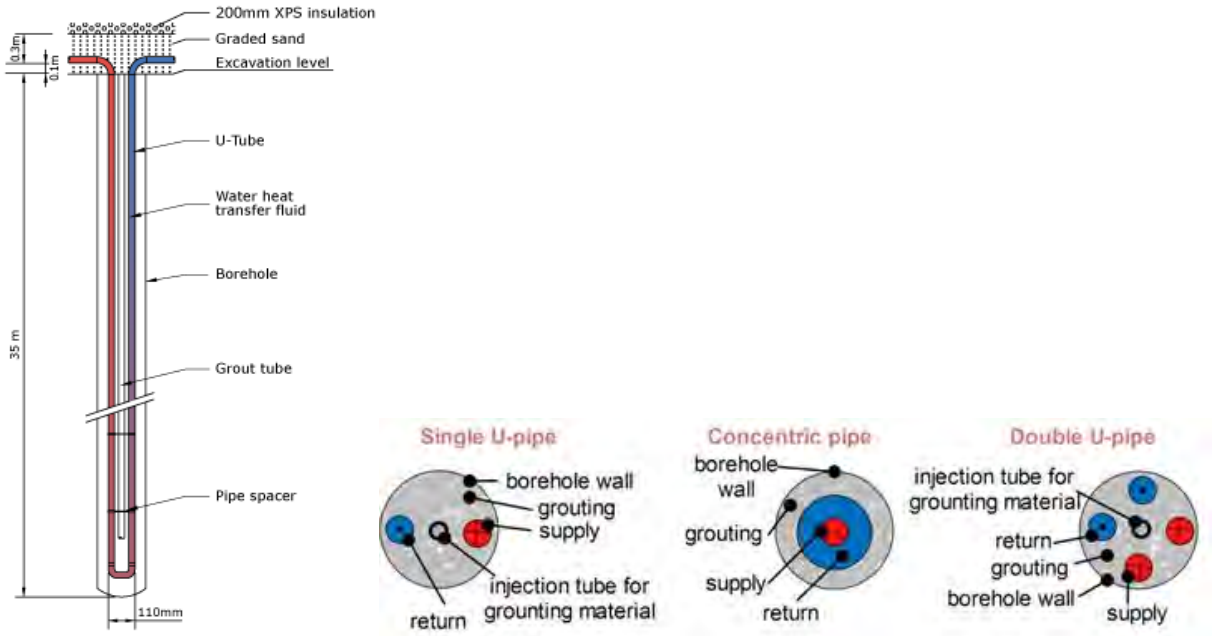

Figure 1.2.3: Vertical closed loop BHE configurations

This research focuses on the effects on the subsoils caused by vertical closed loop BHE. The geothermal heat captation system function is to capture the heat of the ground and to transfer it in the carrier fluid. It consists in vertical pipes filled inside the borehole grout (Figure 1.2.3).

The grout has a sealing function, preventing vertical connection between aquifers. It also has a structural function, protecting pipes from deformations or deterioration. Pipes are of few centimeters diameter (2-4 cm) and could be in plastic (PVC) or metallic material (usually copper). Pipes could have different configurations, as exposed in Figure 1.2.3 (concentric, single and double U) depending on the thermal condition, soil and carrier fluid type. Single-U configuration is the most common, because, if well designed, is the most reliable.

A new typology of GCHP is presented in Figure 1.2.4. It is called *energy pile*, and basically consists in systems in which the borehole heat exchanger is placed inside the buildings piles foundations. As the concrete piles are constructed, flexible plastic pipes are incorporated within the pile reinforcement cages. Upon completion of the foundation works, the sections of pipe-work embedded in the pile are plumbed into the heating /cooling system. The concrete forming the piles provides an ideal energy transfer medium, which allows the energy derived from the ground to be used in the heating and/or cooling of the structure. This technique permits to highly reduce the costs, since it makes not necessary anymore to do specific perforations, but on the contrary it inhibits the possibility to lower the fluid temperature below the 0°C in order to avoid the piles damage.

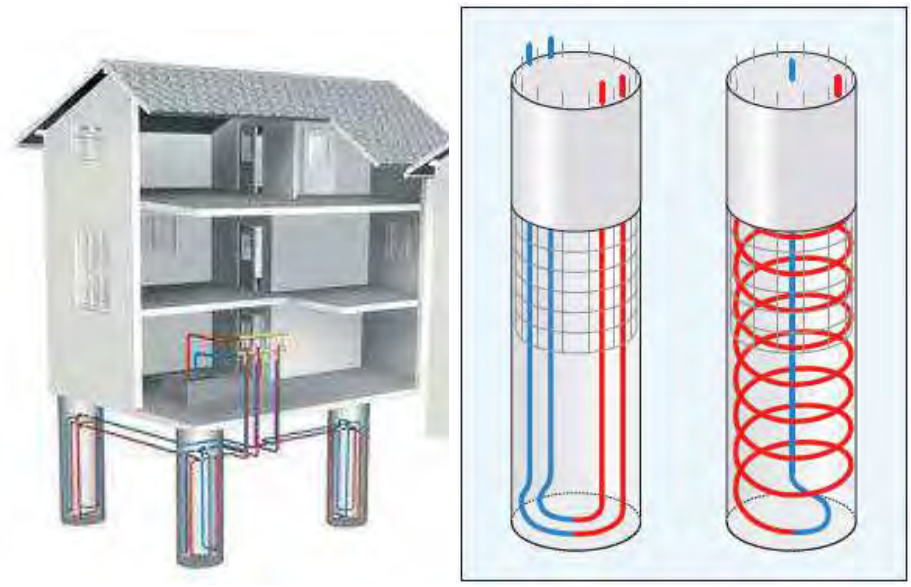

Figure 1.2.4: Energy piles

1.3 Borehole heat exchanger problems

1.3.1 Thermal drift

One of the most important problems to be addressed in the ground source heat pump design is the possible unbalancing of the heat load required from the building during the summer compared to the winter season. If the pump is mostly used in the winter season, extracting heat from the ground, without recharging the subsoil during the summer season, in the long term the soil temperature could be permanently lowered. This effect is called *ground thermal drift* [15].

In highly urbanized areas, where there are several BHE, concentrated and closely installed, the ground thermal drift could be highly amplified because of the interaction between the near boreholes. During the design of geothermal implants, it is necessary to take into account the thermal drift effect and its amplification due to the proximity to others heat boreholes [15].

Ground thermal drift is a situation to be certainly avoided because it could highly affect the whole geothermal plant. A lower soil temperature means a lower carrier fluid temperature, which means a lower heat pump and circulation pump performances, which again means higher energy consumption and higher operational costs. In the long run, the decreased soil temperature may become chronic, especially in highly exploited areas, turning the boreholes as inadequate and under-sized to the heat demand.

1.3.2 Under-sizing

Geothermal systems are very efficient systems and permit to reduce the costs for the buildings conditioning. Despite this, their installation requires an high initial investment, principally for the drilling operations voted to the BHE placing. In Italy, vertical BHE installation costs

are usually about 50 to 60 €/meters depth. A medium size heat pump, for residential usage, could cost about 4-5000€ and the necessary radiant panel are around 55 €/m^2. Adding others insulation measures, the costs for a small residential geothermal system could be up to 15-25'000 €[15].

An expedient to lower the initial costs is to add anti-freeze additives to the carrier fluid . It permits to reduce the borehole length, which means to under-size the implant, because it depresses the fluid freezing point below the 0°C, increasing the temperature operational range. In fact, using simply water as working fluid, it is important to not decrease the operation temperature below 1°-2°C, to avoid the fluid freezing and the pump blocking. In order to increase the ground thermal withdrawal, the fluid could be forced to drop even below -5°C.

The ideal anti-freeze additive should be a-toxic, not inflammable, not corrosive and with good thermal properties. Normally in Europe, as carrier fluid, is used a mixture of water and ethylene glycol ($C_2H_6O_2$) or propylene glycol ($C_3H_8O_2$) at 20% concentration [51]. Ethylene glycol and propylene glycol are almost inert and with low freezing point, but on the contrary they are toxic and with high environmental impact if accidentally dispersed. In USA are also used saline solutions (corrosives) or methanol (toxic and inflammable).

The equation 1.3.1 explains the relation of heat transfer between the ground and the carrier fluid in stationary conditions. This is the basic relation used in every method to size the borehole length. The term R indicates the thermal resistance of the ground and, conveniently modified, could include the non-stationarity of the process.

$$q = L \cdot \frac{T_g - T_f}{R} \tag{1.3.1}$$

Where:

q	is the thermal flux between the ground and the carrier fluid [W]
L	is the total length of the pipe [m]
T_g	is the temperature of the ground before the BHE installation [°K]
T_f	is the average temperature of the carrier fluid [°K]
R	is the thermal resistance of the ground [(m °K)/W]

Equation 1.3.1, even if simplified, basically shows the relationships between the parameters to take into account in BHE design.

Considering for example a BHE already installed (then of fixed length), to cover an increase in the heat demand (q) during a particularly cold winter, it is necessary to increase the ΔT between ground and fluid. Another situation in which it is necessary to decrease the operating temperature carrier fluid is when the ground parameters change (e.g. after several years due to the ground thermal drift or due to groundwater level variations). In this case, fixed the thermal flow (q) and pipes length (L), the decrease in the ground temperature (T_g) or the increase in the ground thermal resistance (R), requires the decrease in the fluid temperature (T_f). As already

said, the case of under-sized BHE (L) to lower the installation costs, also requires the decrease in the fluid temperature.

Anyway this habit, course permits to work with an grater temperature range and to reduce the initial costs, but in the long run it would be disadvantageous. First of all because more energy is needed to lower the carrier fluid temperature, increasing the operational costs, but also for the thermal stresses induced into the surrounding grout and subsoil. The ice formation outside the well could damage the sealing grout and also change the heat exchange conditions of the ground. Moreover the soil freezing could cause others problems that will be discussed in the following chapters.

Chapter 2

Hydro-geological setting of Venice area

The research investigate the Venetian subsoil. This chapter will describe and analyze the study area from the geographical, hydrological and geological point of view.

2.1 Geographical location and lagoon morphology

Figure 2.1.1: Geographical location of the study area.

From a geographical point of view, the study area is the coastal and lagoon urban area of Venice, situated in the Veneto region, north-east side of Italy (Figure 2.1.1). The area is located at the east border of the Po Valley, insisting in the Venetian lagoon, located in the northern Adriatic Sea (45°N, 12°E) (Figure2.1.2).

The area is highly anthropized and is strongly affected by the human activities insisting in.

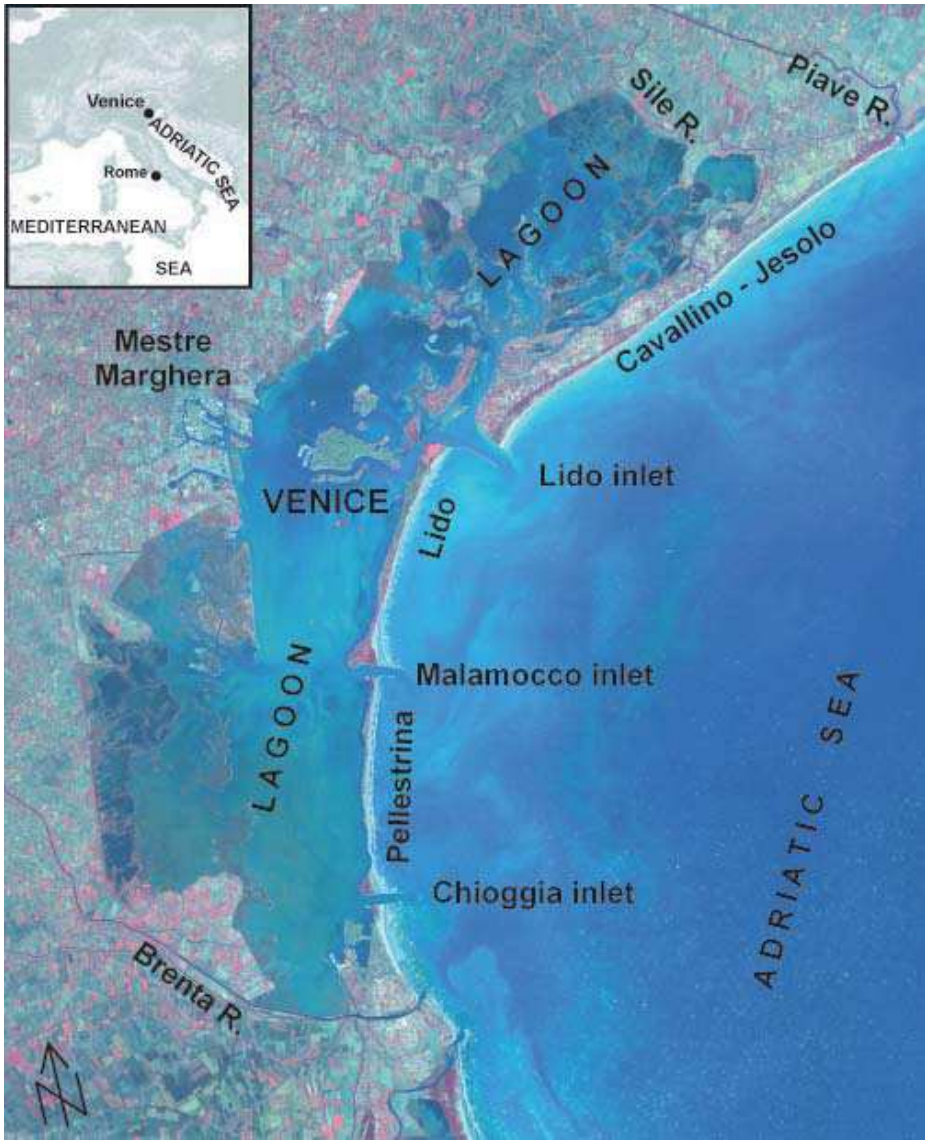

Figure 2.1.2: Venice lagoon aerial view[11].

The lagoon of Venice is the largest lagoon in Italy, and the most important survivor of the system of lagoons which in Roman times characterized the upper Adriatic coast from Ravenna to Trieste. Bounded by the Sile River to the North and the Brenta River to the South, the Venice Lagoon is oblong and arched in shape. It covers an area of about 550 km2, being 50 km long and 8–14 km wide. Its morphology consists of shallows, tidal flats, salt marshes, islands and a net of channels. The lagoon boundaries also include fish ponds, reclaimed areas and the coast that is presently interrupted by three inlets, namely Lido, Malamocco and Chioggia, which permit water exchange with the Adriatic Sea (Figure 2.1.2). The present setting of the Venice Lagoon is mainly the result of a number of human interventions [11].

2.2 Geological setting

The area of Venice is located in a complex foreland setting near the pinchout of both the Southalpine and the Apenninic wedges.

The most recent lithological sequence is characterized by Holocene lagoon and coastal deposits, *Caranto* and Pleistocene continental deposits (Figure 2.2.1). Holocene deposits are more recent and of marine origin, Pleistocene deposits instead are alluvial, caused by the divagation of Bacchiglione and Brenta river. Caranto is the most recent stratum of Pleistocene deposits so it marks the border between the two lithological formations [47] [11]. Caranto is an overconsolidated sandy-clay, very hard and compacted, gray-brown colored. Because of its hardness, it is easily recognizable during perforations so it considered the guide layer all over the lagoon area. As it is possible to see in Figures 2.2.1 and in the extract of the Geological Sys-

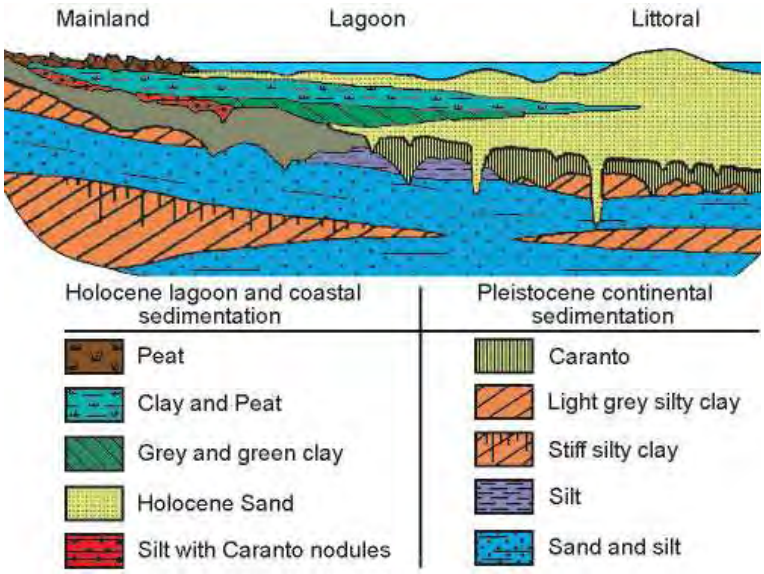

Figure 2.2.1: Holocene-Pleistocene stratigraphical sequence across the central Lagoon of Venice [47]

tems chart of Provincia di Venezia (Figure 2.2.2) Caranto is a discontinuous layer of about 1-2 m thickness, which has a oblique descendent trend from land to sea, with direction NW-SE. In particular, in the study area, city of Venice, Caranto is about 4 to 10 meters deep.

Figure 2.2.2: Deep map of the Caranto layer (table 2, Geological chart [40])

Figure 2.2.3 describes the shallow structure of the subsoil of the city of Venice. It is possible to notice the lithological sequences, consisting in clayey and sandy horizons, of the Holocene and Pleistocene deposits, divided by the Caranto layer. The figure also emphasizes (enlargement) the paleochannel structure which characterizes the city of Venice subsoil.

2.2.1 Stratigraphical context

From the point of view of the geothermal heat exchanger, we are interested in the first 150 meters depth.

The subsoil is characterized by an alternation of sandy and cohesive horizons because of its alluvial and marine origin. In Figure are presented extracts from the table 1 of the Hydrological system chart of the Provincia di Venezia. It is shown the clay subsoil with the sandy intercalations and paleoalves, where insists the confined aquifers and which are the preferential path of salt intrusion from the lagoon.

2.3 Hydrological setting

The hydrology of the area is characterized by the **groundwater aquifers system**, the **surface water system** (Brenta river, south, and Piave river, north) and the **lagoon.**

As regards the groundwater, the area has a complex system of aquifers confined inside the sandy horizons between cohesive layer (see Figure 2.2.4). Confined aquifers are recharged from

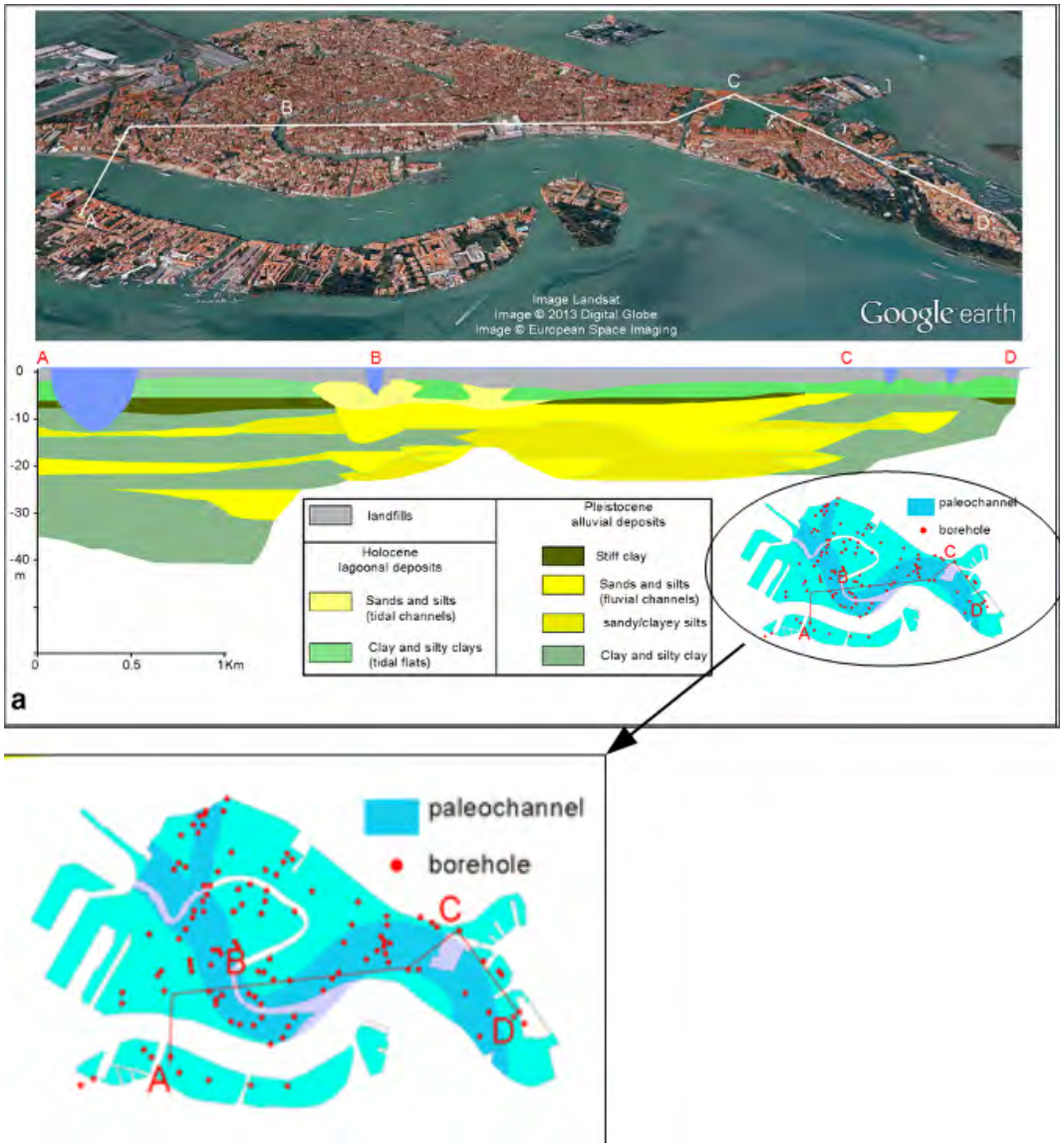

Figure 2.2.3: Architecture of the shallow subsoil of Venice along the alignment A–D[48]. Enlargement of paleochannel structure.

the Alpine foothill belt near Vicenza and have a NW-SE direction, to the sea. Freatic aquifer are recharged by rainfall events and connected with the streams and affected by lagoon tides.

Brenta river, Bacchiglione river and Piave river are the most important streams which affect the study area. Their divagations and floods contributed to create the alluvial plane in which the area insists. Others minor streams and channels are presented into the area: Sile, Dese, Naviglio-Brenta, Taglio-Nuovissimo flow directly into the lagoon. These streams continuously recharge the freatic aquifer, are source of fresh water for the lagoon and, at the same time a path way for the salt intrusion.

The Lagoon of Venice (Figure 2.1.2) is the largest lagoon in the Mediterranean. It extends for about 50 km along the coast and has an average width of 15 km. It covers an area of 550 km2 and has a micro-tidal regime: the Adriatic tides govern water exchange in the Lagoon and

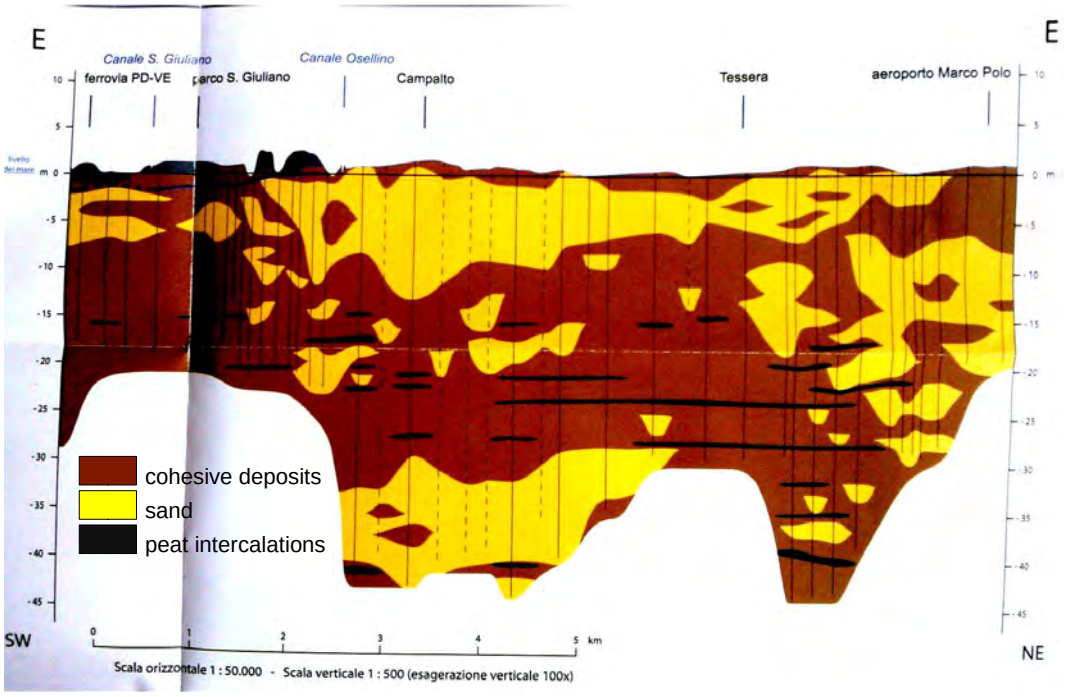

Figure 2.2.4: Stratigraphy of the coastal area of Venice (table 1, hydrological chart extract [40])

have a mean tidal excursion of 35 cm during neap tides and about 100 cm during spring tides. Particular atmospheric conditions such as strong southerly winds (*sirocco*) and low atmospheric pressure produce frequent storm surges which can increase the maximum water level producing extensive flooding of the historical city center of Venice. Only 5% of the Lagoon has a depth greater than 5 m, and 75% is less than 2 m deep; the average depth is 1.2 m. The Lagoon proper forms part of a tripartite ecosystem: catchment basin, lagoon and adjacent upper Adriatic. It is connected with the Adriatic Sea by three inlets (Lido, Malamocco, Chioggia), permitting water and sediment exchange driven by the tidal cycle. The average water volume is approximately 390×106 m3, and the amount of salt water that flows in and out during each tidal cycle amounts to around one-third of the total volume of the Lagoon. The Lagoon has a drainage basin of 1850 km2, which the main contributors are the rivers Silone (23.1%), Dese (21.1%), Naviglio-Brenta (14.3%) and Taglio-Nuovissimo (13.2%), the latter two being partially channelized. The most important tributaries are located in the northern basin which, on average, receives more than 50% of the annual total load. This hydrological pattern creates a typical brackish environment with a salinity gradient that ranges from 10 ‰ near the mainland border to 32‰ at the inlets [35].

2.3.1 Salt intrusion

The aim of the research is to investigate the interaction of the salinity with cohesive subsoil during the thermal stress induced by borehole heat exchanger. This is because in this area, but also in most of coastal areas, the salt intrusion in subsoil is a process to be take into account

because of its effects on the hydrology and soil geochemistry of the area.

As discussed before, the hydrology of the area is interested by presence of the lagoon which is connected with the firsts groundwater aquifers. The magnitude and the rise of saline contamination will depend on a complex balance between the lagoon water level and the amount of the fresh groundwater flux [35]. During high rainfall period, i.e. when piedmont recharge and streamflows are significant compared to the lagoon water level, then the salt intrusion is slightly extended. On the contrary, when the lagoon water level is particularly high (for example during high tides induced by Sirocco wind) the salt water could intrude the aquifers even for many kilometers from the coast. Salt intrusion mechanism could moreover be facilitated by paleoalves presented in the area, which directly connect aquifers with lagoon. The most permeable sediments in the paleochannels constitute the preferential pathway of the salt water rise (Figure 2.3.1)[37].

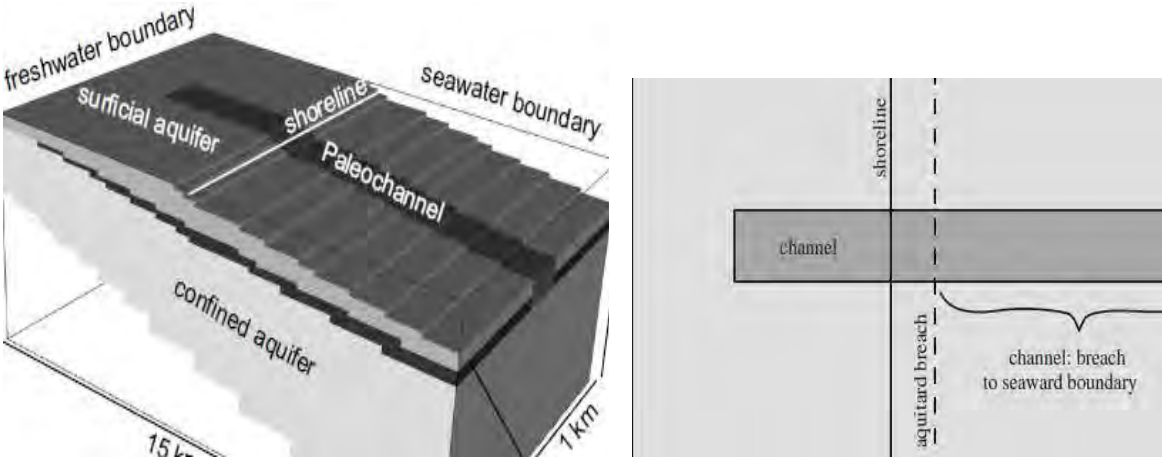

Figure 2.3.1: Paleochannels salt intrusion mechanism [37].

The dynamics of saltwater intrusion along a profile perpendicular to the Venice Lagoon margin has been studied by an electrical resistivity tomography time lapse experiment [18]. The accurate processing and interpretation of the entire data set allow to point out the evolution of the saltwater contamination process at different time and spatial scales, and to investigate the correlation between the salt fate with rainfall events, seasonal fluctuation of groundwater recharge, and tidal level variations. The monitoring results show that the salt contamination affects the shallow subsoil all over the measuring period [18].

The salt intrusion strongly affect the subsoil of the area, particularly of the city of Venice, which is surrounded by the lagoon, and the immediate coastal area.

In order to evaluate the magnitude of the salt intrusion, is also important to take into account the salt concentration in the intruding salt water. If the salinity value of the sea water is almost a constant value, the amount of the lagoon salinity is quite variable, not only in time but also in space. It depends on the balance between the fresh continental water and the salt marine water, which entry and exit the lagoon according with the meteorological conditions. Also the spatial location of the rivers outlets and marine inlets influence the salt concentration distribution along

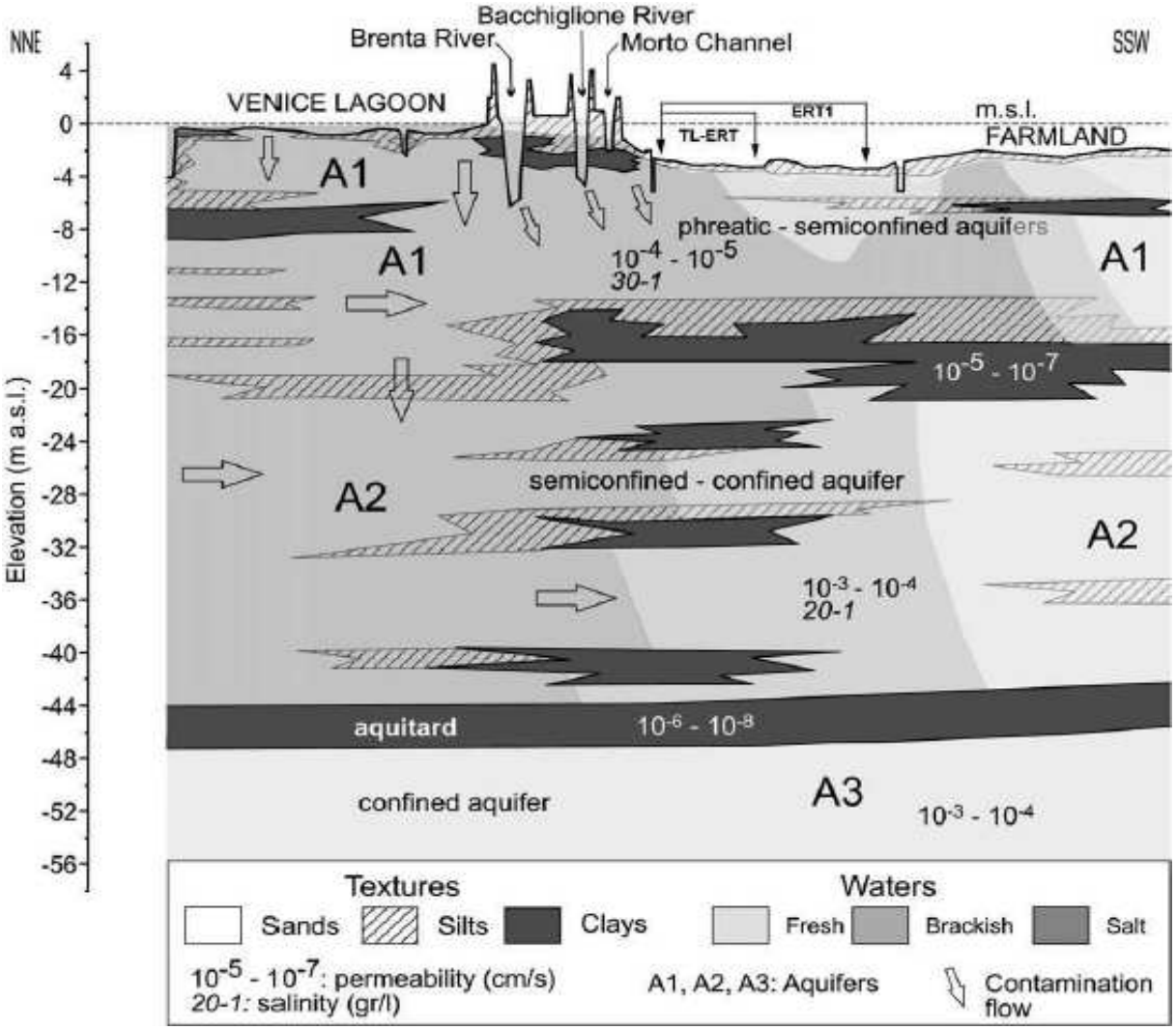

Figure 2.3.2: Sketch of the hydro-geological conceptual model of salt intrusion movements in the study area [18].

the lagoon. In order to give an idea of this, the Figure2.3.3 presents the results of an investigation done in 2003-2005 [23]. The salinity range, in the study area, is around the 3%.

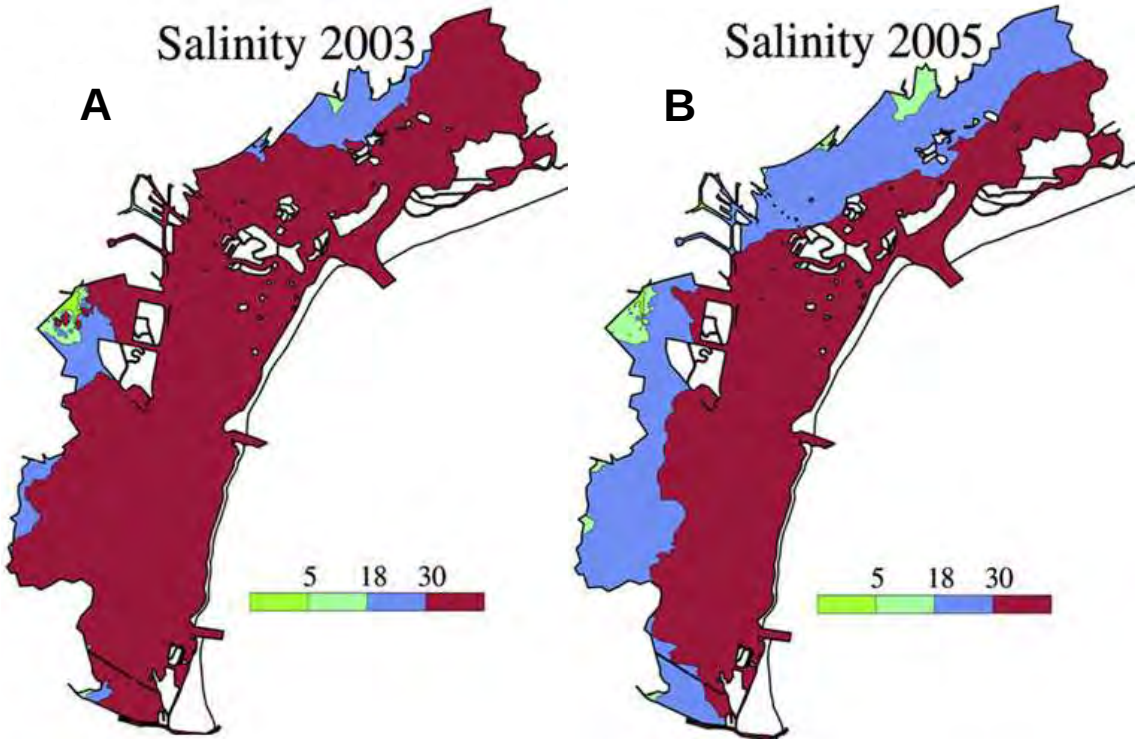

Figure 2.3.3: Salt concentration in lagoon water [23].

Chapter 3

Mechanical behavior of clay sediments

The research focuses on cohesive sediments, which are much more subjected to the thermal stress than coarse grained ones, because of their susceptibility to water content variations and presence of ions.

This chapter will deal with clay mechanical behaviors and changes produced by freeze-thaw processes. The mechanical behavior of clays subjected to thermal stress, especially freeze-thaw processes, have been studied mainly regards the *frost heaving*. Frost heaving is an upwards swelling of soil during freezing conditions caused by the formation of big ice lenses which grow towards the soil surface, upwards from the depth in the soil where freezing temperatures have penetrated. Differential frost heaving can damage buildings foundations and crack pavements. It is a serious problem in regions where prolonged freezing conditions can occur.

As seen in the previous chapter, the study area is subject to saline intrusion, then will evaluate in which way the presence of ions can affected these processes.

3.1 Clayey sediments

3.1.1 Composition and structure

Clay minerals are complex silicates of aluminum, magnesium, and iron. Two basic crystalline units form the clay minerals: (1) a silicon - oxygen tetrahedron, and (2) an aluminum or magnesium octahedron. A silicon - oxygen tetrahedron unit, shown in Figure 3.1.1 (a), consists of four oxygen atoms surrounding a silicon atom. The tetrahedron units combine to form a silica sheet as shown in Figure 3.1.2 (a). Note that the three oxygen atoms located at the base of each tetrahedron are shared by neighboring tetrahedral. Each silicon atom with a positive valance of 4 is linked to four oxygen atoms with a total negative valance of 8. However, each oxygen atom at t he base of the tetrahedron is liked to two silicon atoms. This leaves one negative valance charge of the top oxygen atom of each tetrahedron to be counterbalanced. Figure 3.1.1 (b) shows an octahedral unit consisting of six hydroxyl units surrounding aluminum, or a magnesium, atom. The combination of the aluminum octahedral units forms a gibbsite sheet (Figure 3.1.2 (b). If

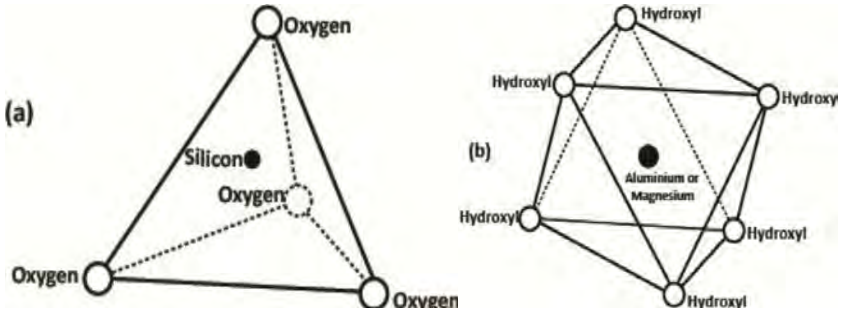

Figure 3.1.1: (a) Silicon-oxygen tetrahedral unit. (b) Aluminum or magnesium octahedral unit[31]

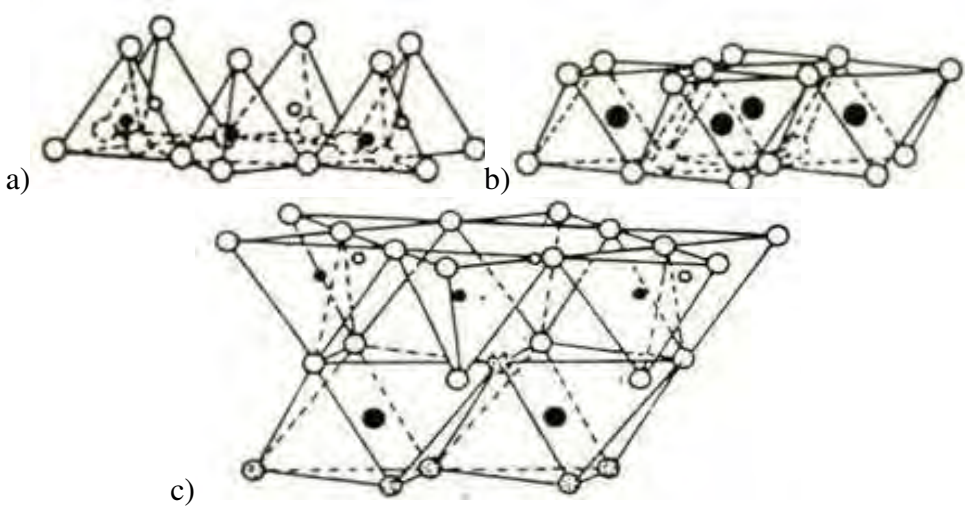

Figure 3.1.2: (a) Silica sheet. (b) Gibbsite sheet. (c) Silica-gibbsite sheet [31]

the main metallic atoms in the octahedral units are magnesium , these sheets are referred to as brucite sheets . When the silica sheets are stack ed over the octahedral sheets, the oxygen atom replaces the hydroxyls to satisfy their valance bonds.

Clay minerals with two-layer sheets. Some clay minerals consist of repeating layers of two - layer sheets. A two - layer sheet is a combination of a silica sheet with a gibbsite sheet, or a combination of a silica sheet with a brucite sheet. The sheets are about 7.2 Å thick. The repeating layers are held together by hydrogen bonding and secondary valence forces.

Kaolinite is the most important clay mineral belonging to this type (Figure 3.1.3). Other common clay mineral that fall into this category are *serpentine* and *halloysite*.

The most common **clay mineral with three-layer sheets** are *illite* and *montromorillonite* (Figure 3.1.4). A three-layer sheet consists of an octahedral sheet in the middle with one silica sheet at the top and one at the bottom. Repeated layers of these sheets form the clay minerals. Illite layers are bonded together by potassium ions. The negative charge to balance the potassium ions comes from the substitution of aluminum for some silicon in the tetrahedral sheets. Substitution of this type by one element for another without changing the crystalline form is know as *isomorphous substitution* . Montmorillonite has a similar structure to illite. However,

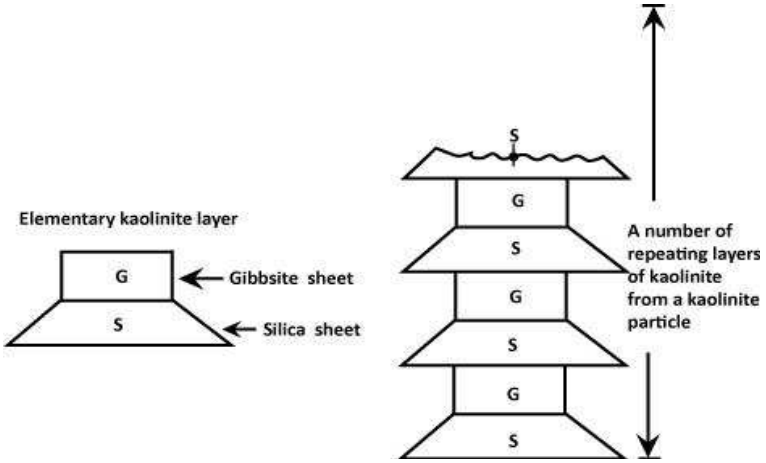

Figure 3.1.3: Kaolinite structure [31]

unlike illite there are no potassium ions present, and a large amount of water is attracted into the space between the three-sheet layers.

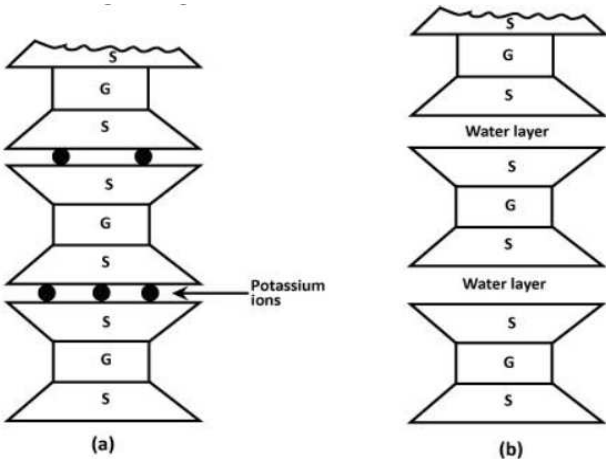

Figure 3.1.4: Structures of (a) illite and (b) montmorillonite [31]

The surface area of clay particles per unit mass is generally referred to as *specific surface*. The lateral dimensions of kaolinit platelets are about 1'000 to 20'000 Å with thicknesses of 100 to 1000 Å. Illite particles have lateral dimensions of 1000 to 5000 Å and thickness of 50 to 500 Å. Similarly, montmorillonite particles have lateral dimensions of 1000 to 5000 Å with thickness of 10 to 50 Å. If we consider several clay samples all having the same mass, the highest surface area will be in the sample in which the particle sizes are the smallest. So it is easy to realize that the specific surface of kaolinit will be small compared to that of montmorillonite. The specific surfaces of kaolinite, illite, and montmorillonite are about 15, 90, and 800 m2/g, respectively.

3.1.2 Diffuse double layer

Some salt precipitates (cations in excess of the exchangeable ions and their associated anions) are also present on the surface of dry clay particles. When water is added to clay, these cations and anions float around the clay particles (Figure 3.1.5). At this point, it must be pointed out that

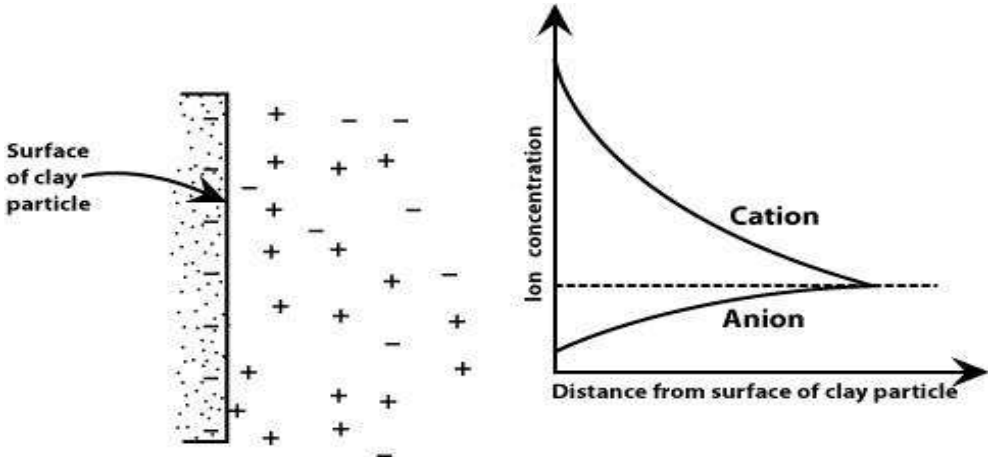

Figure 3.1.5: Diffuse double layer [31]

water molecules are dipolar, since the hydrogen atoms are not symmetrically arrange around the oxygen atoms (Figure 3.1.6a). This means that a molecule of water is like a rod with positive

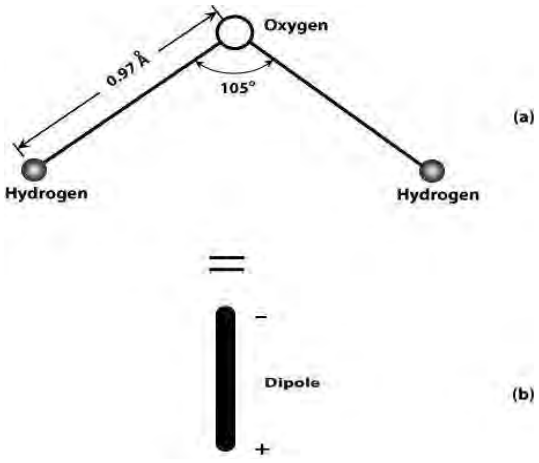

Figure 3.1.6: Dipolar nature of water [31]

and negative charges at opposite ends (Figure 3.1.6b). There are three general mechanisms by which these dipolar water molecules, or *dipoles*, can be electrically attracted toward the surface of the clay particles (Figure 3.1.7).

- a. Attraction between the negatively charged faces of clay particles and the positive ends of dipoles.
- b. Attraction between cations in the double layer and the negatively charged ends of dipoles. The cations are in turn attracted by the negatively charged faces of clay particles

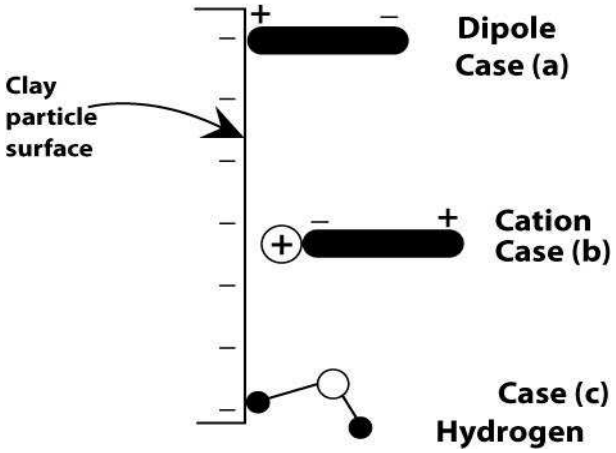

Figure 3.1.7: Dipolar water molecules in diffuse double layer [31]

- c. Sharing of the hydrogen atoms in the water molecules by hydrogen bonding between the oxygen atoms in the clay particles and the oxygen atoms in the water molecules.

3.1.3 Flocculation and dispersion

In addition to the repulsive force between the clay particles there is an attractive force, which is largely attributed to the Van de Waal's force. This is a secondary bonding force that acts between all adjacent pieces of mater. The force between two flat parallel surfaces varies inversely as $1/x^3$ to $1/x^4$, where x is the distance between the two surfaces. Van der Waal's force is also dependent on the dielectric constant of the medium separating the surfaces. However, if water is the separating medium, substantial changes in the magnitude of the force will not occur with minor changes in the constitution of water.

The behavior of clay particles in a suspension can be qualitatively visualized from our understanding of the attractive and repulsive forces between the particles and with the aid of Figure 3.1.8. Consider a dilute suspension of clay particles in water. These colloidal clay particles will undergo Brownian movement and, during this random movement, will come close to each other at distance within the range of inter-particle forces. The forces of attraction and repulsion between the clay particles vary at different rates with respect to the distance of separation. The force of repulsion decreases exponentially with distance, whereas the force of attraction decreases as the inverse third or fourth power of distance, as shown in Figure 3.1.8. Depending on the distance of separation, if the magnitude of the repulsive force is greater than the magnitude of the attractive force, the net result will be repulsion. The clay particles will settle individually and form a dense layer at the bottom; however, they will remain separate from their neighbors (Figure 3.1.9a). This is referred to as the *dispersed* state of the soil. On the other hand, if the net force between the particles is attraction, flocs will be formed and these flocs will settle to the bottom. This is called *flocculated* clay (Figure 3.1.9b).

As we discussed in diffuse double layer theory, the presence of salt hydrates the clay parti-

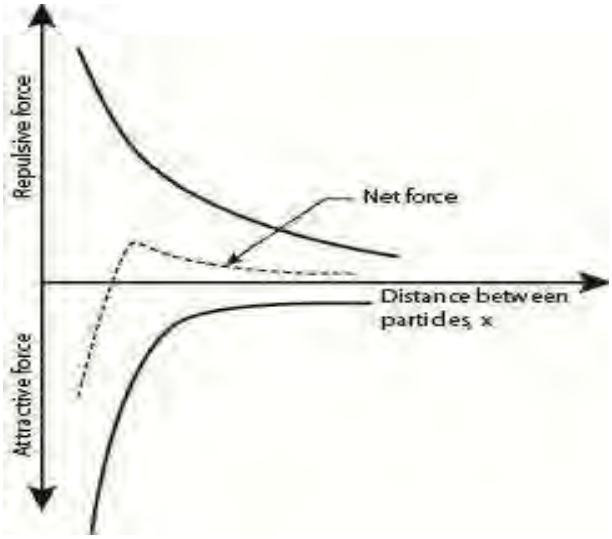

Figure 3.1.8: Attractive and repulsive forces involved in dispersion and flocculation of clay in a suspension [31]

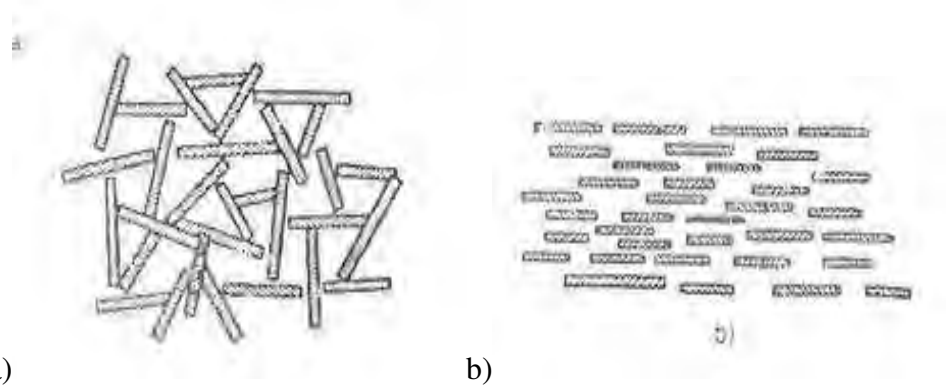

a) b)

Figure 3.1.9: (a) Flocculation and (b) dispersion of clay

cles creating an *adsorbed water layer*, AWL. The thickness of the AWL depends on the type of cations and, influencing the distance between particles, affects the clay structure:

- big monovalent cations such as **Na+** and **K+** weakly bound with clay particle permitting an high hydration. The result is a **thick AWL** and a **dispersed** state.
- bivalent cations, **Ca++** and **Mg++**, strongly bound with particles, do not allowing the bounding of much water. **Thin AWL** and **flocculated** state.

Sumner and Naidu [45] divided cations in good and poor flocculators (Table 3.1).

Depending on the structure of the particles (flocculated or dispersed), the soil matter have different behaviors (Table 3.2). Because of its house of cards structure, the flocculated state gives to the soil an high strength, low compressibility and high permeability, allowing water to pass through the pores between the particles. On the contrary, the dispersed state behaves as an impermeable layer and, as the AWL of the clay particles is thick, the soil counts with high compressibility but little strength resistance.

Ion	Relative Flocculating Power
Sodium Na^{+}	1.0
Potassium K^{+}	1.7
Magnesium Mg^{++}	27
Calcium Ca^{++}	43

Table 3.1: Relative flocculating power [45].

Clay particles state	Flocculated	Dispersed
Cations	Ca^{2+}, Mg^{2+}	none or Na^{+}, K^{+}
Compressibility	low	high
Swell potential	low	high
Strength	high	low
Hydraulic conductivity	high	low

Table 3.2: Behavior of flocculated and dispersed clay particles

We saw the effect of salt concentration on the repulsive potential of clay particles. Even with poor flocculator as $Na^{+}$and K^{+}, high salt concentration (EC[1] > 4 *Siemens/m*) will depress the double layer of clay particles and hence the force of repulsion. We noted earlier in this section that the Van der Waal's force largely contributes to the force of attraction between clay particles in suspension. If the clay particles are suspended in water with a high salt concentration, the flocs of the clay particles formed by dominant attractive forces will give them mostly an orientation approaching parallelism (face-to-face type). This is called *salt-type flocculation* (Figure 3.1.10) [31].

Figure 3.1.10: salt-type flocculation [31]

[1]Electrical conductivity (section 4.3)

3.2 Freeze-thaw processes

Soil freeze-thaw processes are an important topic in cold regions engineering. The frost heave and the consequential thaw settlement have a strong impact on the stability of constructions such as embankment, buildings, pipelines, roads etc.. Freeze–thaw is a weathering process which considerably changes the engineering properties of soils. Therefore, the influence of freeze–thaw must be taken into account for modeling of stress–strain behaviors in stability and deformation analysis for slopes, embankments and cuts in cold regions with soil layers experiencing freeze–thaw cycling [43, 1].

Another engineering field of study of these processes is the *ground freezing* technique in geotechnic. Ground freezing is a construction technique used in circumstances where soil needs to be stabilized so it won't collapse next to excavations, or to prevent contaminates spilled into soil from being leached away.

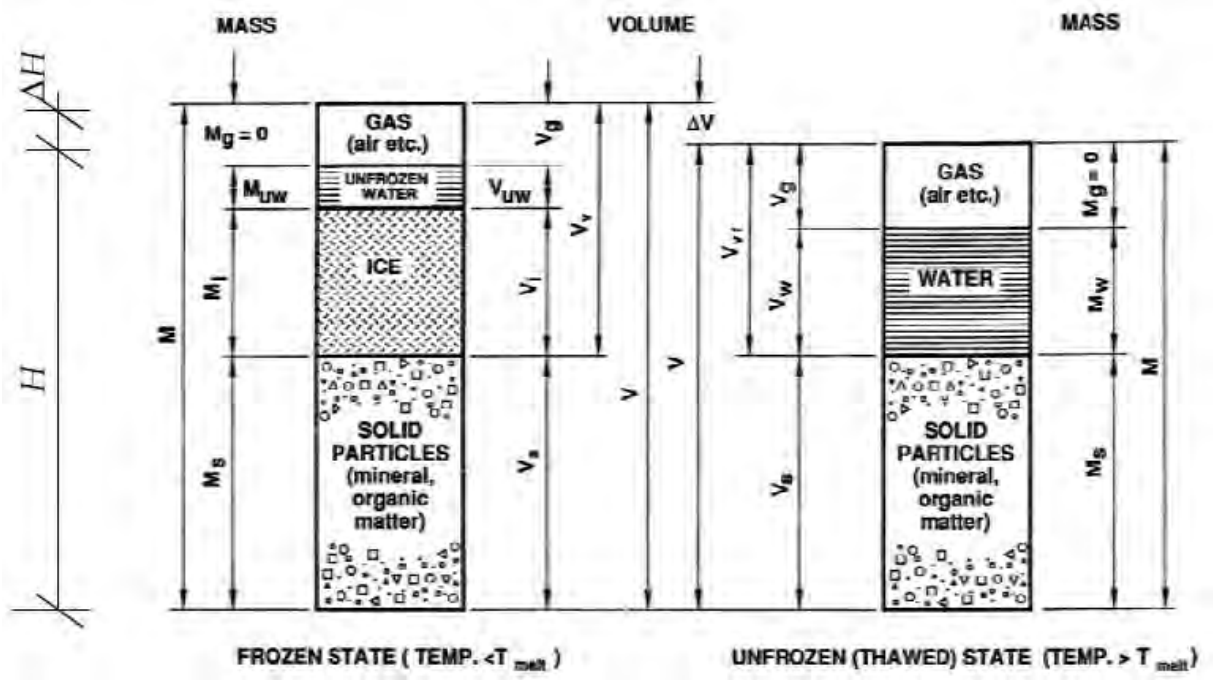

Figure 3.2.1: Phases of a frozen and thawed soil [3]

Frozen soil is a system of four different phases: soil particles, ice, water and air (Figure 3.2.1). Mechanical properties depends on the amount of each phase. In fact, in frozen soil, the strongest bonds are ice-cement ones which are responsible of the soil strength [4, 34].

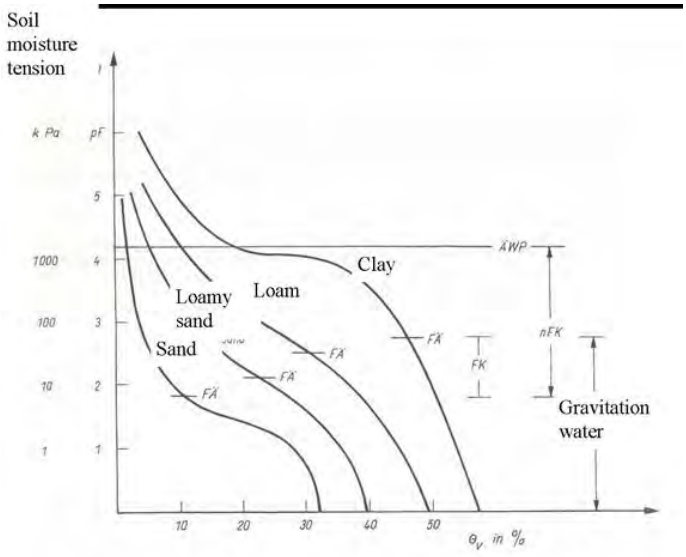

Figure 3.2.2: Different texture soils water absorption tension

The amount of the water phase is different for each soils texture because it depends on the specific area of the soil particles. Smaller particles, with an higher specific area, could retain more water (Figure 3.2.2). This is the same of the capillary effect and its called *matric potential*. Fine-grained soils in saturated conditions have a significantly higher water content compared to coarse-grained ones and for this reason are more susceptible to freezing-thawing [34]. Consequence of these attraction forces which bond water to soil particles is the **Gibbs-Thompson effect**: water in soils, especially in clayey ones, does not freeze at zero degrees but at a lower temperature depending on how much strong it is bonded [34, 3, 29].

3.2.1 Physical mechanism and effects

From a microscopical point of view the freezing mechanism is shown in Figure 3.2.3. During freezing, ice lenses start grow from free water among the soil pores. Then, as the temperature decreases, the weakly bonded water is attracted to the ice. As the temperature continues to fall then more bonded water is “ripped” from the particles to enlarge the ice lenses until an equilibrium is reached. For a given soil the amount of the frozen water depend on the temperature reached. A percentage of unfrozen water will always remain because strongly bonded to the clay particles [27, 41]. Ice formation has a “dewatering” effect on the soil, similar as when you dry the soil resulting in a water suction to the freezing front. Water is attracted to the freezing front due to a water content gradient [34, **?**].

From a macroscopical point of view, when this process occurs in cold regions, due to the climatic conditions, freezing proceeds downwards from ground level and the freezing front is parallel to the ground (Figure). The water is sucked from the aquifer to the freezing front, forming large ice lenses in the sub soil which continue to expand causing the dangerous phenomenon of frost heave. In fact, the frost heave cause a soil swelling much more than the normal

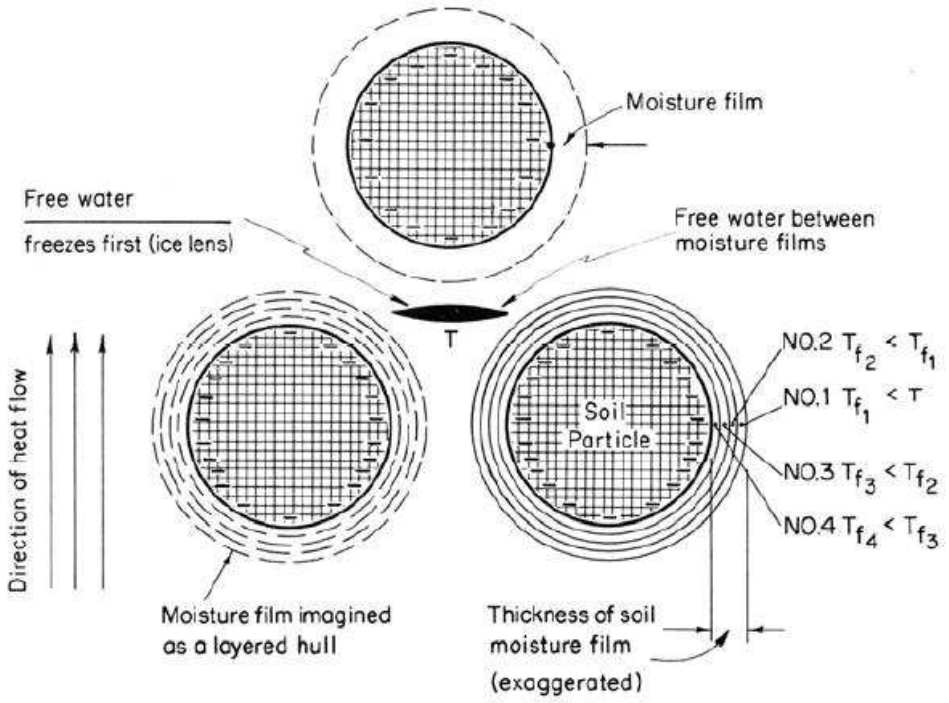

Figure 3.2.3: Freezing of free and bonded water in soil [41]

expansion of the water content precisely because of the water suction from the aquifers [34, 4].

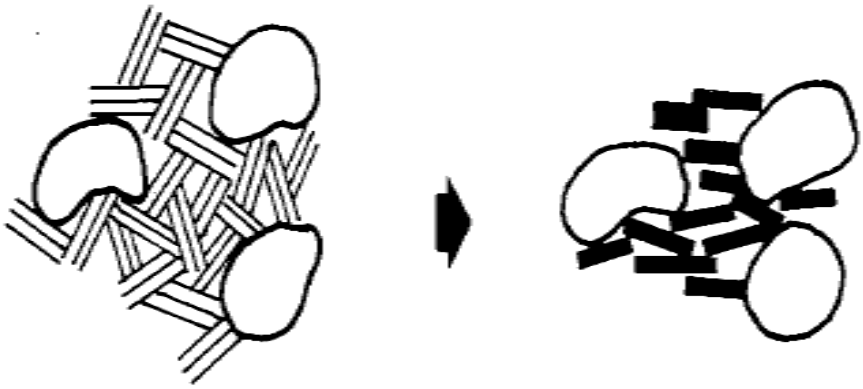

Figure 3.2.4: Particles aggregates and macro-pores formation [12]

Water freezing increases its volume of about the 9%. When water expands among the soil particles, ice lenses start craking the soil structures enlarging the pores, causing a consolidation pressure which packs the soil particles into aggregates (Figure3.2.4)[12]. When temperature arises and ice melts, the result is an increasing of the hydraulic permeability because of the soil macro-pores and cracks induced by the freezing. If we consider the natural condition of a the subsoil, the soil particles are subjected to the site pressure. If thawing occurs under site pressure conditions, macro-pores collapse and water is expulsed resulting in an over-consolidation which not occurs in soils which do not experience the freeze-thaw process [12][17].

Tests on soil compressibility in either field or laboratory conditions were conducted by Goldstein [24], Zhukov [53] and Chamberlain [12]. Based on result of these tests, compressibility curves were constructed, consisting of three characteristic regions. In the first region the change in the coefficient of relative deformation occurred mainly due to the melting of ice inclusions and reduction of macro pores, which results in destruction of soil structure. In the second region, the variation of the porosity was due to the further destruction of the frozen soil with complete disappearance of macro pores and deformation of destroyed the soil structure under constant stress. In the third region with the increasing stress the consolidation of the mineral particles leads to the soil compression (Figure 3.2.5) [17].

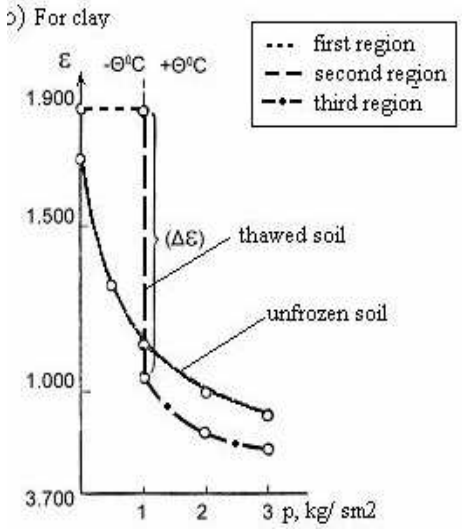

Figure 3.2.5: Compressibility curve of frozen and unfrozen clayey soil [53].

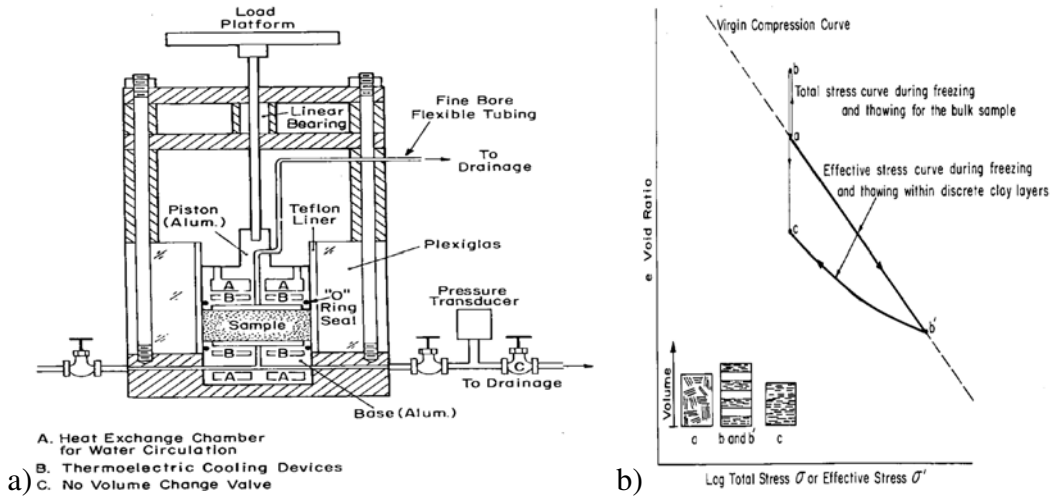

Figure 3.2.6: Chamberlain test apparatus (a) and thaw consolidation curve (b) [12].

Chamberlain studied freeze-thaw processes. His test apparatus (Figure 3.2.6) consists of a tephlon-lined plexiglass cylinder, with a 63,5 mm inside diameter and 152,4 mm outside diameter. The fixed base and movable piston contain stainless steel porous plates with provisions

for drainage and flushing. The piston is sealed by mean of a rubber "O" ring lubricated with light machine oil. the drainage line from the base leads to a calibrated burrett and pore pressure transducer, while the line from the piston leads to a constant head device. A screw pump and a system of valving permit falling head permeability tests to be conducted. Both the base and the piston contain thermoelectric cooling devices for controlling unidirectional freezing. A constant temperature circulating bath provides for long-term stable heat removal. The load was applied in increments. The sample was frozen from the bottom and upon completation of freezing the sample was allowed to thaw uncontrolled at approximately 22°C. In Figure 3.2.6b are presented the consolidation curve which describe the physical process involved in terms of effective stress ($\bar{p} = p - u$). A clay soil is fully consolidated ($u = 0$) to point a on the virgin compression curve where the effective stress is equal to the applied stress. The sample is then frozen unidirectionally with free access to water, and in terms of total stress undergoes a net increase in void ratio to point b due to ice expansion and the intake of water from the reservoir. However, during freezing the large negative pore water pressures that develop cause an increase in effective stress immediately below the freezing front. Discrete bands of clay and ice form as the freezing front propagates, the clay bands being over-consolidated to point *b'*. Upon thawing, the effective stress path within the discrete bands of clay is depicted along line *b'-c* to point c where the pore pressures are in equilibrium with the applied load, and the material has undergone a net decrease in void ratio from point a to point c [12].

Chamberlain's researches shown that freeze-thaw produces an increasing in vertical hydraulic conductivity even if the void ratio decreases. It's because the cracks and macropores produced by the freezing process work as preferential path way of the water flow. Results sug-

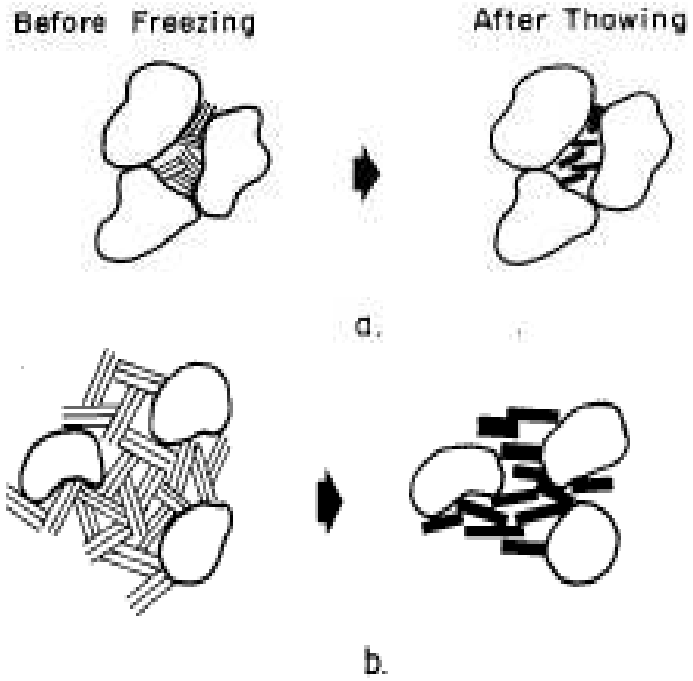

Figure 3.2.7: Schematic consolidation process for (a) clayey silt and (b) silty clay [12]

gest that also the particles grain size play a role in the process (Figures 3.2.7a and 3.2.7b). In the first case (a) the coarser grains control the packing and the clay particles are free to move in the voids. The result is a less consolidation, due to the coarser grain structure, but an increasing in permeability (horizontal and vertical), because of the clay particles compaction in voids. On the contrary, when the sand or silt grains are not in contact (Figure 3.2.7), but floating in a clay matrix, compressibility and permeability are both controlled by the arrangement of clay particles. Void ratio is reduced because of the collapse and rearrangement of the clay packets and permeability increases along the shrinkage cracks that form during freezing [12].

Schematic overview of the freeze-thaw process of a clayey soil under natural conditions:

1. Temperature decreases until reaching the freezing temperature (below 0°C). Ice lenses start growing from the free water among soil particles.

2. Temperature continues to decrease ripping the bounded water to the particles. Water suction from warmer regions to the freezing front. The ice crystals continue to expand cracking the soil original structures, forming macro-pores and consolidating soil particles into packets.

3. When temperature arises, ice melts removing its structural bonds. Macropores collapse and most of the water is expulsed

The result is an **irreversible consolidation** and an **increasing in hydraulic conductivity** compared to a soil which never experience the freezing process.

3.2.2 Cyclical freezing and thawing

In the previous section was discussed the freezing and thawing mechanism, but what happens when the process is cyclical? In fact, the soil freezing induced by borehole heat exchanger is a seasonal process because, in this situation, the soil only freeze in extreme climatic condition, i.e. when the pump requires more heat than that for which it was designed. Also in cold regions the soil is subjected to cyclical freezing and thawing, depending on the climatic conditions.

Chamberlain and Gow [12] and Eingenbrod [22] found that freeze-thaw leads to densification of soft, normally-consolidated clay samples, but other studies showed the opposite to occur for dense samples. Considering these results, Viklander [52] proposed a *residual void ratio* e^{res} for freeze-thaw, which means that both loose and dense soils may attain the same void ratio after a number of freeze-thaw cycles (Figure 3.2.8). Figure 3.2.8 shows an exponential trend of the void ratio to the residual value, both for loose and dense soils. It suggest that the firsts freeze-thaw cycles are the most efficient and the lasts do not have significant influence on the soil rearrangement. In fact, other tests (Boynton and Daniel [10], Othman and Benson [38] and Viklander [52]) showed that neither the permeability nor the soil volume changes significantly after three to five freeze-thaw cycles and that the first cycle has the greatest influence (Figure 3.2.9).

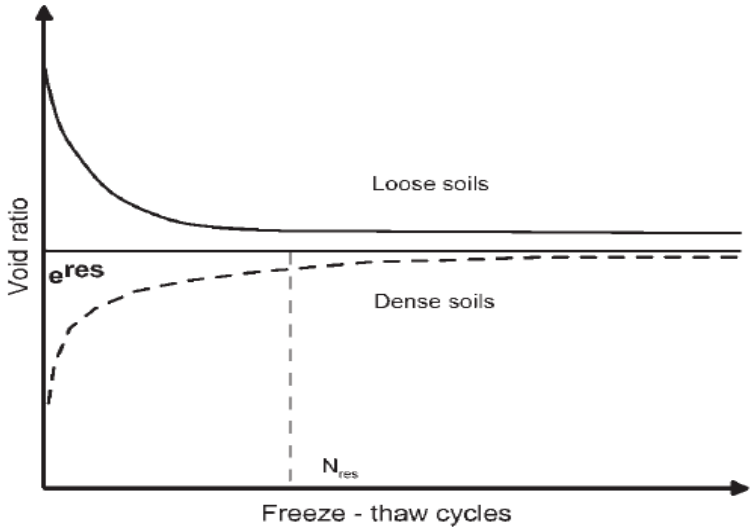

Figure 3.2.8: Residual void ratio in terms of freeze-thaw cycles [52]

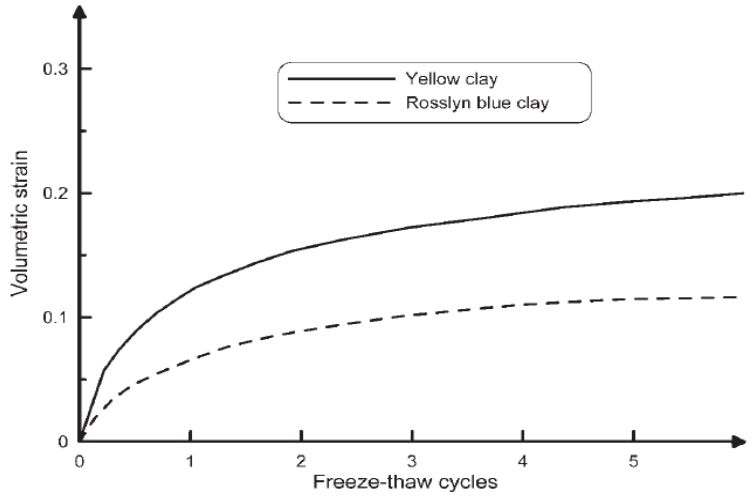

Figure 3.2.9: Relationship between volumetric strain and number of freeze-thaw cycles[22]

Freeze-thaw cycles seems to have effects also on the mechanical properties of the sediments. For example Graham and Au [25] tested high-quality natural clay samples to develop oedometer consolidation curves (Figure 3.2.10). They observed that the effect of bonding was lost after five freeze-thaw cycles (dashed line in Figure 3.2.10). It is not clear to what extent freeze-thaw destroyed the effect of over-consolidation as there may have been a reduction in the preconsolidation pressure. The consolidation line appears to approach that of the normally consolidated reconstituted sample, but as yet this has not been confirmed [43].

Bing and He [8] emphasized the destructive effect of the freeze-thaw cycles on soil structure, concerning its mechanical characteristics. Figure 3.2.11 shows the stress–strain curves for the saline loess after various freeze–thaw cycles with a salt content and water content of 2 and 15%, respectively. When the sample has not experienced cyclical freezing and thawing (the number of freeze–thaw cycles C equals zero), the curve reveals an apparent brittle failure mode. The

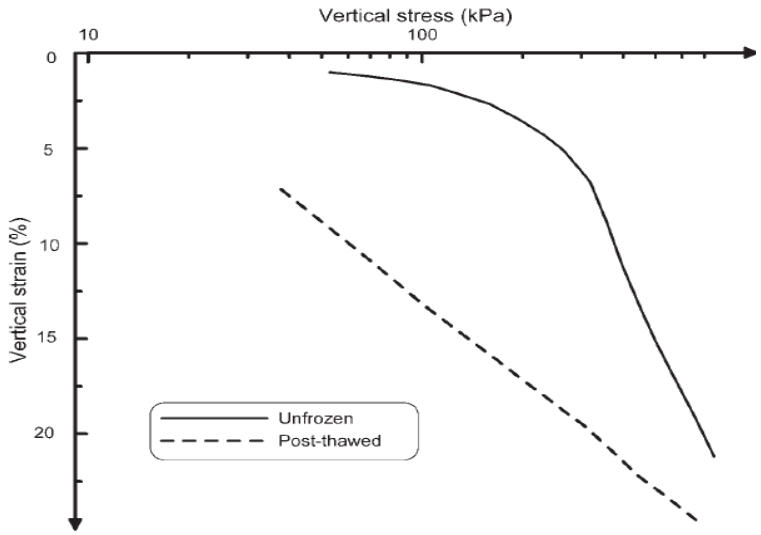

Figure 3.2.10: Oedometer consolidation curves for a clay in unfrozen and post-thawed states [25]

curves with the cyclical freezing and thawing are approximately similar and do not exhibit the yield stage. It is because the samples itself have a stress rearrangement when cyclical freezing and thawing experienced [8]. With increasing numbers of freeze–thaw cycles, the initial portion of the curve is shorter; in other words, the initial moduli of the samples decrease. And it reaches the peak stress with the descent of the ultimate strain point to a lesser failure strain. As the strain progresses, the samples are likely to reach ultimate stress until they reach a weaker plastic failure. Also, the failure stress and the failure strain decrease with the increase in number of freeze–thaw cycles [8]. Also this experiment (Figure 3.2.11) suggests that the firsts cycles are the most effective on the soil rearrangement. In fact after one cycles the soil has no more the yield stage.

Concluding, freezing and thawing seems to have a destroying effect on the soil structures because of the ice expansion which breaks the bonds. It is reflected in a decreasing of the mechanical properties. If the freezing and thawing were cyclical, the rearrangement is completed after 6-7 cycles, even if the firsts cycles are the most effective, until a new equilibrium status is reached with different physical and mechanical features.

3.3 Salt effect

The presence of solutes in the pore solution could strongly influence soil physical properties during freezing and thawing in two important ways: **freezing point depression** and **unfrozen water content**. These properties affect such basic soil parameters as thermal and hydraulic conductivity, effective specific heat, soil strength and stability.

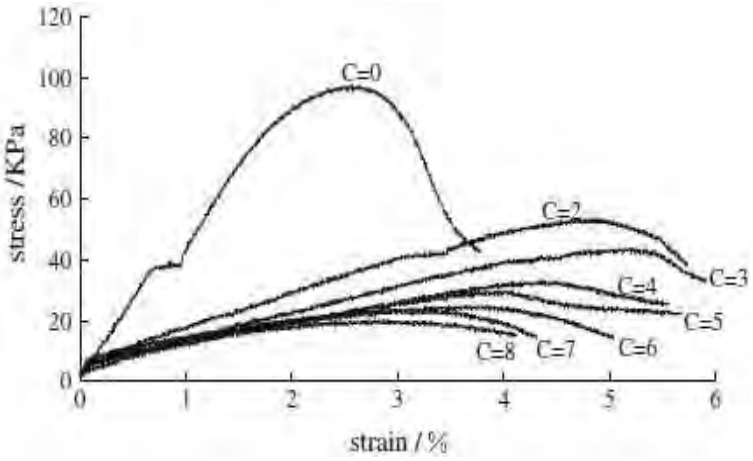

Figure 3.2.11: Stress–strain curves for the loess after cyclical freezing and thawing at S = 2%, W = 15% (C is the F-T number of cycles) [8]

3.3.1 Salt in the liquid phase

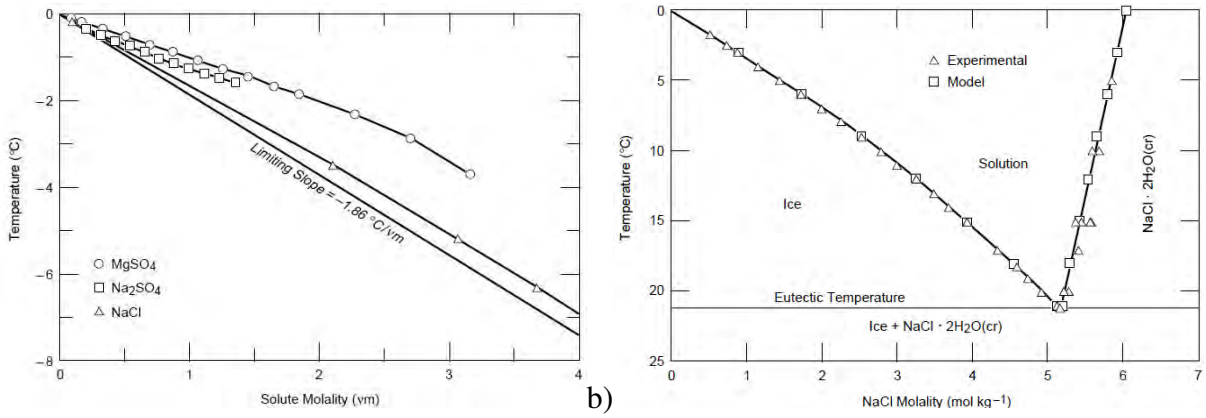

a) b)

Figure 3.3.1: (a) Freezing-point depression for three salt solutions. (b) Stability diagram for the NaCl–H_2O system at subzero temperatures [34]

Solutes lower the freezing point of water. The freezing-point depression in dilute solutions is given by the Van't Hoff equation:

$$\frac{dT}{dm_b} \approx -RT^2/(55{,}5 \cdot \triangle H)$$

where $m_b$is the molality of solute b (mol kg–1), T is temperature (K), R is the gas constant (J K–1 mol–1) and ΔH is the enthalpy of fusion of ice (J mol–1). This equation simplifies to:

$$\triangle T \approx -1{,}860\,(\nu m_b)$$

where ΔT is in °C and n is the number of aqueous species resulting from the dissolution of the solute (e.g., 1 for sucrose, 2 for NaCl, 3 for CaCl2) [34]. This equation is general for dilute solutions and holds for all chemical species regardless of their degree of dissociation.

However, departures from the limiting slope of –1.86°C/nm are apparent at concentrations > 0.2 nm (Figure 3.3.1a). These departures are most significant for electrolytes that dissociate into ions of higher valences (i.e., $MgSO_4$ > Na_2SO_4 > NaCl). Part of the explanation for the deviations from the limiting slope are attributable to ion pairing between oppositely charged species, which decreases the true concentration of chemical species in solution. In general, the strength of ion pairing is proportional to the product of the ionic charges. Therefore, di-divalent ion pairs are much stronger than uni-univalent ion pairs.

For a few salts, primarily highly soluble chlorides and sulfates, it is possible to construct complete phase diagrams at subzero temperatures. A phase diagram for the H_2O–NaCl system at subzero temperatures (Figure 3.3.1b) is very useful in describing the change in the solution phase as ice and NaCl precipitate during the freezing process. Assume an initial NaCl concentration of 1.00 mol kg–1 and an initial temperature of 0°C. As this solution cools below 0°C, the NaCl concentration will remain constant until the temperature reaches –3.3°C, when ice, largely a pure phase, will begin to precipitate, concentrating NaCl in the remaining unfrozen solution. If equilibrium is maintained between the solution and ice phases during freezing, then the NaCl concentration in solution will follow the ice–solution equilibrium line, increasing in concentration as temperature decreases until it reaches the *eutectic composition* at –21.2°C and 5.17 mol kg^{-1}, at which point the residual solution will solidify as a mixture of ice and NaCl*$2H_2O$.

The process for which the salt is concentrated in the liquid phase during freezing is called *salt exclusion*. The soluble salts are excluded from the ice and remain in the unfrozen liquid phase upon freezing of a salt solution. As a result, salt concentration in the solution increases consistently as temperature is lowered, i.e., as more water freezes. This increased salt concentration affects the freezing point depression of the remaining water and shifts it to lower temperatures [7].

Summarizing, solutes in the liquid phase decrease the freezing point and increase the unfrozen water content at a certain temperature.

3.3.2 Salt in porous media

Freezing point and unfrozen water content

Freezing saline soils are complex ice-water-ions-soil systems in witch all of these factors and their interactions have to take in account.

The pure NaCl– H2O phase diagram (Figure 3.3.1b) neglects soil solid–water interactions and as a consequence only demonstrates qualitatively what might occur in a soil. As we discussed before (3.1.1) clay particles have a great specific charged area which interact with water dipoles and solutions ions. In fact, it is well known that the water located within the range of forces emanating from the soil-particle surfaces freezes at a temperature lower than that of pure bulk water (Gibbs-Thompson effect), the magnitude of the reduction in freezing temperature at a point within the pore fluid depends upon the distance to the particle surface, the chemical composition and structure of the particle surface [49]. Adding dissolved solutes to the pore

solution, the volume of water influenced by the mineral surface is reduced due to collapse of the bound water film (double layer theory 3.1.2).

Treatment	Added Solute Content e, meq/g soil	Salt Type	W_u = 0.2 g/g: Freezing Point, °C	W_u = 0.2 g/g: Freezing Point Shift,* deg Observed	W_u = 0.2 g/g: Freezing Point Shift,* deg Calculated	W_u = 0.15 g/g: Freezing Point, °C	W_u = 0.15 g/g: Freezing Point Shift, deg Observed	W_u = 0.15 g/g: Freezing Point Shift, deg Calculated
Untreated soil	($\sim 1 \times 10^{-2}$)	natural, mixed	−0.31	0	0	−0.81	0	0
+0.072 g 0.5 N NaCl solution/g soil	3.6×10^{-2}	1-1	−0.98	0.67	0.67	−1.70	0.89	0.89
+0.072 g 1.0 N NaCl solution/g soil	7.2×10^{-2}	1-1	−1.88	1.57	1.34	−3.05	2.24	1.79
+0.072 g 1.5 N NACl solution/g soil	10.8×10^{-2}	1-1	−2.40	2.09	2.01	−4.00	3.19	2.68
+ 0.477 g dimethyl sulfoxide/g soil	0.611 (mmol/g)	nonelectrolyte	−6.42	6.11	5.68	−8.90	8.09	7.58

* Freezing point shift equals freezing point of untreated soil minus freezing point of treated soil.

Figure 3.3.2: Table of calculated and observed freezing point depression shifts due to solute addition in a Suffield silty clay soil [7]

Banin and Anderson [7] developed a "pure solution theory" in order to predict the unfrozen water content and freezing point shifts in saline soils. Figure 3.3.2 presents the comparison between theoretical and experimental results. They found excellent agreement between experimental measurements and a theoretical solute model at low solutes concentrations and a small but consistent underestimate (10–20%) of the experimental freezing point at higher solutes concentrations. The studies suggested that this discrepancy was due to the inhomogeneous distribution of salt in water because of the negative adsorption of anions (anion repulsion) near negatively charged surfaces, which resulted in abnormally high salt concentrations in the bulk solution.

Yong et al. [49] developed an unfrozen soil water model that explicitly accounts for negative salt adsorption using diffuse double-layer theory. Differently from the "pure solution theory" of Banin and Anderson, Yong also take into account the soil type interaction with the freezing water, considering also the water bounded to the particles. Yong compared the theoretical values with experimental results, obtained for montmorillonite, kaolinite and grundite for various concentration of NaCl at different subfreezing temperatures. Graphical results are presented in Figure 3.3.3.The model showed excellent quantitative agreement with a montmorillonite soil sample but only qualitative agreement for kaolinite and grundite soils. This discrepancy was attributed to the model requirement for interlamellar migration of water in soil freezing, which is a reasonable assumption for montmorillonite but not for kaolinite or grundite.

Bing and Ma [9] have performed several experiments in order to understand how salt content, water content, ion sort as well as type of soil affect the freezing point of the soils. Four different grain size soils were investigated: silty clay along the Qinghai-Tibet Railway (QTR), Lanzhou loess (silt), silty sand along QTR, and Lanzhou sand. They found that, at the same water content and salt content, the freezing point of clay soil is lower than that of sandy soil and the smaller soil particles, the lower the freezing point. The effect of soil particle size on

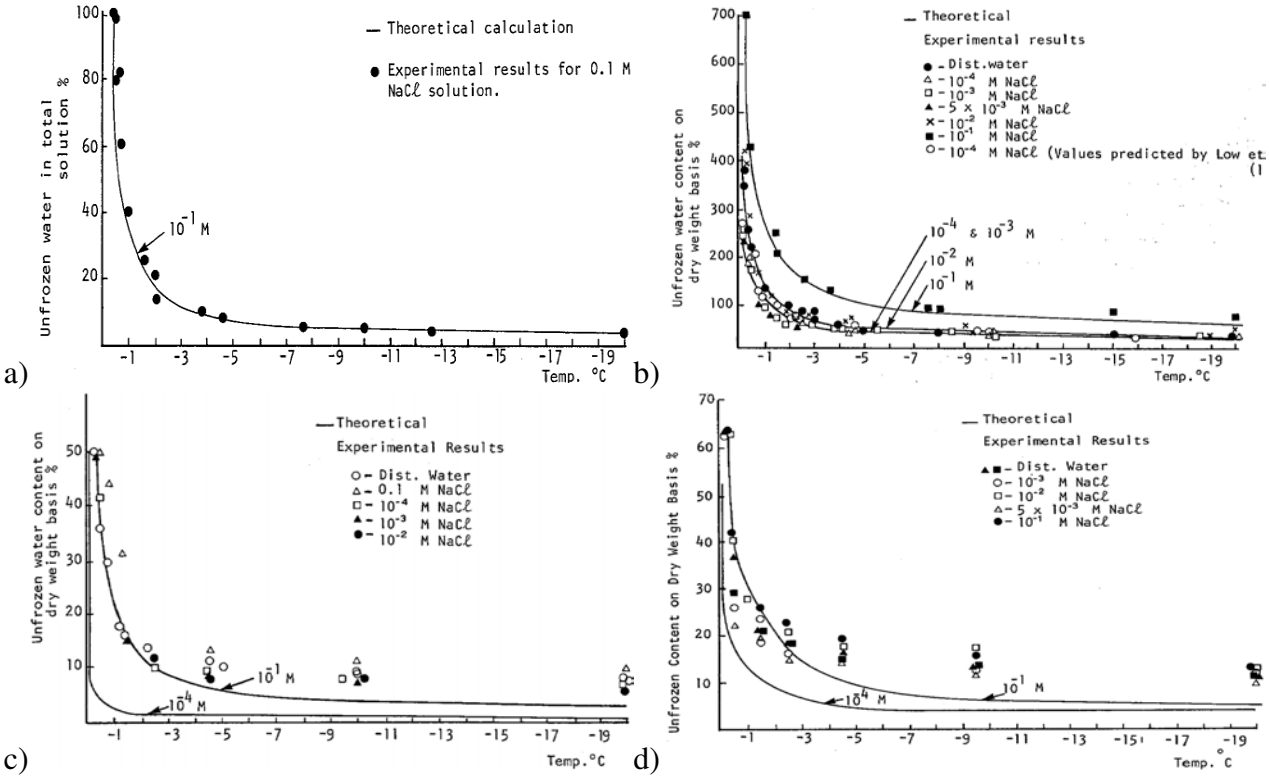

Figure 3.3.3: Comparison of theoretical and experimental results of (a) sodim chloride solution, (b) montmorillonite, (c) kaolinite and (d) grundite with various sodium chloride concentrations [49]

the freezing point decreases with increasing water content. It is because the Gibbs-Thompson effect, which capillary effect is one consequence. The greater the specific area, the larger the adsorption between water molecules and salt particles and the thickness the water film around the soil particles, which leads to a lower freezing point. Adsorption decreases as the soil particles size increases, sand-sized particles have a much thinner water film around the soil particles and will freeze at a higher temperature. In fact, because of the same effect, the freezing point decrease with the decreasing of the water content. With lower water content the water film on soil particles is more bounded and the potential of capillary water or adhesive water increases and it is mere difficult for water to freeze. On the contrary with higher water content the water film increases and there are much more free porous water which could easily freeze at higher temperatures. Figures 3.3.4 shows the influence of the water content at different salt concentration on the freezing point of a silty clay. As regards the salt type, the anion in this study with the strongest influence on the freezing point was Cl^-, followed by $CO_3^{2-}$and SO_4^{2-}(Cl^-> CO_3^{2-}> SO_4^{2-}). The cation among the salts in the study with the strongest influence on freezing point was K^+ followed by Na^+ and Ca^{2+} (K^+> Na^+> Ca^{2+}). The salt that greatly depress the freezing point is NaCl. Of course the most important factor which influence the freezing point is the salt concentration. Both for depressing the freezing point of the free solution and for electrical interactions with soil-water. Results are presented in Figure .

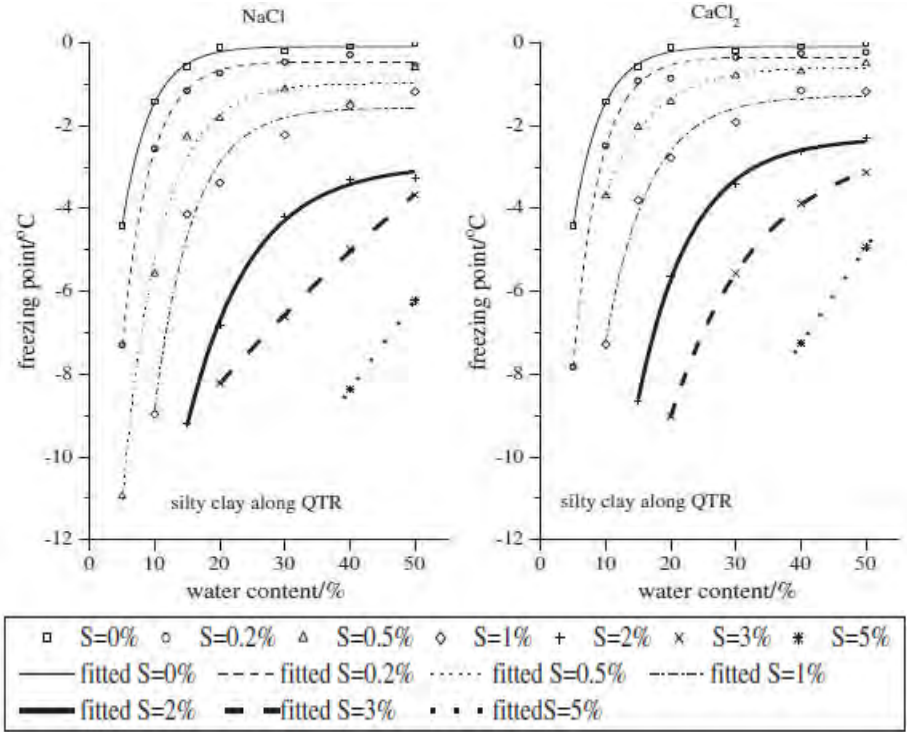

Figure 3.3.4: Freezing point depression for a silty clay at different water content and with different salt concentration (NaCl and $CaCl_2$) [9]

Water movement

The physics of moisture movement in freezing and frozen soils is an important topic in order to investigate phenomena such as the frost heave and permeability in frozen soils.

As we discussed in section 3.2.1, during freezing, water flows to freezing front due to a dewatering because of the ice formation. The *non-equilibrium thermodynamic approach* [**?**] theoretical explains the water transport mechanism. Fluxes are written as explicit functions of both direct and coupled transport phenomena. The water flux is the result of different gradients:

$$j_w = -L_{wh}\nabla T/T - L_{ww}\nabla pl - L_{ws}\nabla\pi - L_{we}\nabla\varepsilon$$

where:

$$j_w = water\,flux$$

$$\nabla T = temperature\,gradient$$

$$\nabla pl = hydrostatic\,pressure\,gradient$$

$$\nabla\pi = solute\,concentration\,gradient$$

$$\nabla\varepsilon = charge\,gradient$$

$L_{wx} = water\,flux\,transport\,coefficient, related\,to\,the\,x\,component\,(heat, water, solute\,and\,electric)$

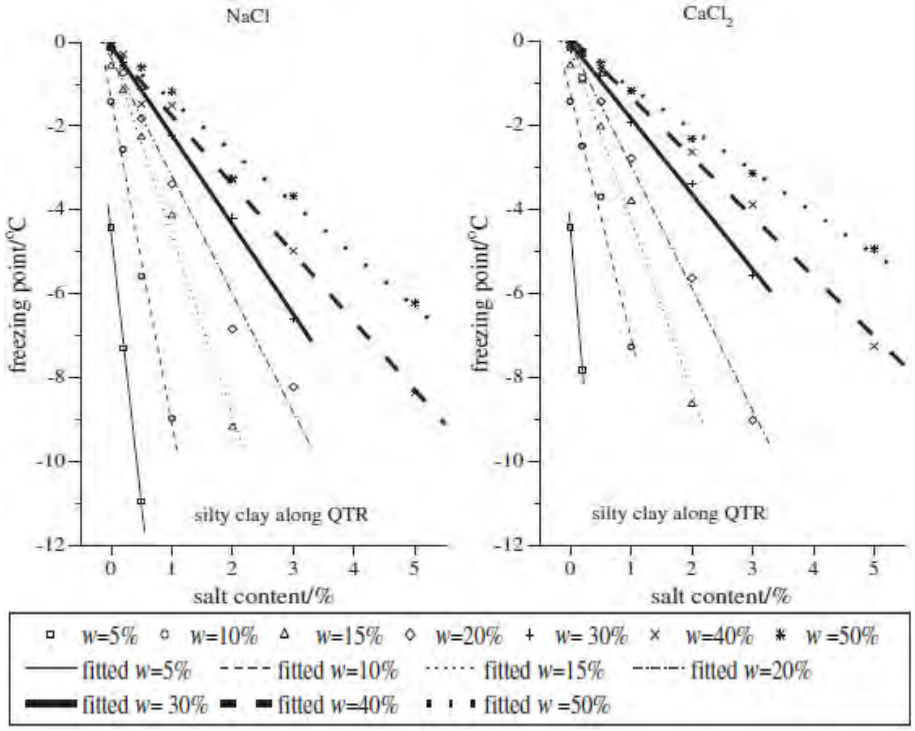

Figure 3.3.5: Freezing point depression induced by salt concentration for different water content in silty clay [9]

Water flux driving forces in frozen porous media are summarized in Table 3.3. Water moves in soil (j_w) in response to changes in the chemical potential of water, which is related to gradients in the hydrostatic pressure (∇pl) (Darcy's Law), temperature (thermo-osmosis), solute concentration (capillary-osmosis) and electrical potential (electro-osmosis) (Table 3.3).

Flux	∇T	∇pl	∇_π	∇_ε
j_w	Thermo-osmosis	Darcy's Law	Capillary osmosis	Electro-osmosis

Table 3.3: Water flux driving forces in porous media [**?**]

In general, water moves from warm to cold, from regions of low solute concentration to high solute regions and from high-moisture zones to low-moisture zones [**?**]. Chemical potentials of water due to gradients of hydrostatic pressure, solute concentration and temperature interact additively to create a strong thermodynamic sink for liquid water at the freezing front (Figure 3.3.6). As soils freeze from the top downward, the thermal gradient will induce an upward flow of water to the freezing front. Solutes are largely excluded in the freezing process, and maximum solute concentrations are generally found immediately in front of the freezing front [34]. This solute (or osmotic) gradient will generally induce an upward movement of water. And last, freezing of soil water, which is analogous to soil drying, creates a strong sink for water and induces an upward movement of water to the freezing front. Under subzero temperatures some soil water remains unfrozen as thin films around soil particles and serves as an avenue for the movement of both water and solutes in frozen soil. From 0°to –1°C there is an exponential

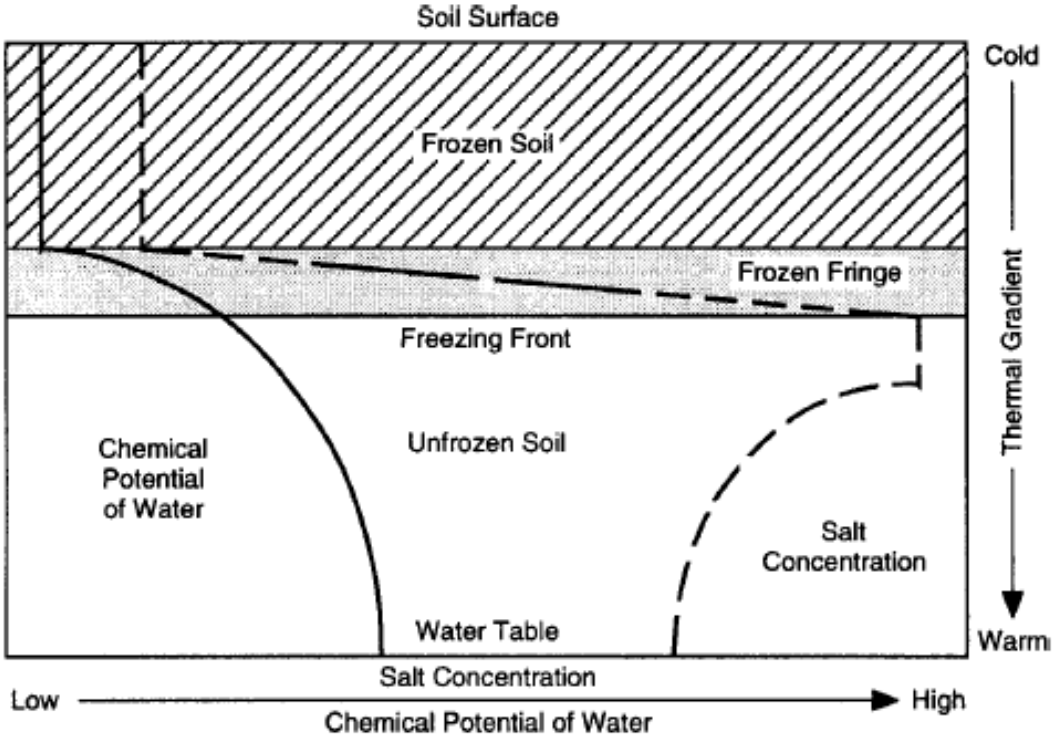

Figure 3.3.6: Schematic representation of gradients in freezing soil system [34]

decrease in the hydraulic conductivity (L_{ww}, in the water flux equation) of a frozen soil from 10^{-8} to 10^{-12}, 10^{-14} m/s; below –1°C the hydraulic conductivity remains essentially constant [**?**]. Solutes can theoretically increase the water flux, in part because of the direct effect on water diffusion (L_{ws} in the equation) but also because of indirect effects on freezing-point depression, unfrozen water content and increases in the thickness of soil moisture films [4, 34]. Despite these theoretical considerations, it appears that the dominant effect of solutes is generally a reduction in hydraulic conductivity (L_{ww}) that overwhelms the other terms in the water flux equation. As a consequence, water flux to the freezing front is generally reduced by solutes [12, 34, 49].

Salts can interact with soil particles, causing them to either aggregate or disperse, depending on solute type and concentration [32]. This, in turn, will affect soil permeability and the resultant water flux.

Soil strength

Freezing, per se, invariably increases the mechanical strength of soils because of the strong bonding between ice and soil particles.

Freezing and thawing can either increase or decrease soil strength, depending on the degree of thaw weakening. With respect to clays, Chamberlain [12, 14, 13] concluded that strength increases can be expected where there is an increase in consolidation and density during freezing and thawing; decreases in mechanical strength can be expected with highly cemented clays and

clay soils that are highly over-consolidated before freezing.

As discussed in section 3.2.1, clay aggregates are produced by freezing. After thawing, these aggregates swelled and dispersed, depending on electrolyte concentration, in a manner similar to aggregates formed by drying. The presence of salts in soils generally decreases mechanical strength [12, 34, 13]. This decline in mechanical strength with increasing salt concentration is generally attributed to a lowering of the freezing point and, as a consequence, an increase in unfrozen water content. In addition to unfrozen water films around soil particles, larger unfrozen brine pockets can form during especially rapid ground freezing of saline soils, which also decreases the mechanical strength of soils[13].

Chapter 4

Test materials and methodology

The purpose of this research is to investigate the effects of salt concentration on freeze-thaw processes of Venice subsoil, induced by the under-sizing of geothermal heat exchangers. To do this was necessary to develop a laboratory protocol and a test procedure *ad hoc*. In order to evaluate the possible environmental hazards, the experiments focused on the irreversible settlements induced in sediments which experience the freezing and thawing. For this purpose a normal oedometer was modified in order to simulate the one-dimensional deformation and drainage conditions that soils experience in the field during freezing and thawing. As the subsoil of Venezia area are rich in clayey sediments (Chapter 2) and the clayey soils are the most subject to changes induced by freezing and thawing, the sample chosen for the experiments is a silty clay, taken from a drilling in the study area and described in the next section 4.1.

4.1 Sample characterization

4.1.1 Geographical and geological characterization

The soil sample derives from a continuous core drilling performed by the company Superjet International S.p.A. [46].

The drilling is located in the municipality of Venice, Tessera, via Triestina n. 214, in the area of the hangar D of the Marco Polo airport (Figure 4.1.1).

The sampling was performed with a simple core barrel of 101mm inner diameter, for 25 meters depth from the ground-level. Figure 4.1.2 shows the sample used in the experiments, called SJ, which corresponds to the material from 7 to 7.5 meters depth (Figure 4.1.2).

In Figure 4.1.3 is presented an elaboration of the stratigraphy of the core drilling. This stratigraphy presents a sequence of silty-clay impermeable horizons and sandy layers, more permeable, perfectly according with the overall stratigraphy of the area (Figure 2.2.4), already studied in section 2.2.1.

The material used for the experiments (SJ) is taken from the silty-clay layer at 7 meters depth. According with the geological characterization, in the sampling area the Caranto layer,

Figure 4.1.1: Geographical location of the sample drilling [46].

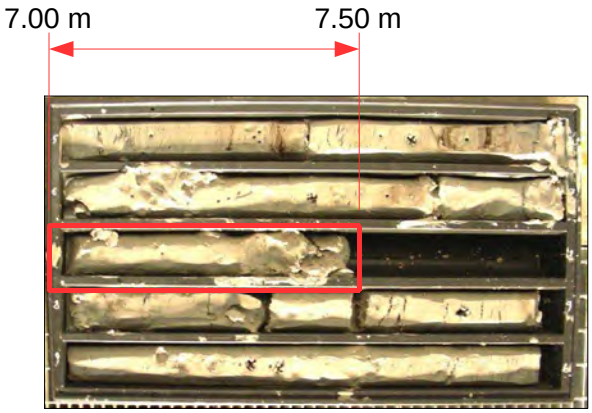

Figure 4.1.2: Sample SJ taken at 7 to 7.5 meters depth.

which divides Pleistocene and Holocene sediments, is at the ground level, or not deeper than 2 meters (Figure 2.2.2). Then SJ sample belongs to continental Pleistocene deposits.

4.1.2 Geotechnical and mineralogical characterization

The geotechnical characterization of the sample was performed at the Laboratory of Geotechnical Engineering of the University of Padova at ICEA Department.

Attemberg limits are defined. The Attemberg limits are a basic measure of the critical water contents of a fine-grained soil, which divided the different state of the soil: solid, plastic, and liquid. They can be used to distinguish between silt and clay, and it can distinguish between different types of silts and clays [33].

The **plastic limit** is determined by rolling out a thread of the fine portion of a soil on a flat, non-porous surface. The procedure is defined in ASTM Standard D 4318 [5]. If the soil is plastic, this thread will retain its shape down to a very narrow diameter. The sample can then

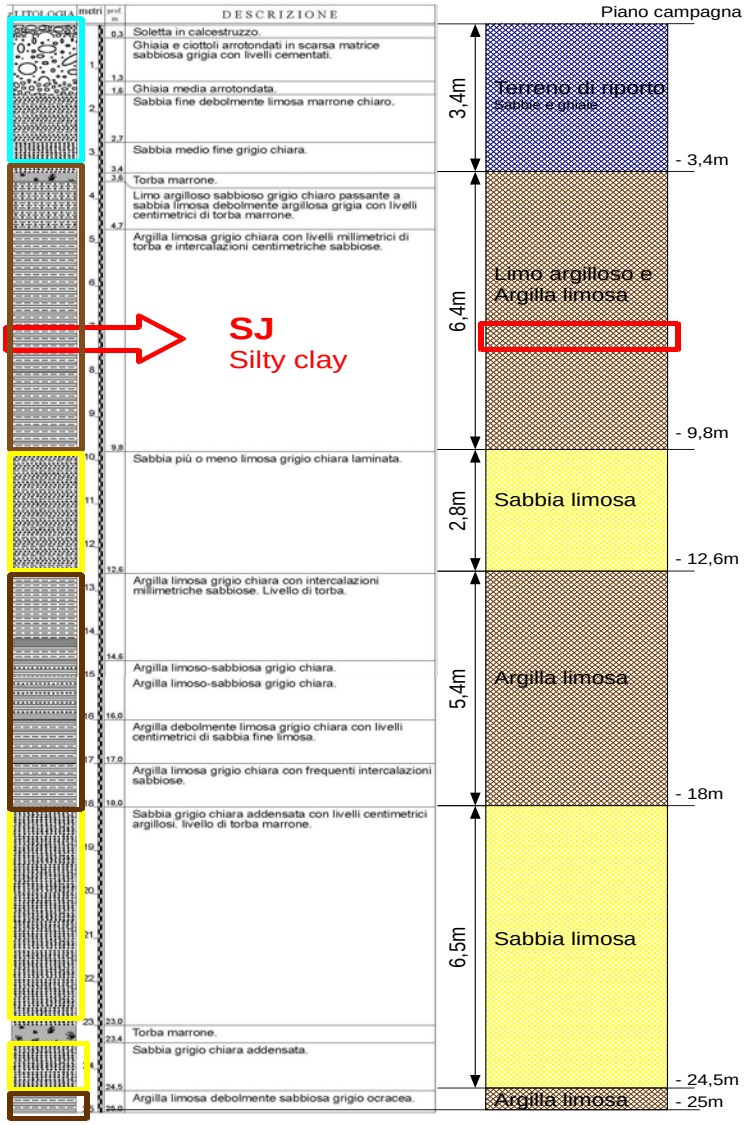

Figure 4.1.3: Schematic elaboration of the stratigraphy from the sampling.

be remoulded and the test repeated. As the moisture content falls due to evaporation, the thread will begin to break apart at larger diameters. The plastic limit is defined as the moisture content where the thread breaks apart at a diameter of 3.2 mm (about 1/8 inch).

The **liquid limit** (LL) is often conceptually defined as the water content at which the behavior of a clayey soil changes from plastic to liquid. Actually, clayey soil does have a very small shear strength at the liquid limit and the strength decreases as water content increases; the transition from plastic to liquid behavior occurs over a range of water contents. The precise definition of the liquid limit is based on standard test procedures described below. Casagrande standardized the apparatus and the procedures. Soil is placed into the metal cup portion of the device and a groove is made down its center with a standardized tool of 13.5 millimeters (0.53 in) width. The cup is repeatedly dropped 10 mm onto a hard rubber base at a rate of 120 blows per minute, during which the groove closes up gradually as a result of the impact. The number

of blows for the groove to close is recorded. The moisture content at which it takes 25 drops of the cup to cause the groove to close over a distance of 13.5 millimeters (0.53 in) is defined as the liquid limit. The test is normally run at several moisture contents, and the moisture content which requires 25 blows to close the groove is interpolated from the test results. The Liquid Limit test is defined by ASTM standard test method D 4318 [5]. The test method also allows running the test at one moisture content where 20 to 30 blows are required to close the groove; then a correction factor is applied to obtain the liquid limit from the moisture content.

The **plasticity index** (PI) is a measure of the plasticity of a soil. The plasticity index is the size of the range of water contents where the soil exhibits plastic properties. The PI is the difference between the liquid limit and the plastic limit (PI = LL-PL). Soils with a high PI tend to be clay, those with a lower PI tend to be silt, and those with a PI of 0 (non-plastic) tend to have little or no silt or clay [33].

The **activity** (A) of a soil is the PI divided by the percent of clay-sized particles (less than 2 μm) present. Different types of clays have different specific surface areas which controls how much wetting is required to move a soil from one phase to another such as across the liquid limit or the plastic limit. From the activity, one can predict the dominant clay type present in a soil sample. High activity signifies large volume change when wetted and large shrinkage when dried. Soils with high activity are very reactive chemically. Normally the activity of clay is between 0.75 and 1.25, and in this range clay is called normal. It is assumed that the plasticity index is approximately equal to the clay fraction (A=1). When A is less than 0.75, it is considered inactive. When it is greater than 1.25, it is considered active [33].

LL	39%
PL	23%
PI	16
A	0,48
CF	34%
ρ_g	2,763 g/cm^3

Table 4.1: Sample characteristics. Liquid limit (LL), Plastic limit (PL), Plasticity index (PI), Activity (A), Clay fraction (CF), Grain density (ρ_g).

Table 4.1 presents the laboratory results for the sample SJ. In Figure 4.1.4 is represented the position of the sample on the *Casagrande plasticity chart*, a diagram which classifies fine-grained soil on Attemberg limits bases. On this classification, the sample SJ is an **inorganic clay of medium plasticity**.

The granulometric analysis was performed with the *aerometric test*. The test defines the grain size distribution of the finest fraction measuring the sedimentation times. The sample is dryed at 105°, pulverized in a mortar, and passed through the sieve number 200, with a 0,075mm diameter. Then the passed material is mixed with water and the density of the water is measured at different times. Larger particles settle first, decreasing the density of the suspension.

Sample SJ was found to have a fine fraction (<0,075mm) of 98% and a clay fraction (<0,002)

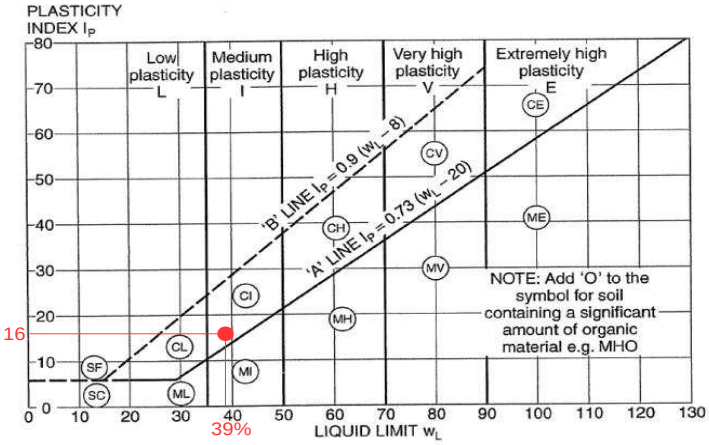

Figure 4.1.4: Casagrande plasticity chart.

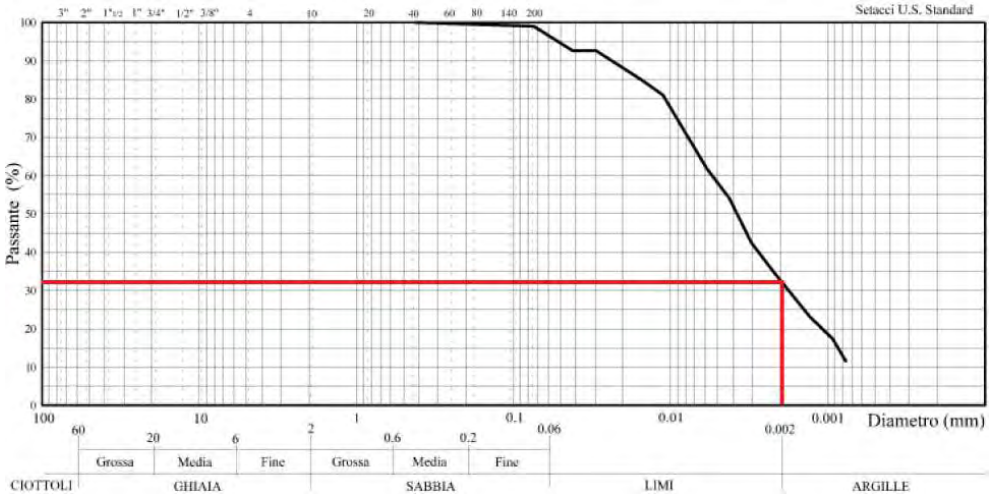

Figure 4.1.5: Granulometric curve SJ.

CF=34%. Figure 4.1.5 shows the granulometric curve of the sample with the CF emphasized.

The mineralogical composition of the sample is:

Phyllosilicates 30%

Quartz 11%

Calcite 42%

Dolomite 15%

Feldspars 2%

Phyllosilicates (mainly illite) are the clay minerals (described in section 3.1.1) and their percentage almost correspond to the clay fraction defined with the granulometric analysis. The low fraction of phyllosilicates qualifies the sample as halfway between silt and clay and almost inactive, precisely as defined with the Casagrande plastic chart (Figure 4.1.4). The sample presents

an high percentage in calcite $CaCO_3$ and dolomite $MgCa(CO_3)_2$, which indicate an evaporitic sedimentation environment, such as exactly the lagoon environment.

4.2 Test procedure

The aim of the experimental analysis is, in particular, to investigate the effects, on soil freezing and thawing, of the salt, simulating the possible salt intrusion in lagoon and coastal areas. For this purpose, were created four samples mixing the SJ soil (previous section 4.1) with a solution at different NaCl concentration (Table 4.2).

	NaCl conc. in added sol. (g/l)	NaCl eq. conc. in the pore sol. (g/l)
SJ 0	0	0,6
SJ 35	35	10,1
SJ 70	70	14,8
SJ 140	140	20,3

Table 4.2: Samples at different NaCl concentrations.

The sample SJ is washed in order to eliminate its original moisture salinity. First it is mixed with five liters of normal tap water and then allowed to settle in a bucket for 6 or 7 days until complete sedimentation (Figure 4.2.1a); the excess water is removed and the procedure was repeated another time. Then the material is processed with a spin-dryer (Figure 4.2.1e) at 3500 rpm for 10 minutes, then mixed with deionized water and processed again with the spin-dryer.

The NaCl solution is prepared (Figure 4.2.1b) mixed with water at least 24 hours before usage, in order to allowed a perfect dissolution of the salt.

The NaCl solution was mixed with the soil. The SJ material was worked with spatulas above a marble table, adding the solution, until obtaining an homogeneous brilliant mixture, malleable but not liquid (Figure 4.2.1c).

The resulting mixture was posed inside a large oedometer cell (internal d = 10cm) under a vertical load of 40kPa (32kg) for five days, to pre-consolidate the soil sample.

After five days of pre-consolidation, electrical conductivity of the sample pore solution measurement, in order to evaluate the salinity (better exposed in section 4.3) . A small amount of the sample is taken and processed in the spin-dryer (4000 rpm for 15 minutes) to extract the pore solution. The extract, in this case, is too small for the EC measurement, so it is diluted with deionized water and the EC value reported to the original with appropriate proportion.

The pre-consolidated sample is then posed into the modified oedometer apparatus in order to performed the thermo-mechanical test (described in section 4.4). The sample is freezed for 18 hours at -6°C and thawed for 6 hours at 55°C under a vertical constant load of 40kPa, cyclically until the specimen has negligible settlement (usually 10-13 cycles). The test simulate the soil freezing and thawing induced by a borehole heat exchanger.

After the thermo-mechanical test, the soil specimen is divided in two half. From one is extracted the pore solution to the electric conductivity measurement. The other is weighed,

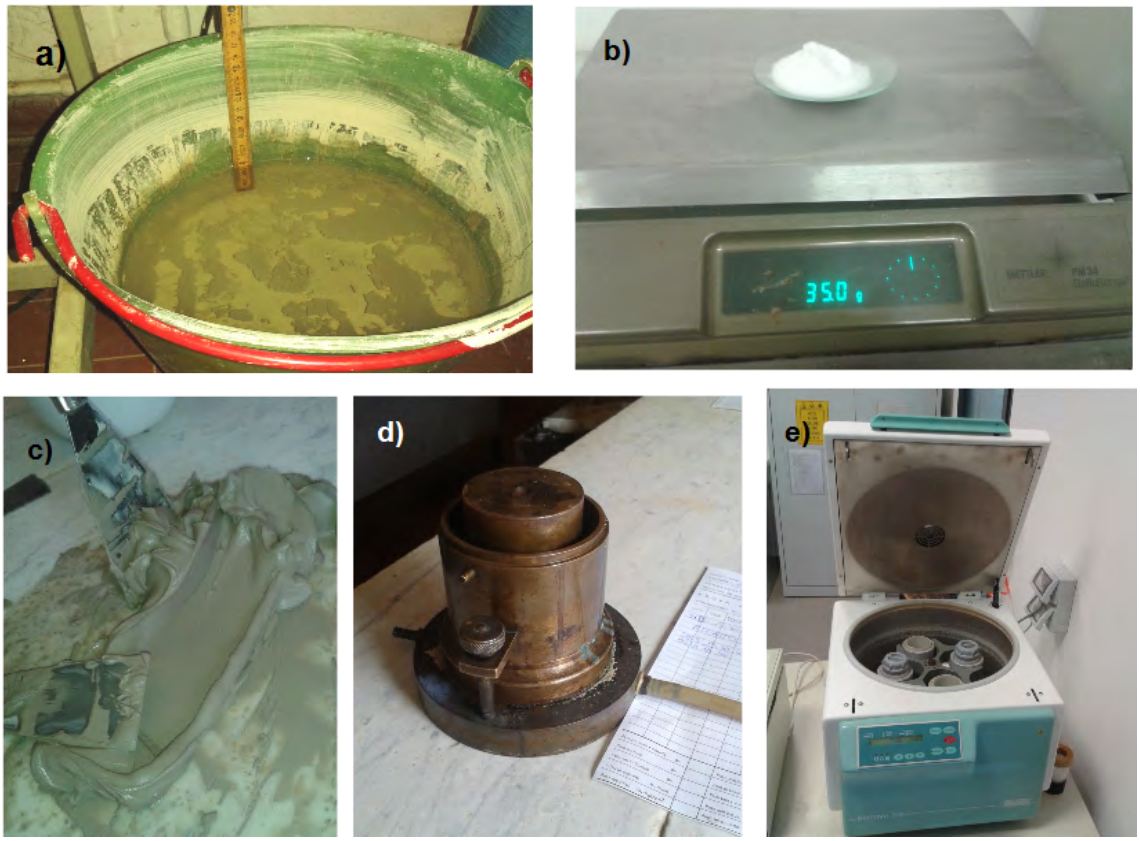

Figure 4.2.1: Test materials. a) bucket for sedimentation; b) NaCl salt; c) sample preparation; d) large oedometer e) spin-dryer.

placed in the oven at 105 ° for 24 hours and then re-weighed, for the calculation of the water content.

The test procedure sequence is then:

1. Sample washing
2. Adding NaCl solution
3. Pre-consolidation
4. EC measurement
5. Thermo-mechanical test
6. EC measurement
7. Water content computation

It is chosen to focus on the effect of the NaCl because we are referring to the effects caused by a probable salt intrusion from the Lagoon. Table 4.3 shows that almost the 86% of the soluble ions presented in marine water are $Cl^-$and Na^+. The Lagoon water has a variable salinity between 5

Ion	Percentage
Cl^-	54,3%
Na^+	31,4%
SO_4^{2-}	7,1%
Mg^{2+}	3,7%
Ca^{2+}	1,2%
K^+	1,1%
others	1,2%

Table 4.3: Soluble ions in marine water.

to 35 g/l (section 2.2.1), depending on the location and on the climate conditions. In the study area, the average salinity is around 20g/l. Knowing this, we tried to get, with the last sample SJ140 almost the same salinity, as a upper limit.

In fact, the sample, before adding the NaCl solution, already has a certain moisture content, derived from its washing. The real salinity of the pore solution is the average between the initial moisture content and the NaCl solution added. Table 4.2 reports the salinity of both added and pore solutions. The salinity value of the pore solution is referred to the extraction of the preconsolidated samples and is obtained converting the EC values into Salinity values using the equation 4.3.1, expressed in the following section 4.3.

4.3 Electrical conductivity and salinity

4.3.1 EC definition and measuring device

The salinity of the sample pore solution is evaluated before and after the thermo-mechanical test, in order to define the differences and the freeze-thaw effect on the soil salinity. Measurements are done on the pore solution, extracted from the sample processing the soil with a spin-dryer at 4000 rpm for 15 minutes (Figure 4.2.1).

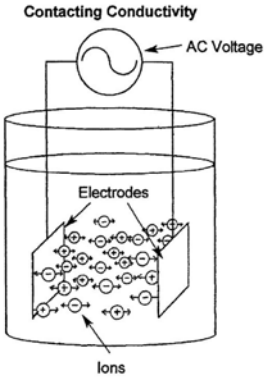

Figure 4.3.1: Electrical conductivity in alternating current.

To evaluate the salinity of the pore solution is used the measurement of the electrical con-

ductivity (EC). In fact, the electrical conductivity is the ability of the ions in solution to conduct electricity. Electrolyte solutions are second kind conductors (unlike metals) because they conduct electricity with mass transit, the migration of ions towards the poles. EC depends on the solute and solution type, temperature, cell geometry and ions concentration. The SI unit of conductivity is Siemens per meter (S/m).

The electrical conductivity of a solution of an electrolyte is measured by determining the resistance of the solution between two flat or cylindrical electrodes separated by a fixed distance. An alternating voltage is used in order to avoid electrolysis (Figure 4.3.1).

$$EC = f_{Temp} \cdot k_{geom} \cdot {}^{1}/_{R}$$

f_{Temp} =temperature correction factor. Referred the value to standard temperature of 25°C.

k_{geom} =cell geometry factor. It takes into account the cell dimensions.

${}^{1}/_{R}$ =conductance. It is the inverse of the solution resistance.

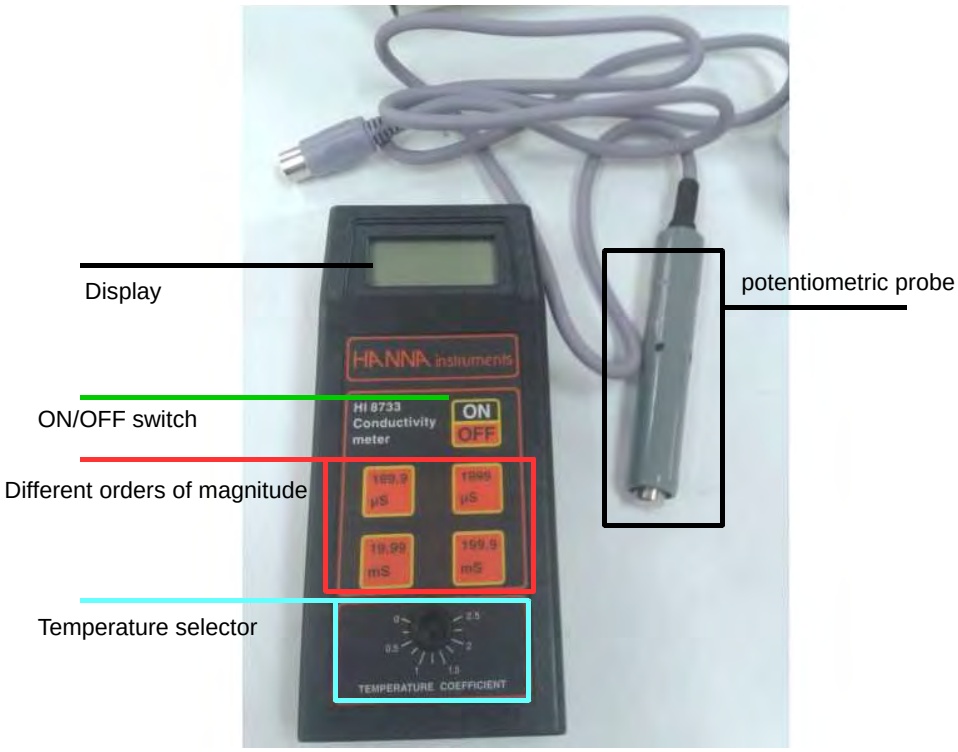

Figure 4.3.2: HI 8733 Conductivity meter. HANNA Instruments.

The EC is measured by HI 8733 Conductivity meter of HANNA Instruments (Figure 4.3.2). Its potentiometer is directly put inside the solution. The instruments automatically correct the value about the cell factor and has a temperature selector which can refer the value to the standard at 25°C. The value is expressed in $\mu S/cm$ or in mS/cm depending on the magnitude of salt dissolved.

4.3.2 EC-Salinity correlation

Electrical conductivity gives the measure of the total ions in the solution. The salinity value is linearly dependent on the EC value. In literature, there are many conversion methods. In the soil chemical analysis [20] normally are used empirical formulas which link EC to TDS[1] with a correlation factor [6]:

$$TDS = k_e \cdot EC$$

TDS is the dissolved solutes, expressed in *mg/l*.

EC is the electrical conductivity at 25°C, expressed in $\mu S/cm$.

k_e is the correlation factor, which varies between 0,55 and 0,8 depending on the solute equivalent mass[6]. For ordinary soil analysis k_e=*0,64* [20].

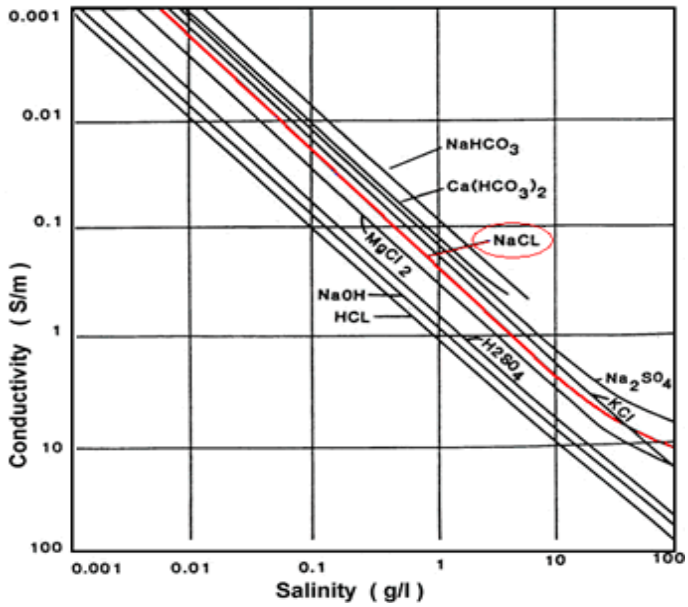

Figure 4.3.3: Electrical conductivity and salinity diagram [26].

Keller and Frischknecht [26], in Figure 4.3.3, present the EC-salinity correlation diagram. It shows almost linear dependence between EC and salinity and that it is different depending on the species of solute.

In order to have a perfect correlation using the tests laboratory device (Figure 4.3.2), the EC of solution at known concentration of NaCl was measured and the results were interpolated to obtain a EC-Salinity conversion law equation:

$$C_{NaCl} = 10^{-9} EC^2 + 4 \cdot 10^{-4} EC + 0,28 \tag{4.3.1}$$

in which C_{NaCl} is the concentration NaCl in the solution expressed in *g/l*.

[1] Total Dissolved Solids. The mass of the fixed residue after the evaporation, at 180°C, of the liquid solvent. Direct measure of the dissolved salts.

The correlation low found (equation 4.3.1) corresponds to the values found in literature.

EC, expressed in $\mu S/cm$, is the electrical conductivity measured in laboratory and referred to 25°C.

C (g/l)	EC microS
0	2
35	66000
70	122000
105	161000
120	180000

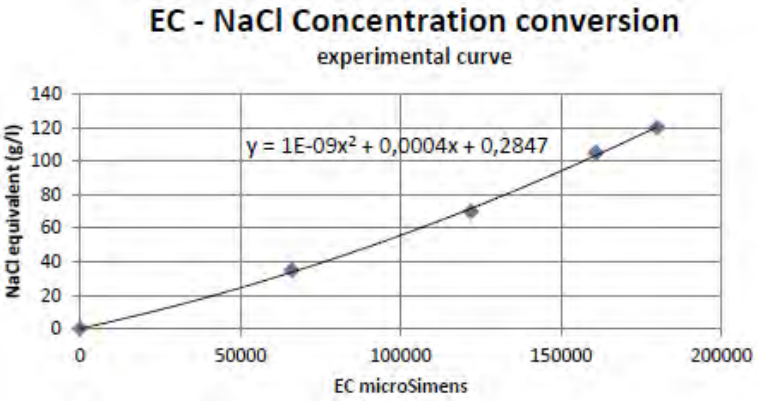

Figure 4.3.4: Experimental EC measures and interpolation curve.

Figure 4.3.4 presents the experimental measures done on five solution at different NaCl concentrations (0, 35, 70, 105, 140 *g/l*) and the resulting interpolation curve, which is used to convert EC values in Salinity values.

4.4 Thermo-mechanical test

The test simulates the response of the soil to the cycling thermal stress (freezing and thawing) induced by a borehole heat exchanger. The temperature range is between -6° to 55°C, which are the extreme operating temperatures of the carrier fluid when anti-freezing solutions are added. The tests focuses particularly on the vertical strains of the soil specimen.

4.4.1 Apparatus

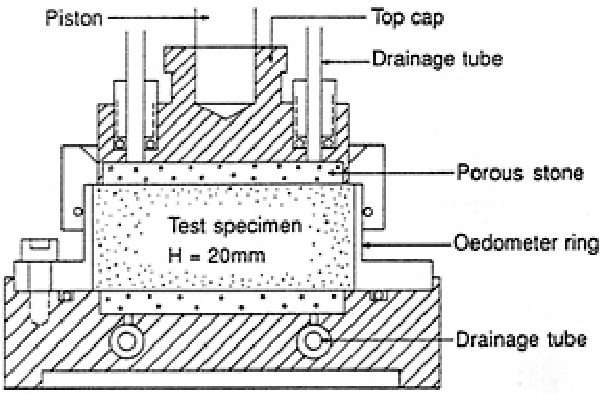

Figure 4.4.1: Standard oedometer.

The apparatus consists in a standard oedometric cell modified in order to operate at controlled temperature.

Standard oedometer (Figure 4.4.1) is essentially a cylindrical soil specimen with cross-sectional area of 39,04cm^2 and height of 20 mm, enclosed in a stainless steel ring. Top cap and base plate are provided with porous stones to which two drainage tubes are connected. Oedometer specimens are mounted with dry filter stones to prevent swelling of the unloaded specimen. Standard oedometer test is designed to simulate the one-dimensional deformation and drainage conditions that soils experience in the field. It is performed by applying different loads to a soil sample and measuring the deformation response.

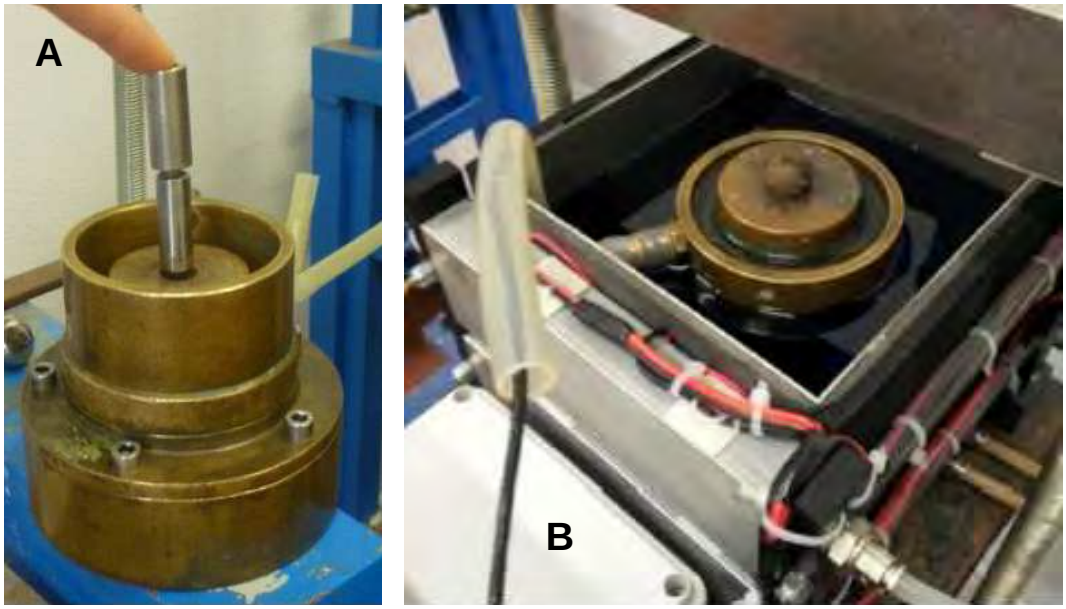

Figure 4.4.2: A) Oedometer cell [51]. B) Stainless insulated chamber with oedometer inside and filled with ethylene glycol [44].

In this thermo-mechanical test, the oedometer cell is inserted into a particular stainless steel chamber of 14x14x13cm dimensions, filled with ethylene glycol where the oedometer could be super-cool or heat through 12 Peltier cells (Figure 4.4.2). The cells are connected together in parallel and are powered by direct current at variable voltage between 5 and 12 volts, depending on which temperature they have to reach.

A Peltier cell (Figure 4.4.3) or thermoelectric heat pump is a solid-state active heat pump which transfers heat from one side of the device to the other, with consumption of electrical energy, depending on the direction of the current. It can be used either for heating or for cooling (refrigeration). Peltier cell is made up of a multiple junction in series of two semiconductor materials (N,P) connected by a copper plate. A driven electric current generate an heat flow from one side to the other.

The chamber is thermal insulated from the environment and the Peltier cells are connected with a cooling system to dissipate the excess heat. The cooling system consists of small water reservoirs in contact with the external side of the Peltier cells and connected with a larger

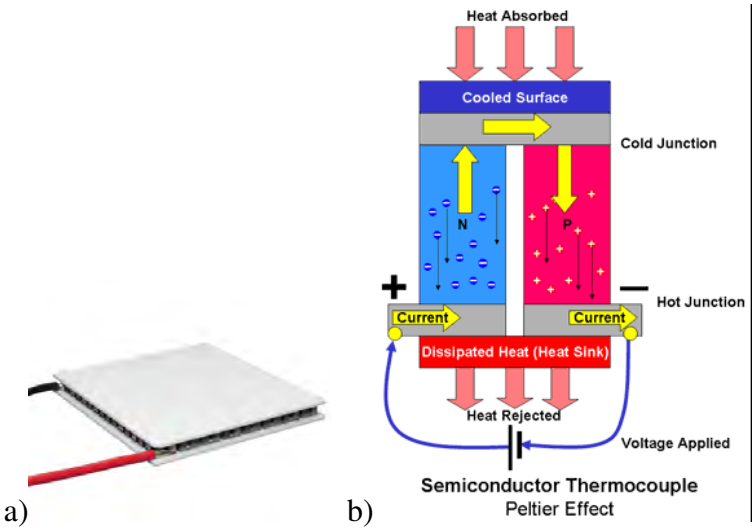

Figure 4.4.3: a) Peltier cell. b) operating scheme.

reservoir (6-10 liters), which takes water directly from the waterway network. The flow is induced by a pump inserted in the delivery circuit.

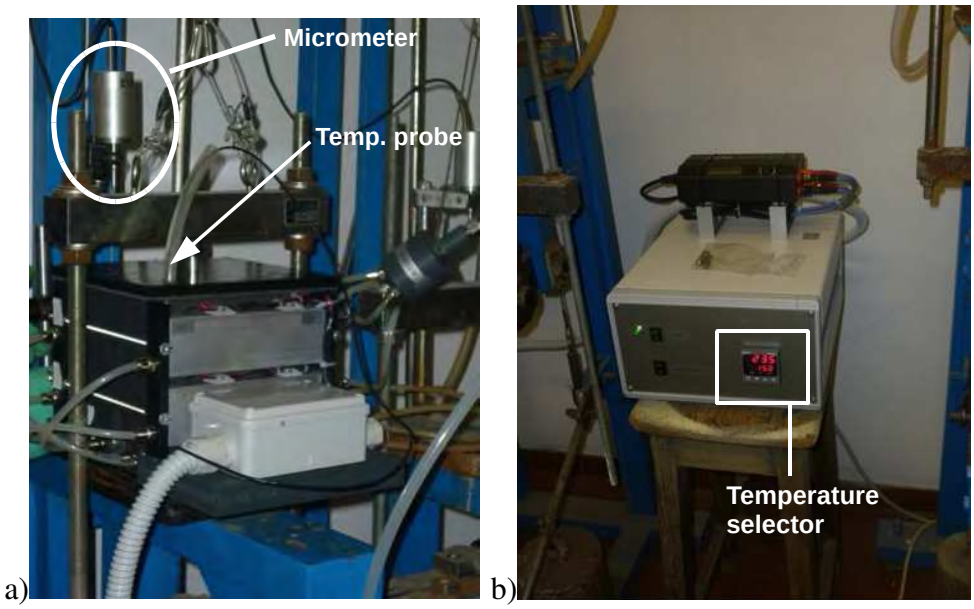

Figure 4.4.4: Thermo-mechanical devices. a) controlled temperature oedometer cell. b) PID device [44].

A inductive displacement transducer (micrometer), connected a PC, records the vertical strain of the specimen. In order to record the temperature values, a thermometric probe PT100 is inserted inside the lower drain, in contact with the porous stone (Figure 4.4.4a).

The electronic power supply of the Peltier cells is regulated by a separate PID[2] controller (Figure 4.4.4b), which acquires the input temperature value, measured by probe PT100, and

[2]Proportional Integral Derivative

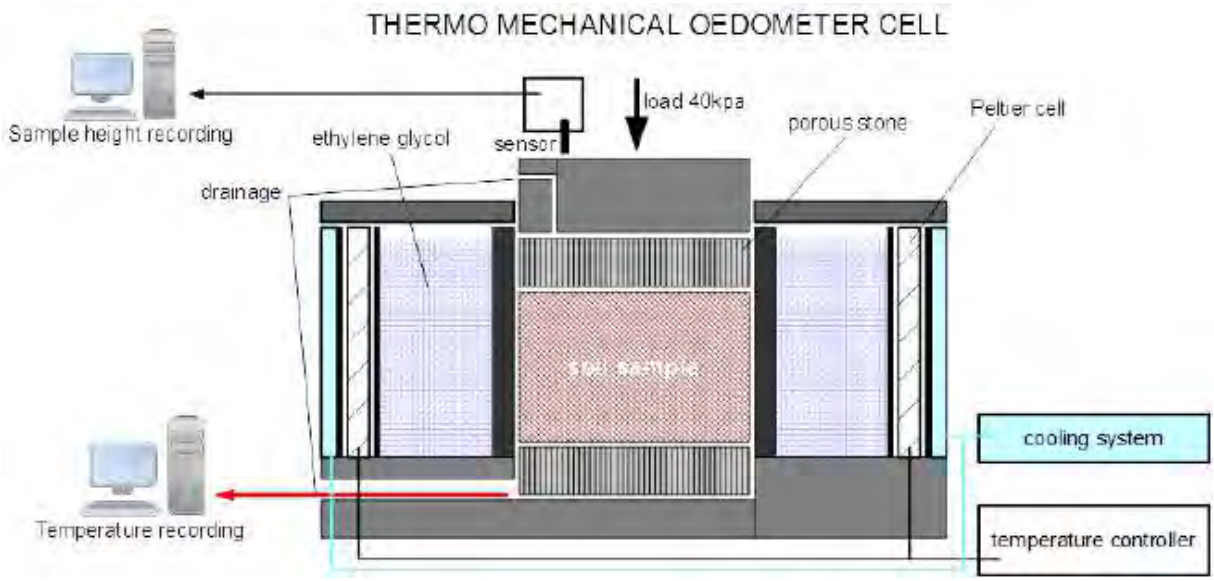

Figure 4.4.5: Thermostatic cell scheme.

compares it with the reference set value. When the temperature set on the PID is equal to the temperature detected, the power supply is interrupted. It is reactivated when the temperature of the sample departs from the threshold of the value established.

Temperature and vertical strain are recorded by two PCs at the same time steps. Time step is define with parabolic law:

$$\triangle\tau = 0,2 \cdot t^2$$

Where:

$\Delta\tau$ is the time step in which the corresponding value is registered

t is the time from the test starting

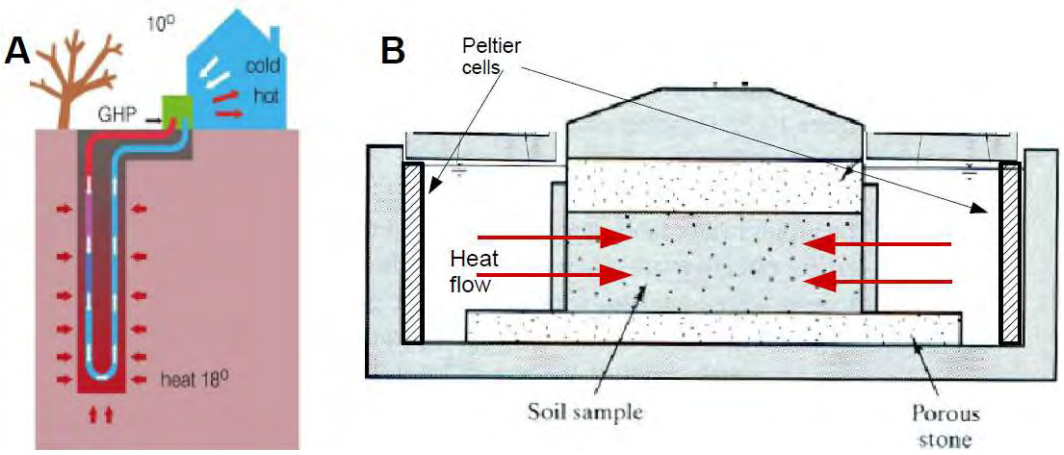

Figure 4.4.6: Heat flow direction scheme. A) *in situ* borehole. B) simulation with laboratory apparatus

Figure 4.4.5 schematically presents the thermostatic cell with a standard oedometer within.

The original element of this research, compared to the others which particularly focused on the *frost heave*, is the application of the FTC to the ground surrounding the BHE. To do this, a change in geometry is required. In fact, the apparatus wants to simulate the thermal alteration induced by the boreholes, i.e. with a horizontal heat flow (Figure 4.4.6A). For this purpose, the Peltier cells are placed on the cell lateral sides, leading a radial heat flow, from the side surface to the center of the specimen (Figure 4.4.6B).

4.4.2 Performed test

The test simulates the extreme thermal stress induced by a borehole on a normal-consolidated clay.

The test is performed with a constant vertical load applied of $40kPa$, i.e. the *in situ* lithostatic effective pressure (4 meters depth, water table at the ground level). The temperature range goes from -6° to +55°C which are the extreme operating temperature of the carrier fluid when anti-freezing solution are added.

After the pre-consolidation, the sample is inserted inside the thermostatic oedometer cell and it is left at 15°C for 5-6 hours to allowed the specimen to consolidate until reaching the zero. During the sample transportation from the preconsolidation oedometer to the thermostatic one, the pressure conditions are disturbed. In this phase the sample experienced an initial consolidation which restores these conditions.

then, from 3:30 pm to 9:30 am (18 hours), the sample is freezed at -6°C.

At 9:30 am to 3:30 pm (6 hours) the sample is thawed to +55°C.

This freezing-thawing process is cyclically repeated until the specimen experienced no, or little (0,02-0,03 mm), settlements for at least two consecutive times. Normally the test stops almost after 10 cycles.

The phases are here summarized:

1. Initial consolidation. 6 hours at 15°C
2. Freezing phase. 18 hours at -6°C
3. Thawing phase. 6 hours at 55°C
4. Stop when $\triangle h_i \leq 0,03mm$ for two consecutive times

Chapter 5

Test results and analysis

Figures 5.3.5, 5.3.6 and 5.3.7, at the end of the Chapter, presents the vertical strain diagrams resulting from the thermo-mechanical tests.

In this diagrams is possible to recognize the different test phases already exposed in section 4.4.2. All the samples starts from 20*mm* height, which is the height of the oedometric cell, then variously consolidated for about 6 hours. This initial consolidation differs form sample to sample because of its dependence on ineliminable differences in the samples preparation, such as initial water content and sample remoulding. Figure 5.0.1 presents the first section of the

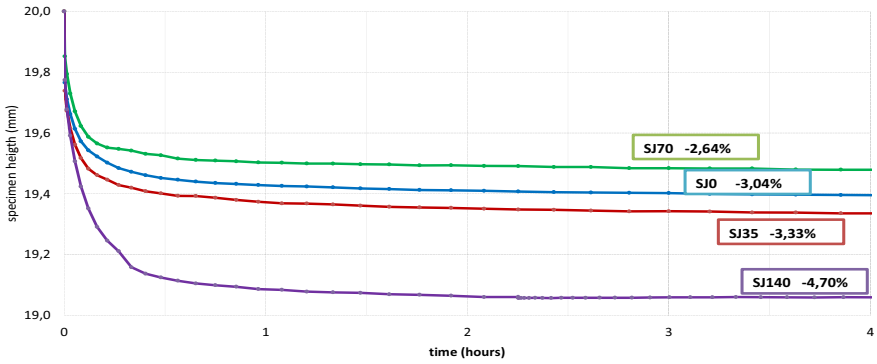

Figure 5.0.1: Initial consolidation phase. Extract from diagram of Figure 5.3.7

samples comparison diagram (Figure 5.3.7) and shows the *initial consolidation phase* of the samples. Most of the consolidation occurs in the first few minutes after the load is applied, then slightly continues for about four hours.

After the initial consolidation phase, the temperature is decrease to -6° and starts the freezing phase, which consists in the sample expansion due to the ice formation. It continues until the temperature is raised to 55°, when thawing phase takes place. During thawing, ice melts and the specimen consolidates. This phase continue until the temperature is decreased again to -6°. Freezing phase and thawing phase compose one cycle (Figure 5.0.2). Freezing and thawing phases and their effects and implications are better exposed and discussed in the following sections, respectively 5.2 and 5.3.

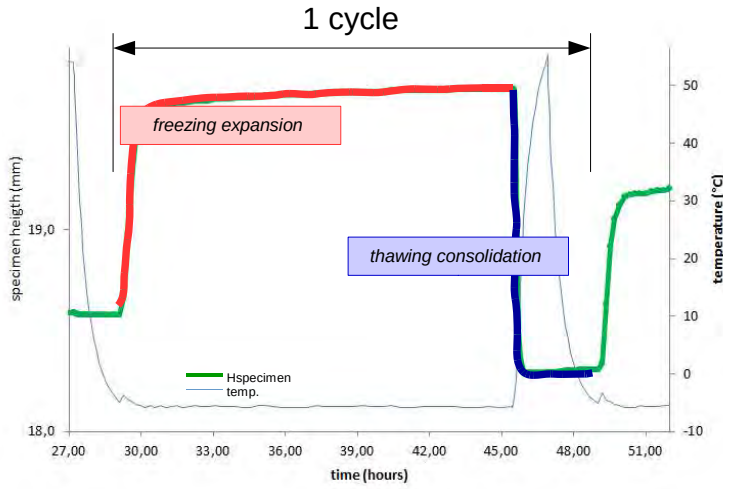

Figure 5.0.2: Freezing and thawing phases. Extract of SJ70 diagram (Figure 5.3.6)

5.1 Salinity and freezing point

Salinity and freezing point are closely linked aspects, as it was already discussed in section 3.3. Salt decreases the freezing point and increases the unfrozen water content.

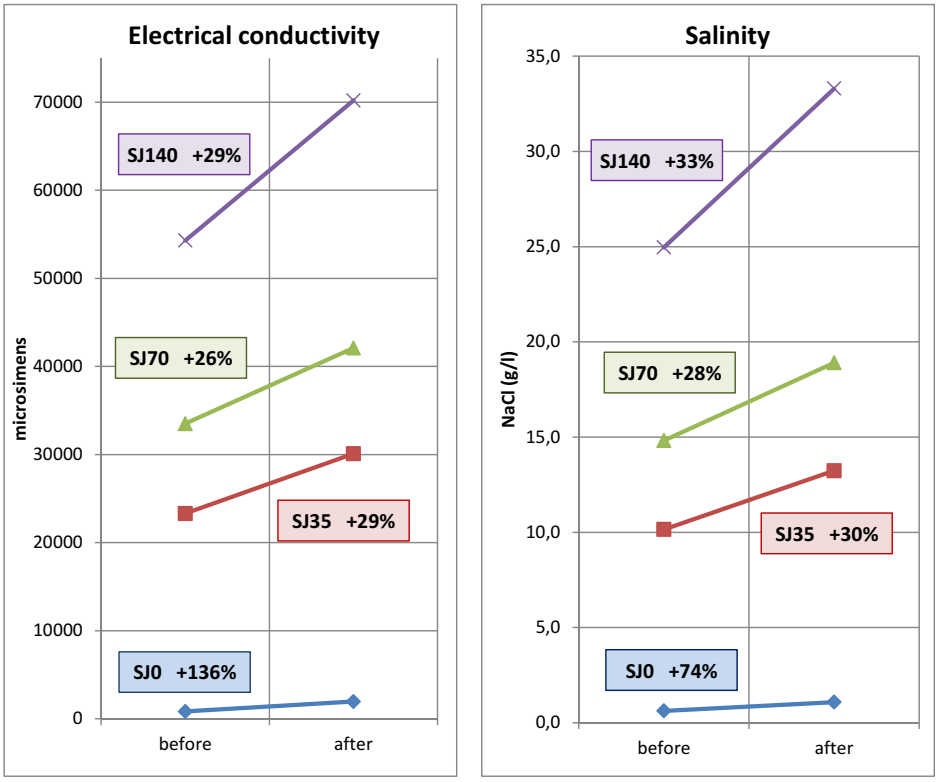

Figure 5.1.1: Increasing salinity effect

Increasing salinity effect As regards the salinity, the measurements performed demonstrates that freeze-thaw cycles, under an applied load, tend to *increase the soil salinity* (Figure 5.1.1)

between the values measured before and after the thermo-mechanical test. Salinity values are calculated from the electrical conductivity measured values using the conversion equation 4.3.1, obtained in section 4.3. Percentages are respect the initial value. Salinity increases of about 30% in samples SJ35, SJ70 and SJ140. The increasing value of the sample SJ0, instead, is higher because it starts from almost zero salinity.

Salinity increasing effect is due to the salt exclusion and the freeze-thaw mechanism (Figure 5.2.3). During freezing, solutes are excluded from the ice formation and remain in unfrozen water near the soil particles. If the concentration exceeds the threshold value, the solution supersaturates causing some salt precipitation. At the same time, ice lenses continue to grow within the macro-pores, forcing the soil particles to aggregate in packets. Probably most of the salt remains confined inside this particles aggregates. During thawing, ice melts, producing almost pure water, which is expulsed from the macro-pores and cracks and than is not able to pass through the packets. As result, the soil increases its salinity every cycle.

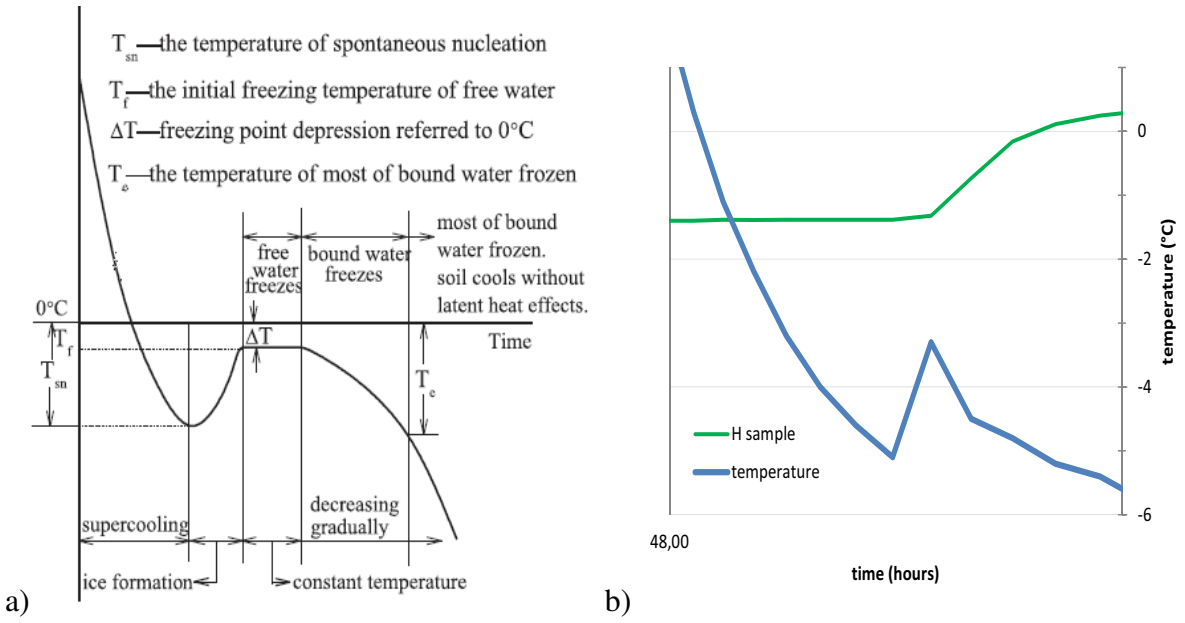

Figure 5.1.2: Freezing soil cooling curve. a) theoretical scheme [9]. b) experimental evidence; extract of SJ70 diagram (Figure 5.3.6)

Freezing point depression effect Kozlowski [28, 29, 30] developed a *"cooling curve"* to describe the temperature trend in a freezing soil (Figure 5.1.2a) [9]. A supercooling is needed to initiate the process of freezing. The pore water does not start to freeze until the temperature drops to the *temperature of spontaneous nucleation* T_{sn}, a few degrees below the melting point of ice. Ice crystal nucleation and crystal growth begins to occur within a few molecules. The abrupt transformation of free water to ice causes water molecules to aggregate to soil particles. As the result of the release of latent heat, during ice formation, the temperature of the system rises again to the initial *freezing temperature*, T_f, at which point it stabilizes for a equilibrium period. As the temperature is forced to more decrease, the extraction of heat leads to successive

freezing of the remaining unfrozen water, which is bounded to soil particles. Thus, the process of soil–water freezing has four stages: (1) spontaneous nucleation, (2) an abrupt transition in temperature as ice formation begins, (3) an equilibrium period of constant temperature, and (4) a gradual temperature decrease [9].

In performed tests is also possible to see the same stages in temperature trend (Figure 5.1.2b). As theoretically described, Figure 5.1.2 shows an abrupt specimen height increasing together with the latent heat release. Unfortunately the process is too rapid and the time step of temperature recording, used in thermo-mechanical tests, is too large to well capture it. In fact, in many cases, the heat latent release stage are jumped over and it is not visible.

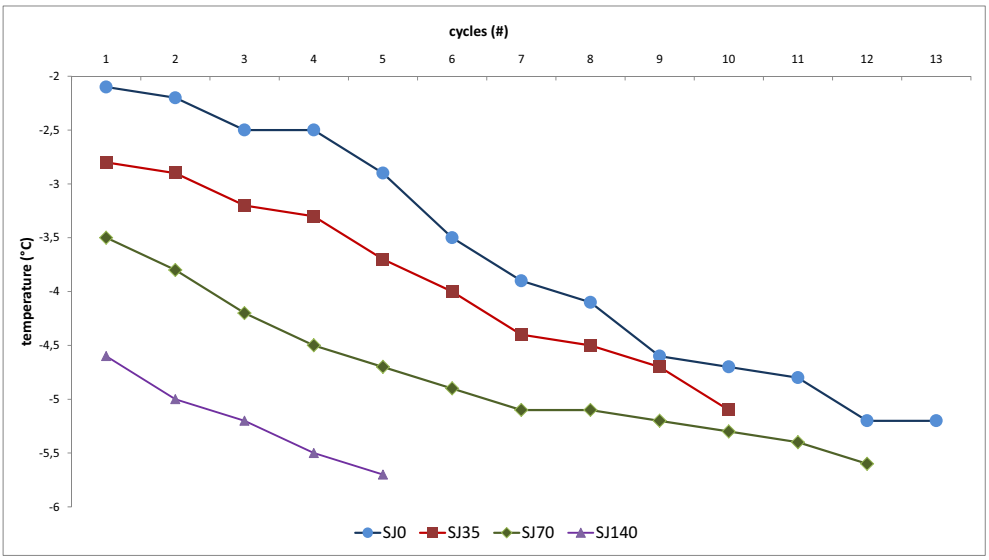

Figure 5.1.3: Freezing point depression

Because of this uncertainty in freezing temperature identification, it is chosen to use the temperature corresponding to the ice melting during thawing phase. In fact the melting temperature correspond to the freezing temperature [9] and, because of temperature linear increasing during thawing, it is better definable. Figure 5.1.3 shows the freezing point versus the number of cycles for each sample. Temperatures data describes only in qualitatively way the process. Anyway data clearly demonstrate the *freezing point depression effect* on soil of the freeze-thaw cycles. In Table 5.1 are reported the values of the freezing point depression for each sample.

	SJ0	SJ35	SJ70	SJ140
n cycles	13	10	13	5
$\Delta T_{1-n}{}^{1}$	3,1°	2,3°	2,5°	1,1°
$\Delta T_i = {}^{\Delta T_{1-n}}/_{n}$	0,24°	0,23°	0,19°	0,22°

Table 5.1: freezing point depression effect

Freezing point depression effect of one cycles is almost 0,2°C. It is grater during the firsts cycles and smaller getting closer to -6°, which is the test limit temperature.

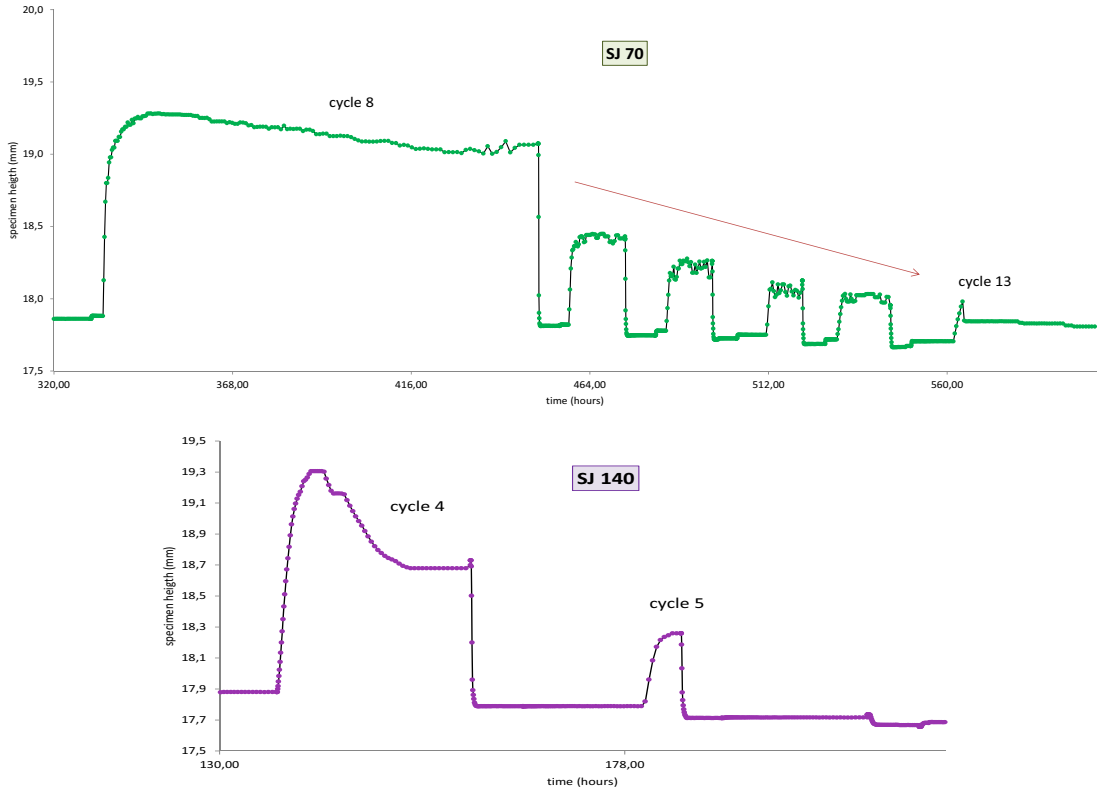

Figure 5.1.4: Particular shapes in freezing phases of SJ70 and SJ140 due to the freezing point reaching the operative temperature (-6°C)

Freezing point depression is the combination effect of two factors. Increasing salinity and water loss. Freezing point decreases with the increasing of salinity, in fact samples with higher solutes concentration starts with a lower freezing point. The increasing salinity effect of cyclical freeze-thaw decrease the freezing point. But this factor alone could not explain the grate freezing point depression of SJ0 which has a final salinity much lower than the others samples. The other factor influencing the decreasing of the freezing point is the capillary effect, or Gibbs-Thompson effect [9, 49]. During thawing some water is expulsed and soil consolidates. It leads to a shorter distance between water molecules and soil particle with thinner water film, increasing the matric potential and consequentially depressing the freezing point. Salinity, water content and particles specific surface are the controlling factors of freezing point depression process and their effect has already been recognized by Bing and Ma [9] (section 3.3.2).

As a consequence of freezing point depression effect, samples stop freezing after a certain number of cycles, that is when the freezing temperature reaches the test limit range temperature, about -6°C. In the 8^{th} cycle of SJ70 and in the 4^{th}cycle of SJ35, vertical strain diagrams show a particular wavy shape (Figure 5.1.4), like the soil is not able to maintain the freezing state but remains in a precarious equilibrium. SJ70 continued freezing fewer and fewer stopping at 13^{th}cycle; SJ140 only had one more little expansion. The reason is because the freezing point of the soil has reached -5°\-6°C, which is the operating test temperature.

5.2 Thawing consolidation

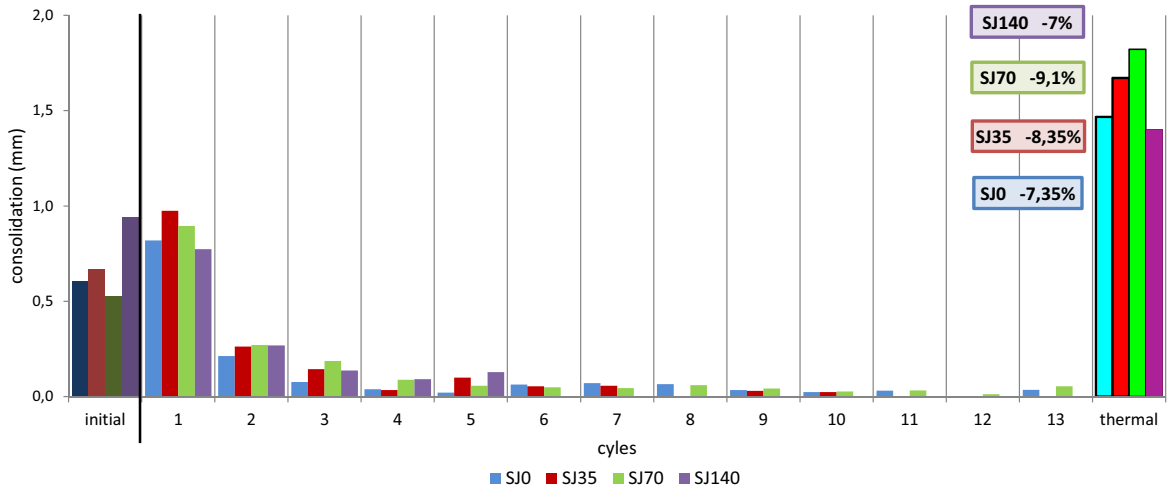

Figure 5.2.1: Irreversible settlements. Initial, for each cycle and total thermal consolidation

The most interesting and important effect of the freeze-thaw cycles is the *irreversible thermal settlement*. Figure 5.2.1 presents the consolidation for each cycles. The consolidation of one cycle is defined as the difference between the lower point of the thawing phase and the lower point of the previous thawing phase, regarding the vertical strain data. As the initial consolidation (Figure 5.0.1) is not due to the thermal stress, it is subtracted from the sum of each consolidation contribution to obtain the *total thermal consolidation*, i.e. the irreversible consolidation caused by the freezing-thawing cycles. Percentages in Figure 5.2.1 are referred to the total initial height of the samples (20mm).

Thermal stress induces in soil samples irreversible settlements from 7% to 9%. Settlements seems to have a decreasing exponential trend. More than half of the total thermal consolidation is carried out in the first cycle, and about the 80% in the first three cycles. Salinity seems to increase the consolidation effect. SJ0, SJ35 and SJ70 have rising settlements while SJ140 less consolidates. In fact SJ140, because of its higher salinity, performs only 5 cycles and only a fraction of the total water can freeze, lowering the final consolidation.

$$water\,content = {}^{water\,weight}/_{dry\,weight}\,[\%]$$

	SJ0	SJ35	SJ70	SJ140
initial water content	34,4%	35,3%	34,6%	36,1%
final water content	26,9%	27,2%	25,5%	27,4%
water loss	7,5%	8,1%	9,1%	8,7%

Attemberg limits	LL = 39%	PL = 23%	IP = 16

Table 5.2: Water content

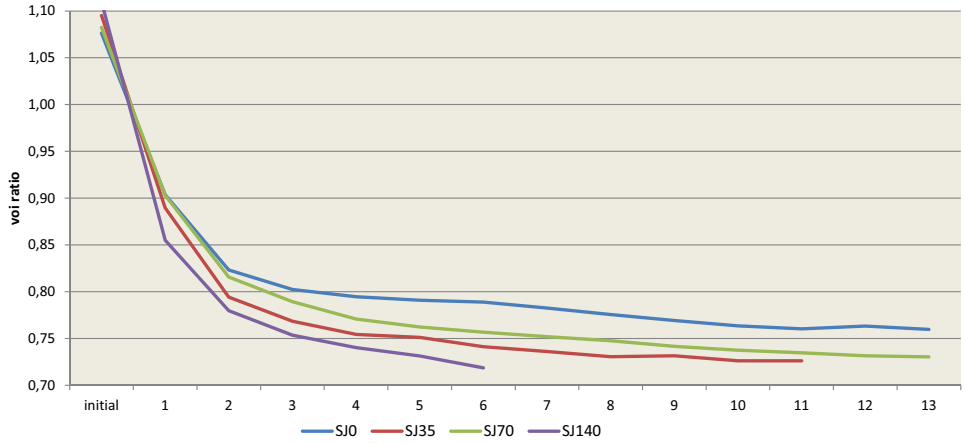

Figure 5.2.2: Void ratio vs freeze-thaw cycles

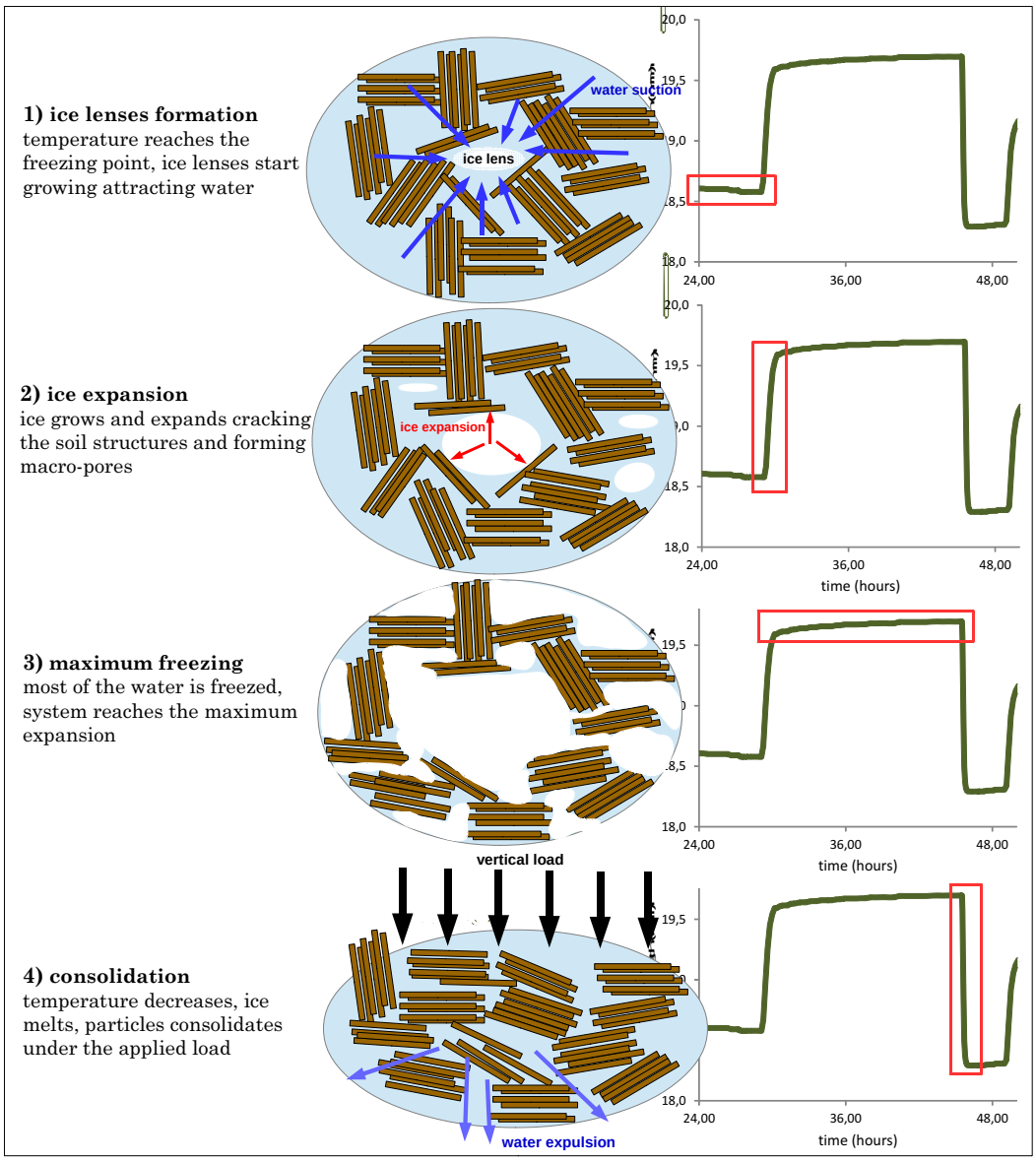

Figure 5.2.3: Freezing and thawing mechanism

Consolidation is related to water loss (Table 5.2) and decreasing of the void ratio (Figure 5.2.2). Void ratio is defined as the ratio between the volume of voids (water and air) and volume of solids (soil grains): $e = V_v/V_s$. Figure 5.2.2 shows the void ratio trend measured in the thawing phases at each cycle. The trend is decreasing exponential as the consolidation. SJ140 has the lowest final void ratio, even if it consolidates less. It is because the initial consolidation phase, which only depends on sample preparation, is included in the final void ratio result, which is then distorted.

In Figure 5.2.3 are schematically summarized the freezing-thawing mechanism. As temperature reaches the freezing point, ice lenses start growing from the free water among the pores. Ice growing attracts water from warmer regions to the freezing front; this phenomenon is called *water suction*. Due to the water suction and freezing expansion, ice lenses continue to expand cracking and destroying the soil previous structure. Soil particles are forced to over-consolidate into packets among the ice. When finally the temperature is decreased, ice melts, macro-pores collapse and soil consolidates under the applied load ($40kPa$). Freezing and thawing results having a dispersing effect on soil particles. The thermal stressed soil results irreversibly over-consolidated compared to unfrozen one.

Experimental evidences (Figure 5.2.1) show that salinity increases the thermal settlement effect. It is probably because SJ35, SJ70 and SJ140 samples EC is much higher than $4000\mu S/cm$, which represent the limit between dispersed and salt-type flocculated structure. Then, even if Na^+ is a bad flocculator, high salinity induces a thinner AWL and salt-type flocculated soil structure (section 3.1.3) [31]. Flocculated structure are more rigid and permeable, and permits an higher water circulation. Moreover, when soil freezes, soil structures is broken and dispersed and, combined with the thinner AWL, the result is an higher consolidation, respect to a lower salty soil (SJ0), which starts with a more dispersed structures.

On the contrary, when salinity is such high to depress the freezing point to operational temperature (-6°C) like SJ140 sample, the percentage of unfrozen water arises until arrest the freezing process of the soil after few cycles (Figure 5.1.4), resulting in a lower degree of consolidation.

Summarizing, the presence of solutes in the interstitial water seems to have two opposite effects on the consolidation process. One due to its flocculation power, which increases the consolidation, and the other due to the depression of the freezing point, which, up to a certain limit, prevent the soil freezing, contrasting the consolidation effect.

5.3 Freezing expansion

When temperature reaches the freezing point, water start to freeze and the specimen expands. Expansion is reasonably due to the water changing phase which increases its volume of about 9%. Not all the water freezes; in section 3.3.2 we already saw that a fraction of water remains unfrozen also at very low temperatures because bounded to soil particles, and we also saw that salinity increases the unfrozen water. So it is expected that the specimens expand more during

the first few cycles, and that saline samples less expand.

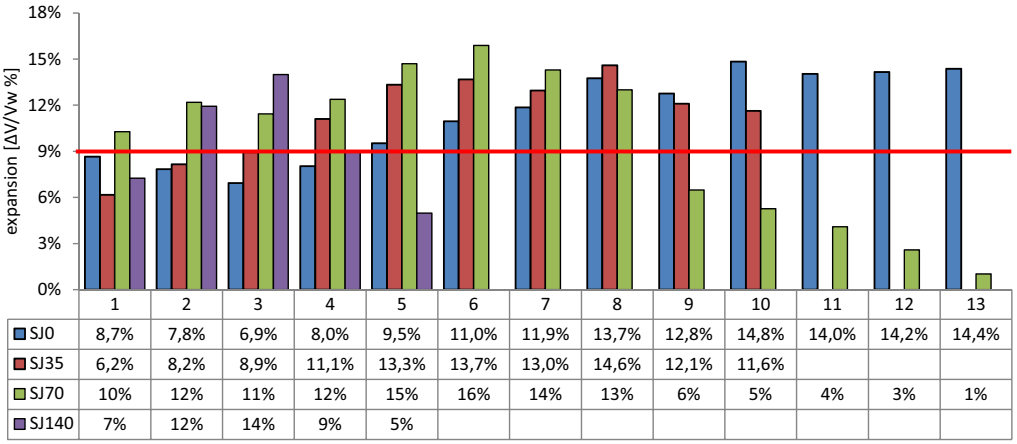

	1	2	3	4	5	6	7	8	9	10	11	12	13
SJ0	8,7%	7,8%	6,9%	8,0%	9,5%	11,0%	11,9%	13,7%	12,8%	14,8%	14,0%	14,2%	14,4%
SJ35	6,2%	8,2%	8,9%	11,1%	13,3%	13,7%	13,0%	14,6%	12,1%	11,6%			
SJ70	10%	12%	11%	12%	15%	16%	14%	13%	6%	5%	4%	3%	1%
SJ140	7%	12%	14%	9%	5%								

Figure 5.3.1: Specimen freezing expansion. Percentage respect the volume of initial water content

Figure 5.3.1 present the specimen expansion for each cycle. Expansion is calculated as the percentage of the increasing volume respect the volume of the initial water content:

$$expansion = \triangle V / V_{w,initial}$$

Unexpectedly in the firsts cycles the expansion is lower and seems to be higher for higher salt concentrations. In fact, SJ0 increases the expansion every cycles, despite the water loss and the increasing salinity. SJ70 and SJ140 which are the most salty, greatly expand already from the second cycle, much more than SJ35 and SJ0.

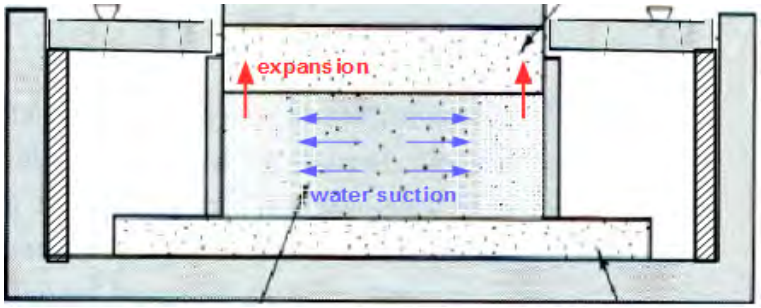

Figure 5.3.2: Inhomogeneous expansion

Specimens expand more than the expansion of the total initial water. The red line in Figure 5.3.1 corresponds to 9% and represents the maximum expansion if all the water freezes. This is an overestimation because it does not take into account the unfrozen water and the expulsed water. The over-expansion is probably due to the inhomogeneous distribution of the water into the soil specimen. In fact, the sample freezes from the outer surface, and the water is sucked to the freezing front (Figure 5.3.2). Cycle by cycle it leads to a grater water content near the sides of the specimen, and consequentially a inhomogeneous soil expansion. So considering

the ice expansion as homogeneous is not representative of the real situation: $\triangle h = \triangle V/A$ is not correct.

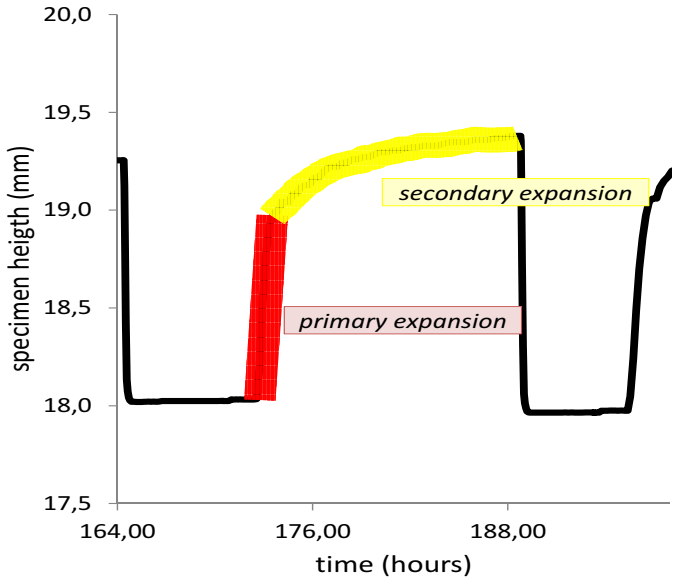

Figure 5.3.3: Primary and secondary expansions

There must be also some other microscopical explanation to this phenomenon, because this theory does not explain why salt seems to increase the effect. In fact, in vertical strain diagrams (Figures 5.3.5 and 5.3.6) a different expansion shape appears in correspondence with the over-expansion. Figure 5.3.3 shows this shape. The normal freezing expansion phase (primary expansion) is followed by a secondary expansion stage. This second phase could represent the freezing of the more bounded water, which occurs for lower water content or for more salty samples. In SJ0 it occurs at the 6^{th}cycle, in SJ35 at the $3^{th}/4^{th}$and for SJ70 and SJ140 since from the firsts cycles. The freezing of the bounded water may occurs in a inhomogeneous way, dislocating the soil particles, which is then measured as over-expansion. Anyway, it is phenomenon difficult to understand only on such tests basis, and it requires more investigation in order to better capture the processes involved.

Remarks

Thermal irreversible settlement

Experimental evidences show that FTC induces an *irreversible settlement* in clayey sediments. The magnitude of the settlement is from 7% (SJ0) to 9% (SJ70).

Salt concentration in the pore solution has two opposite effects. One increases the thermal consolidation due to the thinner AWL induced in clay particles. The other one decreases the final consolidation because of the freezing point depression which prevents the soil freezing.

A *salinity limit* (between 15 g/l and 20 g/l) exists, below of which the consolidation is increased by the salinity, and after which the freezing point depression effect is predominant. In fact SJ70, which has a pore solution salinity of 14,8g/l, had a final irreversible consolidation of 9,1%. SJ140, which is even more salty (20,8g/l) consolidated only 7%.

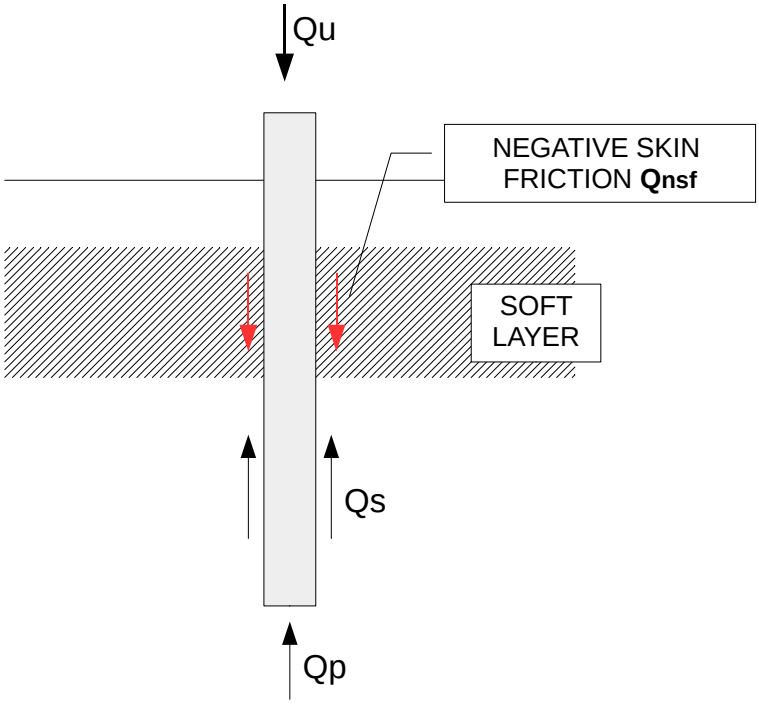

Figure 5.3.4: Negative skin friction in foundation piles

Referring to the BHE in field, the FTC affects at least the portion of ground surrounding the borehole. The thermal consolidation could have *negative skin friction* effect on BHE, similar to foundation piles fixed in compressible deposits which consolidate due to over-loads or to the ground water level reduction. In this case the surrounding soil transmits to the foundation pile a downwards load, decreasing the pile bearing capacity referred to the consolidated layer (Figure 5.3.4). This mechanism in BHE, could damage the borehole or, in case of energetic foundation piles, also damage the overall structure stability.

In field, the magnitude of the settlement could be higher than in laboratory experiments. In fact, litterateurs references about the frost heave in permafrost regions, indicate that the presence of the groundwater leads to a greater ice lenses formation due to the water suction to the freezing front [27, 4].

Hydraulic hazard

Borehole heat exchangers penetrate aquifers and aquicludes and need to be sealed with grouting materials. The sealing of penetrated aquicludes has to be guaranteed in order to prevent unwanted connections of aquifers, which could lead to vertical contamination or unwanted water flux.

Freezing and thawing lead to changes in state of stress, causing damages to the grout and soil structures [2]. As regards the soil, the water suction to the freezing front and the consequential growth of ice lenses near the borehole causes cracking in the soil structures, and the increasing in vertical permeability [27, 14]. This could lead to vertical connection between aquifers and unwanted water flux.

Salt concentration in the pore solution seems to decrease this effect. Salt decreases the soil permeability and increases the unfrozen water content [34], preventing the formation of large ice lenses. Moreover, salt concentration highly depresses the freezing point of the soil-water system, allowing lower operational temperatures without freezing the soil.

Salinity of the pore solution

Experimental evidences show that FTC increases the salinity of the pore solution. The increment, for high NaCl concentrations, was about 30%.

Moreover the experiments indicate that the pore solution salinity have a protecting effect on the possible hazards caused by FTC induced by BHEs, because of the freezing point depression which prevents the soil from freezing.

The salinity of the pore solution is then an important value to take into account in studying FTC processes applied to the ground surrounding the BHEs.

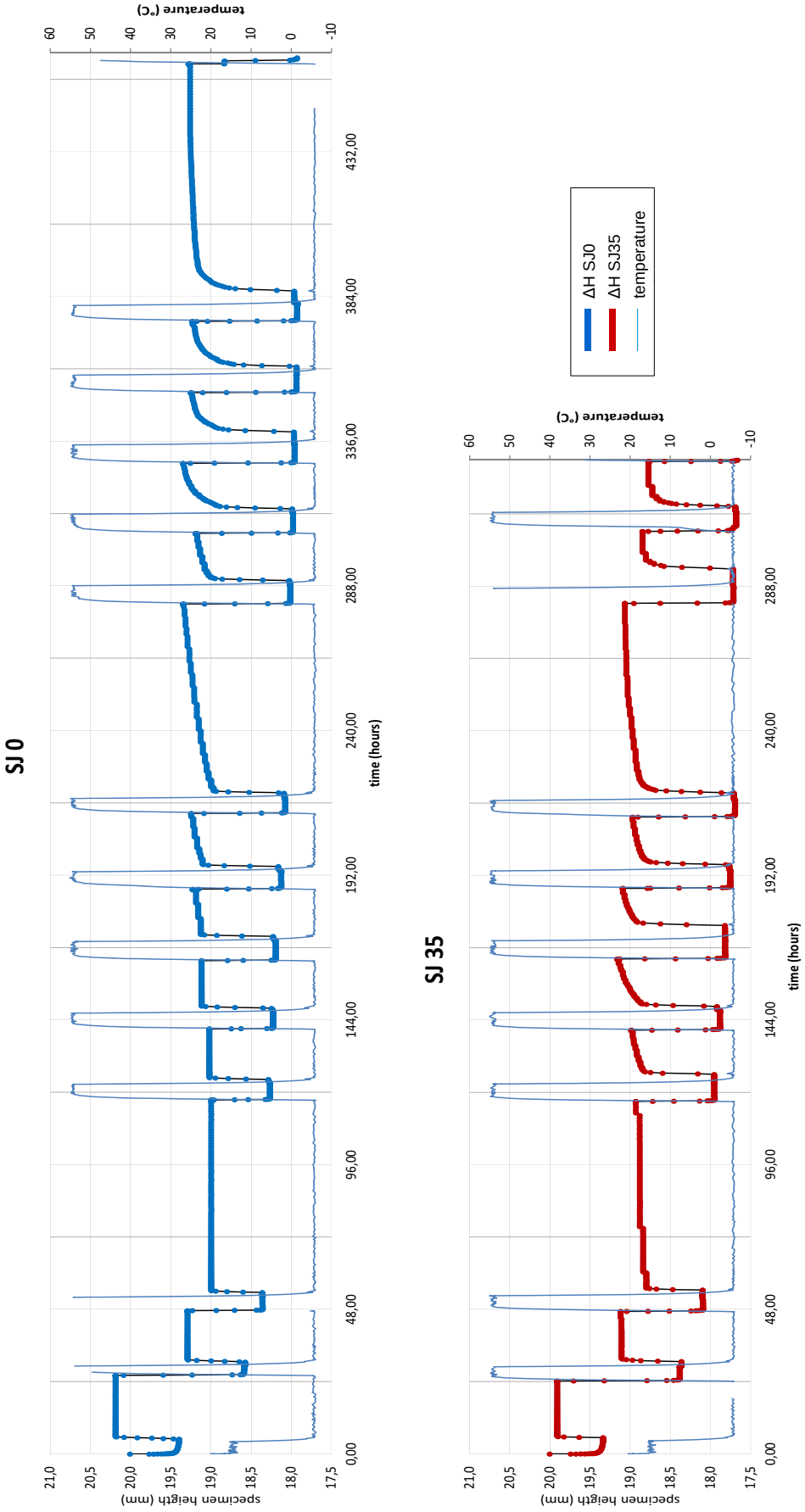

Figure 5.3.5: Vertical strain diagram of samples SJ0 and SJ35 under cyclical thermal stress

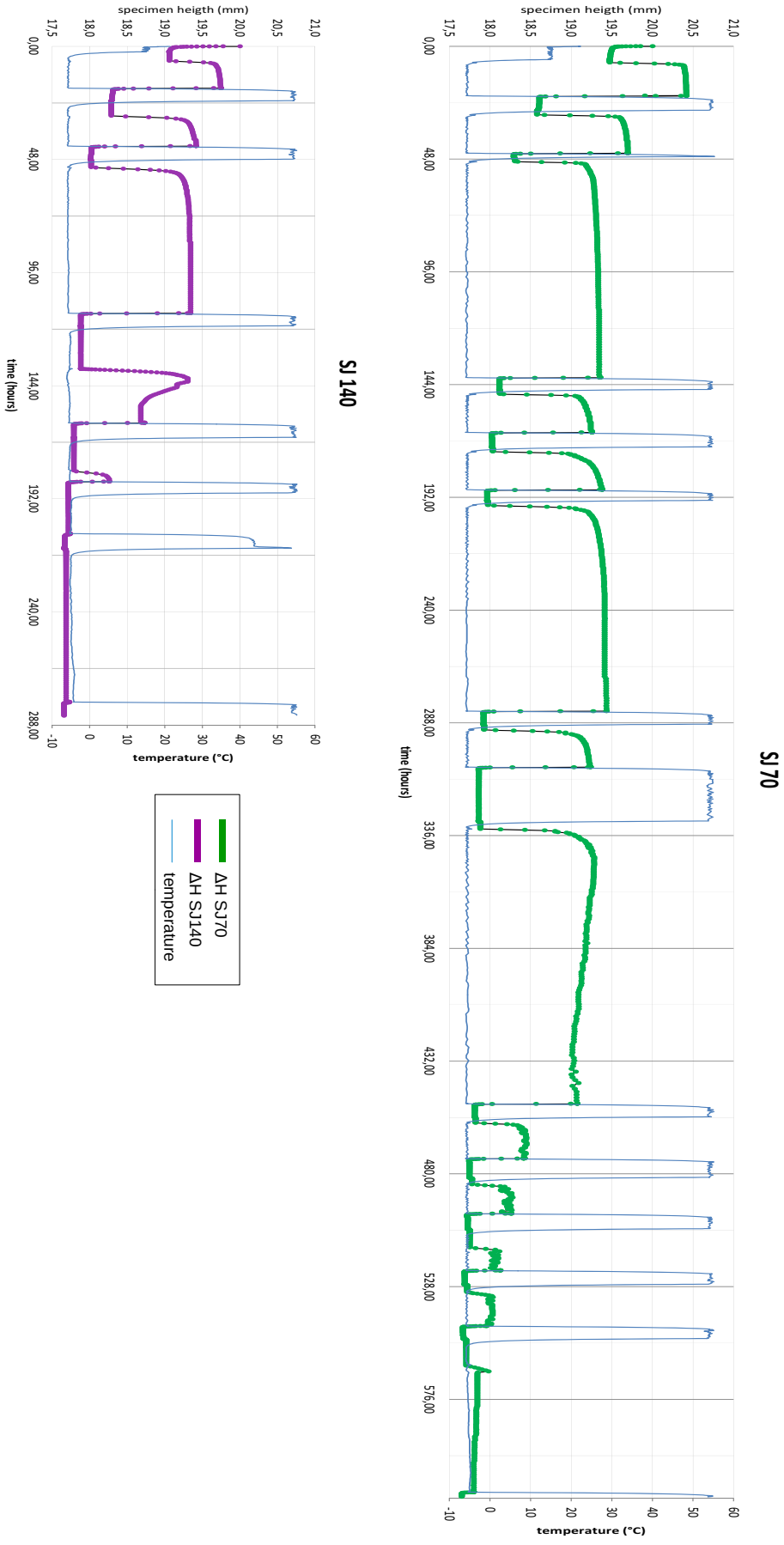

Figure 5.3.6: Vertical strain diagram of samples SJ70 and SJ140 under cyclical thermal stress

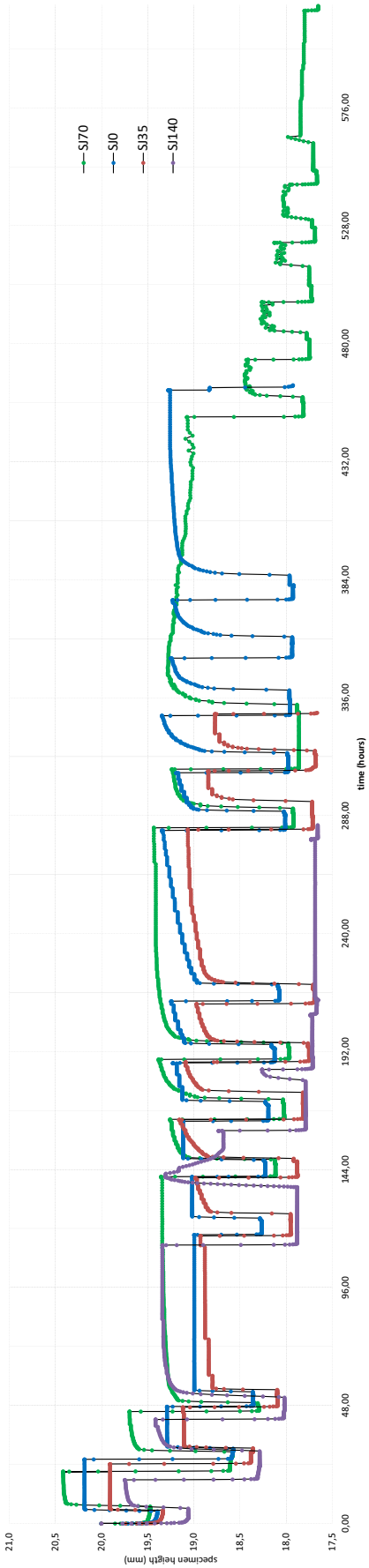

Figure 5.3.7: Comparison between samples vertical strain diagrams

Conclusions

The thermo-mechanical behavior of a Venetian clayey subsoil sample was tested under freeze-thaw cycling conditions, in order to investigate the effects induced in Venetian subsoils by BHE thermal forcing. In particular, the samples were tested at different NaCl concentration to understand the interaction of solutes in freezing soils.

Laboratory experiments show that:

1. Under-sized BHE could induced the freezing and thawing of the surrounding ground, if the soil freezing point is reached by the carrier fluid temperature
2. FTC induces an *irreversible settlement* in clayey sediments of 8% of magnitude
3. NaCl concentration in the pore solution increases the settlement in soils subjected to FTC
4. NaCl concentration in the pore solution depresses the freezing point and increases the unfrozen water in freezing and thawing soils
5. FTC induces a freezing point depression in clayey soils because of the increased salinity and water loss

Future development

Soil freezing and thawing mechanisms are complex and far from being well understood.

The experiments particularly focused on soil thermal settlements and gave only indirect indications on the water movement inside the specimen. Permeability tests would be useful to verify the increase in vertical permeability, in soils which experienced the FTCs performed with horizontal heat flow.

Also the influence mechanism of solutes in FTC processes needs more investigation. Future tests may for example involve other types of solutes, as bivalent cations such as $Ca^{2+}$and Mg^{2+}, which are characteristic cations of marine deposits and have different interactions with clays, compared to Na^{+}.

Performed experiments suggest that also the clayey soil structure, i.e. the microscopical disposition of the particles, has an important influence on the final thermal settlement. Freezing flocculated sediments could result in an higher consolidation because of the destroying effect on FTC coupled with a thinner AWL. Clayey soil structure depends on the solute type and on its

concentration in the depositional environment. While coastal deposits, alluvial and then characterized by fresh water, are mostly dispersed, marine and lagoon deposits have a flocculated structure, because with high Na^{+}, $Ca^{2+}$and Mg^{2+}concentration [41]. Under this assumption, Holocene deposits (flocculated) are more vulnerable to thermal stress consolidation than Pleistocene (dispersed) sediments. In order to investigate these aspects, it would be interesting to perform experiments on undisturbed samples, using tomographies to visualize the soil structure and its changes during every freezing and thawing phases.

Another kind of important analysis is the development of numerical models, but also *in situ* experiments in order to understand which is the soil spatial range, around the well, effectively affected by the thermal stress.

The combined action of these researches will lead the understanding of the real environmental impacts of BHE installation, with the aim of safely increasing and diffusing low enthalpy geothermal technologies.

Acknowledgments

Desidero ringraziare tutti coloro che mi hanno aiutato nella realizzazione della mia Tesi.

In particolare ringrazio Giorgia per avermi aiutato e spronato a fare sempre del mio meglio, ma soprattuto per aver reso più divertente ed appassionante quest ultimo anno di ricerche. Sarà sicuramente uno dei periodi accademici che più ricorderò volentieri. Ringrazio sentitamente il Prof. Sassi ed il Prof. Galgaro per la disponibilità ed i loro preziosi consigli. Inoltre ringrazio Mattia, Micol, Miriam, Laura, Riki e tutti i ragazzi del laboratorio per aver reso più leggere le giornate chiusi là dentro. Un ringraziamento anche al mio amico Totò per avermi dato un paio di idee che ho sviluppato in questa Tesi. Infine un grazie a Giulia che oltre ad aver revisionato il testo, mi ha anche sopportato durante tutta la sua stesura.

Tutte le persone citate in questa pagina hanno svolto un ruolo fondamentale nella stesura della Tesi, ma desidero precisare che ogni errore o imprecisione è imputabile soltanto a me.

Bibliography

[1] Aicarr journal N.15. Pompe di calore, terra o aria?, 2012.

[2] Anberg H., 2014. Testing Procedure: Freeze-Thaw-Cycles on Borehole Heat Exchanger Grouts. 5th European Geothermal PhD day, Darmstad.

[3] Andersland, B.O., Ladanyi, B., 2003. Frozen Ground Engineering, second ed. ASCE Press and John Wiley & Sons, Reston, VA.

[4] Anderson D.M., Morgenstern N.R., 1973. Physics, chemistry and mechanics of frozen ground. A review. In Permafrost: The North American Contribution to the 2nd International Conference on Permafrost, Yakutsk, 13–28 July. Washington, D.C.: National Academy of Sciences, p. 257–288.

[5] ASTM D4318. 10 Standard Test Methods for Liquid Limit, Plastic Limit, and Plasticity Index of Soils. ASTM 2010. Retrieved 2011-02-18.

[6] Atekwana E.A. et al., 2003. The relationship of total dissolved solids measurements to bulk electrical conductivity in an aquifer contaminated with hydrocarbon. Journal of Applied Geophysics 56 (2004) 281–294.

[7] Banin, A., Anderson, M.D., 1974. Effects of salt concentration changes during freezing on the unfrozen water content of porous material. Water Resour. Res. 10 (1), 124–128.

[8] Bing H., He P., 2010. Experimental investigations on the influence of cyclical freezing and thawing on physical and mechanical properties of saline soil. Environ Earth Sci (2011) 64:431–436.

[9] Bing H., Ma W., 2011. Laboratory investigation of the freezing point of saline soil. Elsevier B.V., Cold Regions Science and Technology 67 (2011) 79–88.

[10] Boynton S.S., Daniel D.E., 1985. Hydraulic conductivity tests on compacted clay. ASCE Journal of Geotechnical Engineering 111 (4) 465–478.

[11] Brambati A., Carbognin L., Quaia T., Teatini P., Tosi T. 2003. The Lagoon of Venice: geological setting, evolution and land subsidence.

[12] Chamberlain E.J., Gow A.J., 1979. Effect of freezing and thawing on the permeability and structure of soils. Engineering Geology. 13 (1-4), 73–92.

[13] Chamberlain E.J., 1983. Frost heave of saline soils. In Proceedings, 4th International Conference on Permafrost, July 17–22, Fairbanks, Alaska. Washington, D.C.: National Academy Press, p. 121–126.

[14] Chamberlain EJ, Iskander I, Hunsiker SE. 1990. Effect of freeze-thaw on the permeability and macrostructure of soils. Proceedings of the International Symposium on Frozen Soil Impacts on Agriculture, Range, and Forest Lands. Cold Regions Research and Engineering Laboratory, Hanover, New Hampshire, U.S.A. Special Report 90-1: 145–155.

[15] Chinellato M., 2013. Effetto del congelamento del terreno sulle prestazioni delle pompe di calore geotermiche. Tesi di laurea magistrale, Ingegneria Energetica. Dipartimento di Ingegneria Industriale. Università di Padova.

[16] Chorom M., Rengasamy P., 1996. Effect of heating on swelling and dispersion of different cationic forms of a smectite. Clays and Clay Minerals, Vol. 44, No. 6, 783 790.

[17] Dashjamts D., Altantsetseg J., 2011. Research on Consolidation of Frozen Soils upon Thawing. The 6th International Forum on Strategic Technology.

[18] De Franco R. et al 2009. Monitoring the saltwater intrusion by time lapse electrical resistivity tomography: The Chioggia test site (Venice Lagoon, Italy). Journal of Applied Geophysics 69 (2009) 117–130.

[19] D.Le n.28. Attuazione della direttiva 2009/28/CE su la promozione dell'uso dell'energia da fonti rinnovabili, recante modifica e successiva abrogazione delle direttive 2001/77/CE e 2003/30/CE. 2011

[20] D.M 13/09/1999 e successiva rettifica D.M. 25/03/2002. Metodi ufficiali di analisi chimica del suolo. In recepimento delle normative ISO e CEN.

[21] D.M. 28/12/2012 Incentivazione della produzione di energia termica da impianti a fonti rinnovabili ed interventi di efficienza energetica di piccole dimensioni.

[22] Eigenbrod K.D., 1996. Effects of cyclic freezing and thawing on volume changes and permeabilities of soft fine-grained soils. Canadian Geotechnical Journal 33 (4) 529–537.

[23] Ghezzo M. et al., 2011. Modeling the inter-annual variability of salinity in the lagoon of Venice in relation to the water framework directive typologies. Ocean & Coastal Management 54 (2011) 706 - 719.

[24] Goldshtein H.N., 1948. Deformation of the Earth Road-Bed and Foundations of Structures during Freezing and Thawing, Tr. Vscs. in-ta zhel.-dor. transp., No. 16. Transzheldorizdat.

[25] Graham J., Au V.C.S., 1985. Effects of freeze-thaw and softening on a natural clay at low stresses. Canadian Geotechnical Journal 22 (1) 69–78.

[26] Keller G.V., Frischknecht F.C., 1966. Electrical Methods in Geophysical Prospecting. Pergamon Press : Oxford, UK.

[27] Konrad,J e Morgenstern,N. 1980. A mechanistic theory of ice lens formation in fine grained soils. Can Geot J, vol (17). Pp 473-486.

[28] Kozlowski, T., 2004. Soil freezing point as obtained on melting. Cold Reg. Sci. Technol. 38, 93–101.

[29] Kozlowski, T., 2009a. Some factors affecting supercooling and the equilibrium freezing point in soil–water systems. Cold Reg. Sci. Technol. 59 (1), 25–33.

[30] Kozlowski, T., 2009b. Some factors affecting supercooling and the equilibrium freezing point in soil–water system. Cold Reg. Sci. Technol. 59, 25–33.

[31] Lambe T.W., 1960. Compacted Clay: Structure. Trans. ASCE, vol. 125, pp. 682 - 717.

[32] Lambe T.W., Kaplar C.W., 1971. Additives for modifying the frost susceptibility of soils, Part I. USA Cold Regions Research and Engineering Laboratory, Technical Report 123, Pt. 1.

[33] Lancellotta R., 2012. Geotecnica. Zanichelli editore.

[34] Marion G.M., 1995. Freeze–Thaw Processes and Soil Chemistry. Special Report 95-12.

[35] Molinaroli E., Guerzoni S., Sarretta A., Cucco A., Umgiesser G. 2006. Links between hydrology and sedimentology in the Lagoon of Venice, Italy. Journal of Marine Systems 68 (2007) 303–317.

[36] Muffler P. and Cataldi R., 1978. Methods for Regional Assessment of Geothermal Resources. Geothermic Vol. 7, pp. 53-89.

[37] Mulligan A. E., Evans R. L., Lizarralde D., 2006. The role of paleochannels in groundwater/seawater exchange. Journal of Hydrology (2007) 335, 313–329.

[38] Othman M.A., Benson C.H., 1993. Effect of freeze-thaw on the hydraulic conductivity and morphology of compacted clay. Canadian Geotechnical Journal 30 (2) 236–246.

[39] Perfect E., Groenevelt P.H., Kay B.D., 1991. Transport phenomena in frozen porous media. In Transport Processes in Porous Media. Dordrecht: Kluwer Academic Publishers, p. 243–270.

[40] Provincia di Venezia, 2008. Le unità geologiche della provincia di Venezia. Servizio geologico e difesa. Università di Padova, Dipartimento di Geografia.

[41] Push R. 1978. Unfrozen water as a function of clay microstructure. 1st Int Symp on Ground Freezing, Germany, Bochum. Pp 103-107.

[42] Qi J.L., Ma W., 2008. Influence of freeze–thaw on engineering properties of a silty soil. Wiley InterScience, Permafrost and Periglac. Process. 17: 245–252.

[43] Qi J.L., Pieter V., Cheng G.D., 2006. A review of the influence of freeze–thaw cycles on soil geotechnical properties. Permafrost and periglaical processes. 17, 245–252.

[44] Stefanile L., 2013. Analisi sperimentale del comportamento termo-meccanico di un'argilla di Venezia. Tesi di Laurea Triennale, Ingegneria Civile, Università di Padova.

[45] Sumner M.E., Rengasamy P., R. Naidu., 1998. Sodic soils: A reappraisal. In: Sodic soils: Distribution, properties, management, and environmental consequences. (Sumner M.E., Naidu R., eds.). Oxford University Press, NY, Oxford, pp. 3-17.

[46] Superjet International S.p.A., 10/02/2013. Relazione Geognostica e Geotecnica. Redatta da dott. Freddo A. geologo.

[47] Teatini P., Rizzetto F., Tosi L., Carbognin L., Bonardi M. 2003. Geomorphic setting and related hydro-geological implications of the coastal plain south of the Venice Lagoon, Italy. Hydrology of die Mediterranean and Semiarid Regions (Proceedings of an international symposium held at Montpellier, April 2003). IAHS Publ. no. 278.

[48] Tosi L., Teatini P., Strozzi T., 2013. Natural versus anthropogenic subsidence of Venice. Scientific Reports 3, Article number: 2710.

[49] Yong R.N., Cheung C.H., Sheeran D.E., 1979. Prediction of salt influence on unfrozen water content in frozen soils. Engineering Geology (Amsterdam), 13: 137–155.

[50] Yong R., Boonsinsuk P., Yin C., 1985. Alternation of soil behavior after cyclic freezing and thawing. Balkema A (ed) Proceedings of the 4th international symposium on ground freezing, Rotterdam, The Netherlands, pp 187–195 436 Environ Earth Sci (2011) 64:431–436 123.

[51] Valentini N., 2013. Analisi sperimentale dei terreni coesivi della laguna di Venezia in relazione alla realizzazione di impianti di geoscambio. Tesi di Laurea Triennale, Ingegneria Civile, Università di Padova.

[52] Viklander, P., 1998. Permeability and volume changes in till due to cyclic freeze–thaw. Canadian Geotechnical Journal. 35, 471–477.

[53] Zhukov M.F., 1990. "Korenniye Prichini Deformatsii Zdanii na Vechnoi Merzlote", Osnovaniya i Fundamenti i Mehanika Gruntov 1990 (4), pp. 25-27.